Soft Actuators for Miniature and Untethered Soft Robots

Using Stimuli-Responsive Hydrogels

by

Roozbeh Khodambashi Emami

A Dissertation Presented in Partial Fulfillment
of the Requirements for the Degree
Doctor of Philosophy

Approved April 2021 by the
Graduate Supervisory Committee:

Daniel M. Aukes, Chair
Thomas G. Sugar
Changho Nam

ARIZONA STATE UNIVERSITY

August 2021

ABSTRACT

Soft robots currently rely on additional hardware such as pumps, high voltage supplies, light generation sources, and magnetic field generators for their operation. These components resist miniaturization; thus, embedding them into small-scale soft robots is challenging. This issue limits their applications, especially in hyper-redundant mobile robots. This dissertation aims at addressing some of the challenges associated with creating miniature, untethered soft robots that can function without any attachment to external power supplies or receiving any control signals from outside sources. This goal is accomplished by introducing a soft active material and a manufacturing method that together, facilitate the miniaturization of soft robots and effectively supports their autonomous, mobile operation without any connection to outside equipment or human intervention.

The soft active material presented here is a hydrogel based on a polymer called poly(N-isopropylacrylamide) (PNIPAAm). This hydrogel responds to changes in the temperature and responds by expanding or contracting. A major challenge regarding PNIPAAm-based hydrogels is their slow response. This challenge is addressed by introducing a mixed-solvent photo-polymerization technique that alters the pore structure of the hydrogel and facilitates the water transport and thus the rate of volume change. Using this technique, the re-swelling response time of hydrogels is reduced to $2.4min$ – over 25 times faster than hydrogels demonstrated previously. The material properties of hydrogels including their response rate and Young's modulus are tuned simultaneously. The one-step photo-polymerization using UV light is performed in under 15 sec, which is a significant improvement over thermo-polymerization, which takes anywhere between a few minutes to several hours. Photopolymerization is key towards simplifying recipes, improving access to these techniques, and making them tractable for iterative design processes.

To address the manufacturing challenges, soft voxel actuators (SVAs) are presented. SVAs are actuated by electrical currents through Joule heating. SVAs weighing only 100

mg require small footprint microcontrollers for their operation which can be embedded in the robotic system. The advantages of hydrogel-based SVAs are demonstrated through different robotic platforms namely a hyper-redundant manipulator with 16 SVAs, an untethered miniature robot for mobile underwater applications using 8 SVAs, and a gripper using 32 SVAs.

ACKNOWLEDGMENTS

TABLE OF CONTENTS

LIST OF TABLES

LIST OF FIGURES

Figure   Page

Chapter 1

INTRODUCTION

Traditionally, robots are made of rigid materials such as steel. Rigidity enables robots to perform repeated tasks with high speed and precision. Rigid robots such as the ones used in automotive assembly lines are usually designed for specific tasks and are less applicable in the presence of changes in working conditions. Biological organisms on the other hand perform a wide range of tasks, although with lower precision and speed. Scientists have thus been investigating using soft materials in robots to mimic soft living organisms in terms of adaptability. Figure 1.1-a shows an example of a soft robot that can perform grasping of delicate objects without damaging them, regardless of their shape or surface roughness [1].

Untethered robots are a class of robots that can function independently without any connection to external power supplies or other equipment. Therefore, untethered robots can be used as autonomous mobile robots in remote locations or in situation where the robot needs to move around and perform tasks such as in factory floors or in warehouses. Boston Dynamics' Atlas [1] can be considered as an example of untethered robots as can be seen in Figure 1.1-b.

Miniature robot applications include exploring tight spaces like the human body. Since miniature robots use less material, and the fabrication processes for making miniature robots often utilize precision tooling, automation, or processes that are easily parallelized,and their fabrication methods are less costly, they can be manufactured in large numbers and be used in swarm robotics. The mentioned three categories of robots can be combined to make robots that have the advantages of each. Figure 1.1-c,d,e highlight examples of such

---

[1]https://www.bostondynamics.com/atlas

robots.One example shown in Figure 1.1-c shows a low cost miniature insect-inspired robot that can be used in large numbers to pollinate plants [2].

Miniature, untethered soft robots take advantage of all categories and are the focus of this dissertation as shown in Figure 1.1-f [3]. In this chapter, a brief survey of soft robot technologies is presented. Then, the state of the art in miniature robots is discussed and the limitations of current miniature soft robots is presented. Finally, the contributions of this dissertation which aims at solving some of the challenges are summarized.
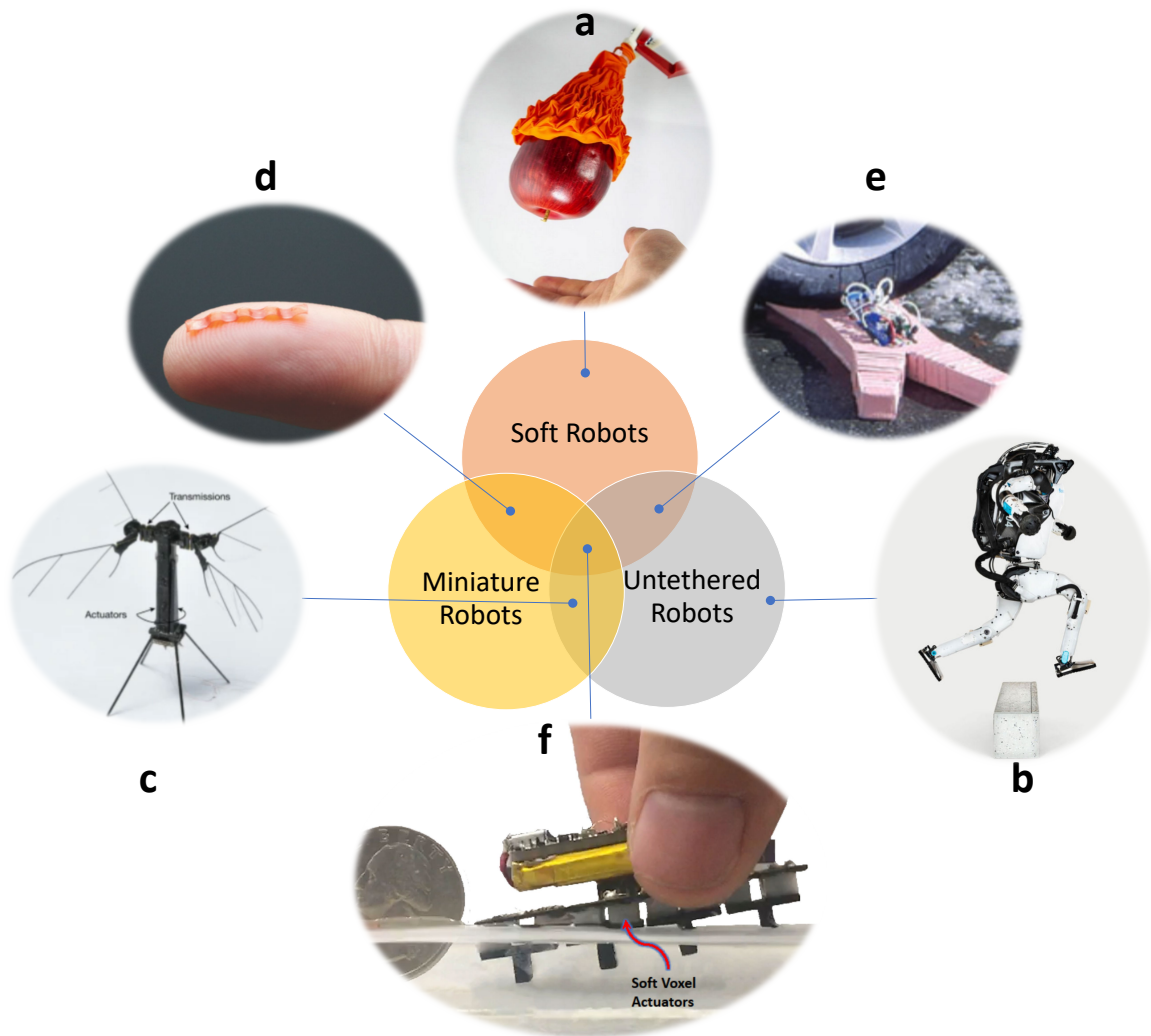
Figure 1.1 a) soft robot [1]. b) Untethered robot [1] c) Miniature untethered robot [2] d) Miniature soft robot [4] e) Untethered soft robot [5] f) Miniature untethered soft robot [3]

1.1 Soft Robotics as an Emerging Field

The majority of biological organisms consist of soft tissue, which provides some advantages to these biological systems. The octopus is the most widely used cited source of inspiration for soft robotics research because of their capabilities; they can deform their body and pass through small openings (Figure 1.2A). Therefore, shape morphing is one of the key advantages of soft organisms. Octopuses can also soften their arm as they wrap it around a bottle cap and stiffen their arms for a tight grip as they turn the cap to open it as shown in Figure 1.2B. Variable stiffness is therefore another aspect of soft organisms. The human hand is another example of a soft system that can demonstrate some of the advantages of compliant materials; it can grasp objects across a wide range of shapes and surface roughnesses without slipping because the soft tissue surrounding the skeletal system passively conforms to different shapes, improving conformance, increasing the contact surface area, and permitting higher forces to be passed to the grasped object. The human hand can also absorb energy from impacts, as it does when catching a baseball, absorbing energy and reducing the risk of damage. The ability to absorb energy also protects the objects and humans in case of a collision. This brings up safety as another important feature of compliance present in soft-bodied animals that can be important in the design of soft robots. Inspired by biology, soft robot developers try to utilize the advantages inherent in soft, compliant matter to achieve safer interactions around humans or more robust locomotion and manipulation in unstructured environments [5, 6, 7, 8].

1.2 State of the Art in Soft Robotics

Early robots were designed to be stationary. They were unaware of their surroundings and operated based on a prescribed set of instructions. Recent advances in sensing has paved the way for to mobile, autonomous, untethered robots. In addition to soft actuators,

3
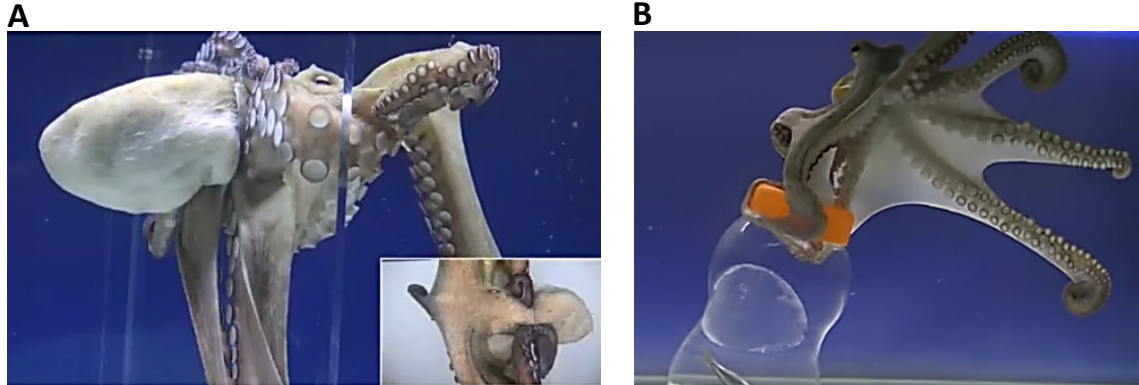
Figure 1.2 A) Octopus squeezing in a tight space while still being able to navigate the pipe. B) Octopus arm wrapping around a bottle when it is soft and then twisting to open the cap when it is stiff. Source: Octolab TV https://youtu.be/303S9kOxd0c

soft sensors and soft computers are thus an integral part of untethered robotic systems. For soft robots, ideally all these components are soft. With special attention paid to soft actuators –which is the focus of this dissertation– the state of the art technology in each category (untethered, soft, miniature robots) is reviewed.

1.2.1 Soft Sensors

Research on soft sensors focuses mainly on stretchable sensors for wearable health monitoring [9, 10]. Since these sensors exhibit characteristics, researchers have focused on solutions for integrating soft sensing into soft robotic systems. Sensors based on liquid metals have been successfully implemented within soft structures to measure strain [11, 12, 13, 14]. Other sensor technologies include piezoresistive [15, 16, 17], capacitive [18, 19, 20, 21], and conductive polymers [22, 23, 24] which rely on the change in resistance or capacitance of the material when they undergo strain.

1.2.2 Soft Computers

Traditionally, the majority of computation in robotic systems is performed by micro-controllers made of hard materials. This is unavoidable and is one of the major limiting factors in the development of entirely soft robots. Soft computers are in their incipient stage; they are based on pneumatic networks and have been demonstrated performing simple logic functions [25, 26]. Another research direction uses living cells as computers [27]. In general, the topic of soft computing requires significant development before it can be successfully implemented within soft robotic structures.

1.2.3 Soft Actuators

Actuators are often the core of robotic designs, and as such, there is a larger amount of research on soft actuators compared to soft sensors and computers. Soft pneumatic actuators (SPAs) [28, 29] are the most widely used category of actuators in soft robotics. Their function is based on chambers made of soft materials that are pressurized using fluids such as air or water. As a result of pressure supplied from external supply lines, the chamber deforms and produce motions such as bending, elongation or twisting. SPAs have high power to weight ratios and exhibit a relatively fast response. Another class of actuators use active materials whose strain is based on an externally-applied stimulus such as heat, light or magnetic field. This class includes shape memory alloys (SMAs)[30], dielectric elastomer actuators (DEAs) [31, 32], liquid crystal elastomers (LCEs) [33, 34], and stimuli-responsive hydrogels [35, 36, 37, 38].

1.3 Challenges Ahead

The focus of early soft robotic research was to identify methods for manufacturing and assembling SPAs and assemble them into functioning prototypes. Early soft robots were

created for tasks such as grasping or were used as stationary continuum manipulators. In these applications, the size and weight of the supporting fluidic equipment was not important because they could be located near the robot and did not have to be transported. In the case of mobile robots, however, all the supporting equipment must be included within the robot, and therefore, careful design is required to meet payload limitations. This challenge becomes more pronounced in the case of miniature robots where there is less space available within their body to include all the accessories. SPAs use passive soft materials such as silicone elastomers for pneumatic actuation and rely on rigid components such as motors and pumps for providing fluidic power; these devices are difficult to scale to millimeter or micrometer-scale robot designs and therefore, manufacturing small-scale soft actuators for applications such as healthcare, wearable devices, manufacturing, and robotics as envisioned by [39] has remained a bottleneck in the development of miniaturized soft robots [40]. This category of soft robots has been the least explored due to this issue, as well as the complexity of scaling down soft fabrication techniques. Though small-scale actuators can be produced using responsive materials such as DEAs, LCEs and hydrogels, these actuators lack sensing and computation– essential subsystems of a true robot. These systems are thus usually used in a human-in-the-loop scenario, where sensing and computation are performed by a human operator. This helps in down-scaling the robots to the micrometer range. These actuators can perform limited robotic functions and have highly specific applications such as to perform a colon tissue biopsy. However, these robots can not function as autonomous robots because they lack sensing and computation and rely on external devices for their operation. For instance, [41] needs a light projecting device to generate the light patterns required for creating deformations and movement in a light-responsive actuator. Another example is a magnetic-responsive actuator [42] which rely on a magnetic field generator for its operation. All this equipment is bulky and requires careful setup and therefore, these types of actuators are not suitable for use in autonomous mobile robots.

Technologies are still needed to create small-scale autonomous soft robots that function similar to biological organisms such as annelids, mollusks, and octopuses. Considering the highly sophisticated structure of living organisms, simultaneous progress in multiple disciplines such as materials science, design, manufacturing and control is required in order to achieve soft robots that are closer to their biological counterparts.

The focus of early soft robots was to identify methods for manufacturing and assembling SPAs and assemble them into functioning prototypes. These early soft robots were created for tasks such as grasping or were used as stationary continuum manipulators. In these applications, the size and weight of the supporting fluidic equipment was not important because they could be located near the robot and did not have to be transported. In the case of mobile robots, however, all the supporting equipment must be included within the robot, and therefore, careful design is required to meet payload limitations. This challenge becomes more pronounced in the case of miniature robots where there is less space available within their body to include all the accessories. SPAs use passive soft materials such as silicone elastomers for pneumatic actuation and rely on rigid components such as motors and pumps for providing fluidic power; these devices are difficult to scale to millimeter or micrometer-scale robot designs and therefore, manufacturing small-scale soft actuators for applications such as healthcare, wearable devices, manufacturing, and robotics as envisioned by [39] has remained a bottleneck in the development of miniaturized soft robots [40]. This category of soft robots has been the least explored due to this issue, as well as the complexity of scaling down soft fabrication techniques. Though small-scale actuators can be produced using responsive materials such as DEAs, LCEs and hydrogels, these actuators lack sensing and computation, which are essential subsystems of a true robot. These systems are thus usually used in a human-in-the-loop scenario, where sensing and computation tasks are performed by a human operator. This can make it possible to scale soft robots to micrometer ranges, though resulting actuators can perform limited robotic

functions and have highly specific applications such as to performing colon tissue biopsies. Because of the sensing and control limitations of small-scale microrobots, such systems, cannot truly function as autonomous robots and rely on external devices for their operation. For instance, the soft microrobot made of LCE described in [41] requires a light-projecting device to generate the light patterns required for creating deformations and movement in a light-responsive actuator. Another example is the magnetic-responsive actuator used in [42] which relies on a magnetic field generator for its operation. This equipment is universally bulky and requires careful setup and comlex computation. Therefore, these types of actuators are not suitable for use in autonomous mobile robots. Technologies are thus still required that enable small-scale autonomous soft robots which function similarly to biological organisms such as annelids, mollusks, and octopuses. Considering the highly sophisticated structure of these organisms, simultaneous progress in multiple disciplines, such as materials science, design, manufacturing and control is required in order to achieve soft robots that are closer to their biological counterparts.

Hydrogels are close to soft tissue in terms of their material properties and the muscle-like contractions in response to external stimuli [36]. They can be tuned to be ion conductive as well as biocompatible. These attributes can help hydrogel soft robots address the core benefits of soft devices namely safety and adaptability [43]. However, the uniform responsive volume change of bulk hydrogels makes them less interesting in robotic applications, which demands complex spatiotemporal reconfigurability [44] - as the dexterity of the octopus's arm demonstrates.

In summary, the challenge for small, untethered soft robots is to create 1) on-demand, 2) time-varying, 3) local deformations in a hydrogel structure. From a structural design perspective, the majority of reported heterogeneous hydrogel structures made up till now demonstrate fixed deformation patterns, such as static shape shifting of sheets, without any interaction with the environment [45, 46, 47], or bending of beams to perform simple grip-

8

ping functions [48, 49, 50]. Only a few methods demonstrate on-demand deformations for interacting with objects [41, 42, 51]; these approaches, however involve bulky equipment (light and magnetic field generators), making them impractical for mobile soft robots or embedded applications. From a materials perspective, there is a need for a powerful but simple synthesis method to broadly tune the material response behavior (volume changing ratio, speed, and stiffness), to meet the requirement of creating a complex robotic structure with spatiotemporal reconfigurability.

1.4 Contributions of this Dissertation

This dissertation demonstrates progress in different areas of material science and manufacturing that together contribute to the field of soft robotics. A set of design decisions are made based on close collaboration with teams of material scientists and roboticists which helps inform progress of one field by considering the requirements of the other.

A bioinspired approach is applied in several design decisions. Biological organisms use electrical signals from the nervous system in conjunction with responsive muscle tissue to perform soft actuation. This combination helps them to be self-contained and also, it is viable across scales from giant octopuses to millimeter-sized worms. Therefore, the first feature that is considered for the design of soft robots is to use a material that is responsive to electrical stimulus. Living organisms are made of cells – another type of simpler building blocks assembled to form a more complex organ. The second requirement imposed is therefore, to use a bottom-up strategy to fabricate complex robots using simple building blocks that are easy to manufacture.

The contribution of this dissertation, as shown in Figure 1.3, can be summarized as follows:

- A novel, temperature-responsive hydrogel material with fast response. This material functions as artificial muscle tissue.

9

- A facile and tunable synthesis method for making soft actuators that is accessible to the soft robotics community, where in-house material synthesis, training, and capability, is more limited than in material-science focused lab spaces.

- A voxel-based assembly approach that uses simple building blocks called soft voxel actuators (SVAs) in the assembly of more complex soft robots. SVAs are easy to manufacture and solve some of the challenges associated with embedding electronics in soft robots.

- The use of electrical Joule heating of SVAs in the generation of a motion/force response. This enables the use of small-footprint microcontrollers and paves the way to embedded and mobile robot applications.

- Realization of hyper-redundant, hydrogel-based, electrically-addressable, miniature soft robots capable of performing tasks that require high degrees of freedom. High dexterity combined with the ability to function in unstructured environments separate our soft robots from previously demonstrated ones.

- Realization of miniature untethered soft robots that weigh only 20g including battery and power supply and does not rely on external equipment or human intervention for its operation.

1.4.1   Dissertation Outline

The following chapters discuss the innovations in materials science and manufacturing methods that lead to the development of miniature untethered soft robots.

Chapter 2: Soft Voxel Actuators: Hydrogel Building Blocks for Bottom-up Assembly of Soft Robots
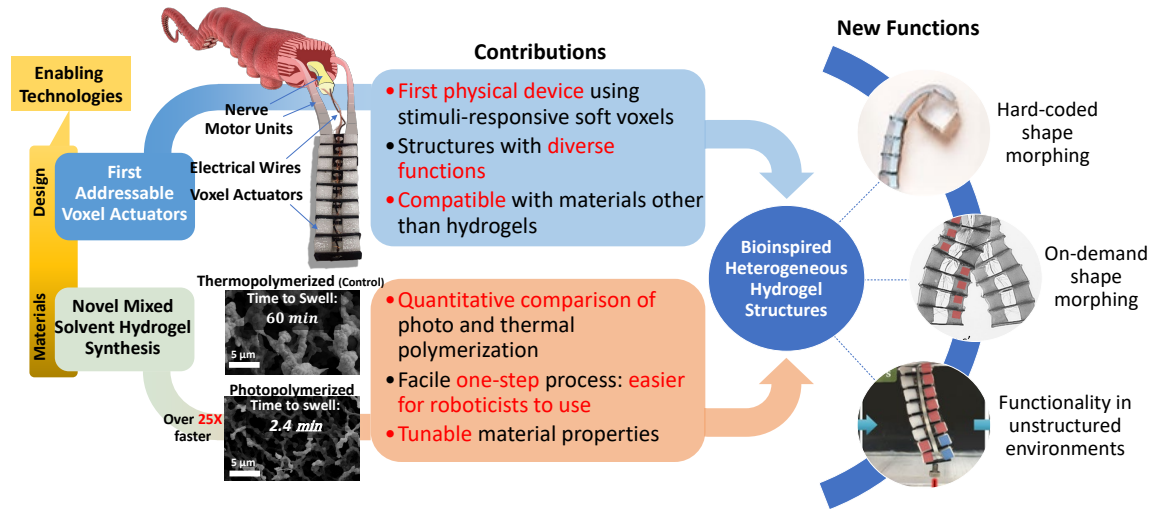
Figure 1.3

This chapter discusses the recipe for preparing temperature-responisve hydrogels. Improvements have been made in the synthesis technique such that it is more accessible to robotic researchers who have less access to material processing facilities. In addition, this recipe results in hydrogels with fast response, solving a challenge that has limited the use of hydrogels in soft robotics. Next, building blocks called soft voxel actuators (SVAs) are introduced that facilitate the manufacturing of soft robots through a bottom up assembly approach. Both the hydrogel and SVAs are characterized in-depth in terms of material properties and actuation properties.

Chapter 3: Heterogeneous hydrogel structures as Miniature Hyper-redundant Soft Manipulators

This chapter is a case study of the application of SVAs towards miniaturizing soft robots while maintaining their high degrees of freedom. Hyper-redundant miniature soft robotic manipulators are developed. It is shown that the use of SVAs enables for the first time the development of such robots. These robots are able to work in unstructured environments, where working conditions might change. This manipulator has 16 actuators in a $40 \times 10 \times 4.5$ mm footprint which, is the highest reported number of degrees of freedom

in a miniature robot of this size and material type.

Chapter 4: Miniature Untethered Underwater Walking Robot

This chapter is a second case study of the application of SVAs and is focusing on the development of untethered miniature robots. This chapter demonstrates that SVAs can significantly reduce the weight and size of such robots, without limiting payload. These robots are fully untethered which means all the electronics and batteries are carried by the robot.

Appendix A: Tracking Control of a Miniature 2-DOF Manipulator with Hydrogel Actuators

The electrical stimulation of SVAs inspired by biology has many advantages and open the doors to equip the robots with artificial intelligence. As a first step, the automatic control of SVAs using a microcontroller is presented in this chapter. Instead of turning the SVAs on and off as explained in Chapter 3, the deformation of SVAs are controlled using a closed-loop control system based on the feedback from vision sensors which record the desired output of the system. A 2-DOF manipulator is fabricated using two SVAs and the position of the tip of the manipulator is controlled. As a final demonstration, a starfish-inspired robot is presented which can move a payload. Closed-loop control enables faster payload transport compared to an open loop control because the trajectory that each foot follows remains near optimal despite different loads and disturbances.

Chapter 2

SOFT VOXEL ACTUATORS: HYDROGEL BUILDING BLOCKS FOR BOTTOM UP

ASSEMBLY OF SOFT ROBOTS

Soft continuum manipulators are suitable for safely interacting with unstructured environments due to their compliance and theoretically infinite degrees of freedom (DOF). However, since current soft actuators resist miniaturization, it has remained a challenge to integrate large numbers of them in a minaturized soft continuum manipulators and mobile robots. Thus, until recently, the state of the art has remained limited to primitive miniature manipulators which have limited functionality. In this chapter we apply a bottom-up voxel-based design and manufacturing methodology to integrate more actuators into soft robot manipulators, while maintaining the small footprints found in prior literature. To solve the challenges associated with miniturizing soft actuators, we introduce soft voxel actuators (SVAs) – an active voxel actuated by an electrical stimulus – that resembles a group of muscle fibers (fascicles) in size, force production, and method of activation. We introduce an approach for manufacturing SVAs, and find their resulting frequency bandwidth and static and dynamic force production capacity. We then demonstrate the advantages of voxel-based fabrication methodologies by assembling $4.5 \times 4.5 \times 4.5 mm^3$ SVAs –which weigh only $100 \ mg$– into a miniature soft, continuum robotic manipulator with 16 DOFs and a $10 \times 40 \times 4.5 mm^3$ footprint. The arrangement of SVAs within this manipulator is inspired by the the arrangement of muscle fascicles in an octopus arm. We finally demonstrate the superiority of SVA-based manipulators over conventional ones when interacting with unstructured environment.
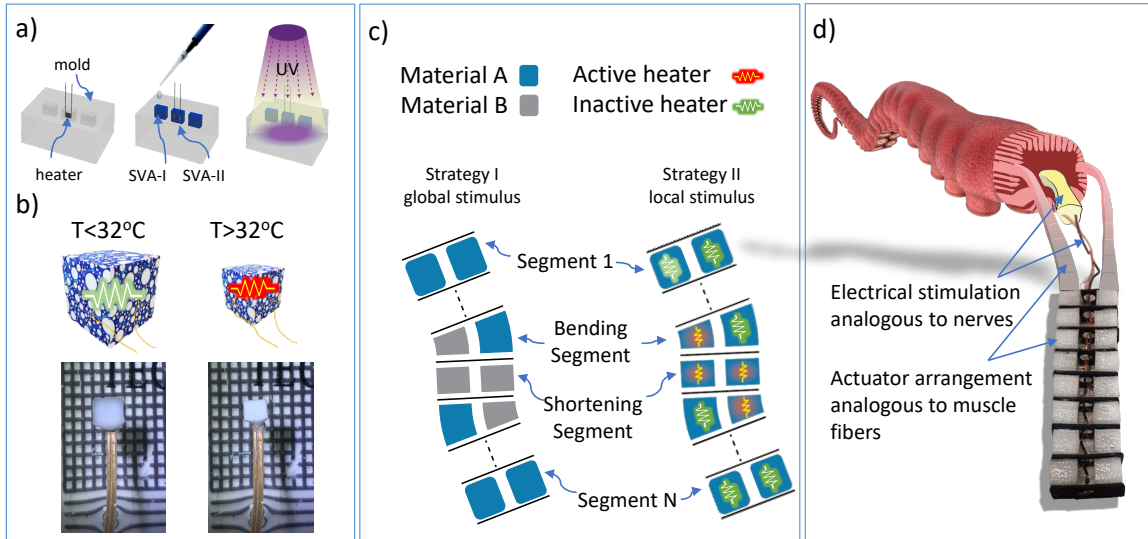
Figure 2.1 Soft Voxel Actuators (SVAs). A) SVA manufacturing steps, B) a SVA in its actuated and unactuated staes C) The voxel-base design and manufacturing methodology based on electrically addressable SVAs has made possible the creation of miniature continuum manipulator with 16 DOFs. D) Biological inspiration

2.1 Background

Inspired by biology, soft robot developers try to utilize the advantages inherent in soft, compliant matter to achieve safer interaction with unstructured environments. While the applications of small-scale soft robots have been demonstrated or envisioned by many research groups [39], miniature and micro-scale soft robots have matured more slowly than their macro-scale counterparts. The majority of soft robots utilize rigid components such as motors and pumps that are difficult to downscale [40] and therefore, manufacturing small-scale soft actuators has remained a bottleneck in the development of miniaturized soft robots. Smart, soft materials have shown promise in solving some of these challenges [52, 53, 54]; these smart materials react to changes in pH, temperature, or electric, magnetic and light fields by producing stress/strain fields in the material to create motions such as bending, twisting, or elongation. These motions have been harnessed for applications

such as drug delivery [55], micro-grippers [56], or other primitive robots [37].

2.2   SVA Fabrication

SVAs are made through a molding process in the form of cubes of different dimensions, as shown in Figure 2.2. The molds are made with PDMS (Sylgard 184, Dow Corning) because of its transparency to UV light and its elasticity, so that the cured hydrogel may be easily and fully demolded without breaking. Since the hydrogel swells from its molded dimensions upon soaking in water, the dimensions of the molds should be selected to be smaller than the required dimensions of the actuator. A nylon mold is prepared using a 3D printer (Markforged, M2) and is used to create the PDMS mold. When selecting Joule heaters, several types of resistive heaters were examined to find the optimum one in terms of manufacturability, durability, and compatibility with other electronic components. Surface mount resistors properties fit well with our needs and therefore are used as the heating elements (Figure 2.2). The value of the resistor should be chosen such that it produces enough heat to set the equilibrium temperature of the SVA from room temperature (25^oC) to above the transition temperature of the hydrogel (32^oC) and cause it to shrink when a 3.7 V supply voltage was connected to it. This actuation voltage is chosen to be compatible with many commonly used microcontrollers that are available on the market. We have used surface mount (SMD) thick film resistors with a resistance of 10 ohms which is shown in Figure 2.2 along with its dimensions. For manufacturing each SVA, a resistor (Joule heater) is positioned inside the mold using an XYZ manual stage (Figure 2.2) before the precursor solution is added and cured along with the gel. The heater is placed at a position equidistant from each side of the mold so that the entire volume of the gel is heated as uniformly as possible to avoid undesired nonuniform deformation of the actuators. PNIPAAm precursor solution is poured into the molds using pipettes while the resistive heater is held in place using grippers. A UV LED (UV 365nm, 10W, Chanzon, China) is used for curing the gels.

15
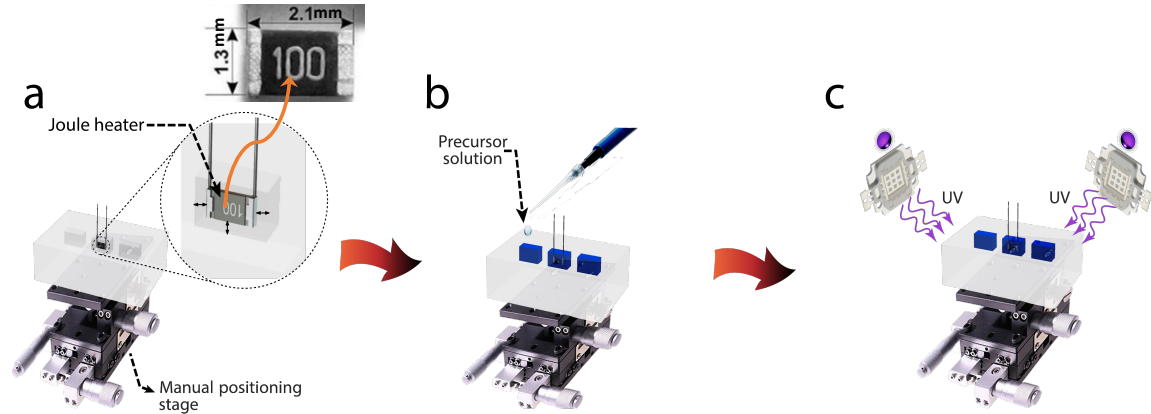
Figure 2.2 Steps for manufacturing SVAs. A) A Joule heater (surface mount (SMD) thick film resistors with a resistance of 10 ohms) is placed in the PDMS mold using an XYZ manual stage. B) Precursor solution is added to the mold. C) Hydrogel is formed by curing the solution under UV light for 10 seconds.

2.3 SVA Force Measurements

The force generated by a SVA is measured using a $100\ g$ load cell with a bridge amplifier (PhidgetBridge 1046_0B, Phidget, Canada) in the setup shown in Figure 2.3. The SVA is placed under the load cell, the Joule heater is activated allowing the SVA to shrink to its minimum volume, and then the linear stage is lowered to bring the load cell in contact with the surface of the SVA as shown in Figure 2.4. The interface between the load cell and the SVA is made from an acrylic plate. In force measurement tests where the SVA expands and pushes against the load cell, this plate just touches the surface of the SVA. In other tests where the SVA contracts, superglue is used to bind the acrylic plate to the SVA, so that the SVA pulled on the load cell as it contracted. The experiment is performed in a water bath at room temperature ($25^{o}C$). The load cell is calibrated while the acrylic plate is underwater but not touching the SVA. A two-point calibration method is used with a $50\ g$ precision weight.

16
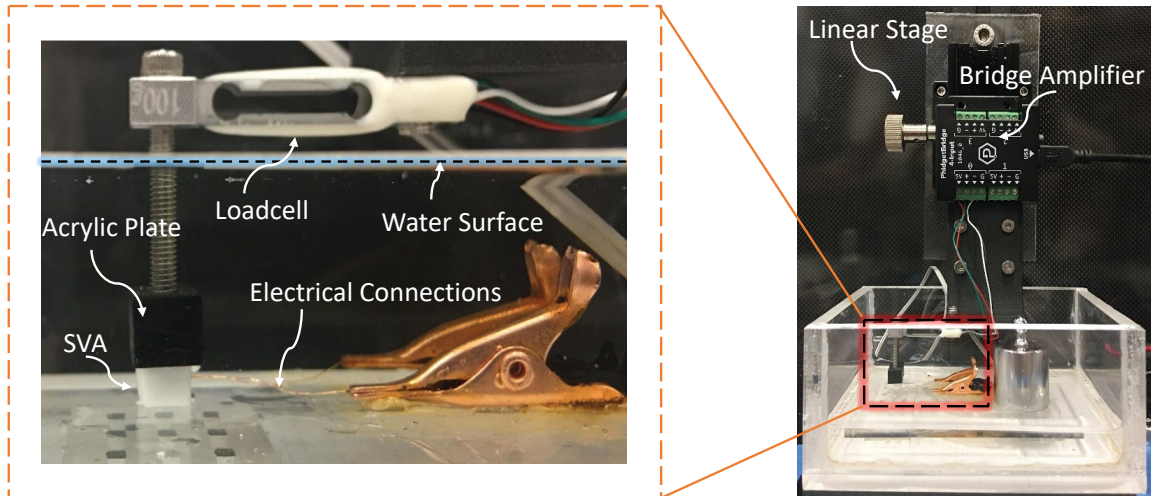
Figure 2.3 Force measurement test setup. SVA force is measured using a load cell and a bridge amplifier.
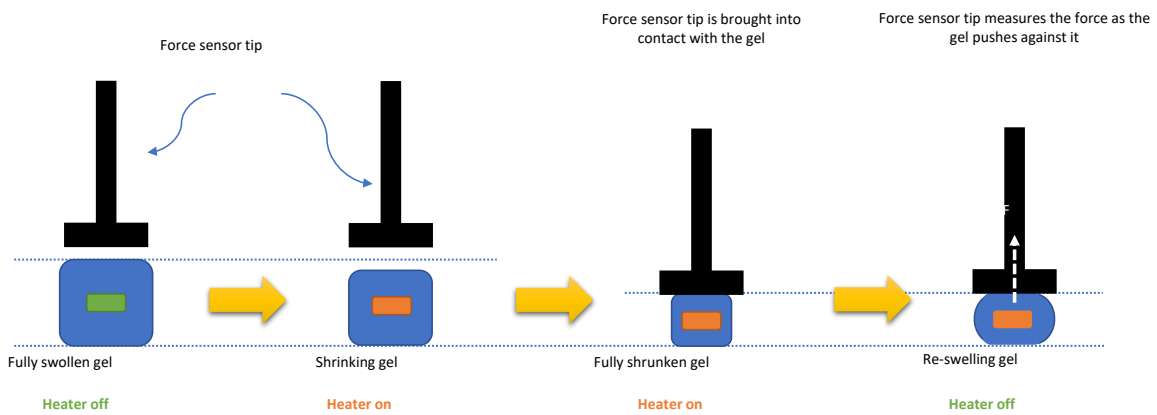
Figure 2.4 Force measurement procedure. Steps of placing the sensor tip on the SVA for compressive force measurement.

2.4 SVA Swelling Ratio Measurements

A commonly studied property of hydrogels, is its swelling ratio, or the measure of the ability of the gel to expand when it absorbs water. Robotics applications that use fast-responding hydrogels such as the one presented in this dissertation require a method of characterization of the hydrogel swelling that is compatible with experimental data-collection procedures that last on the order of minutes rather than hours. This helps to
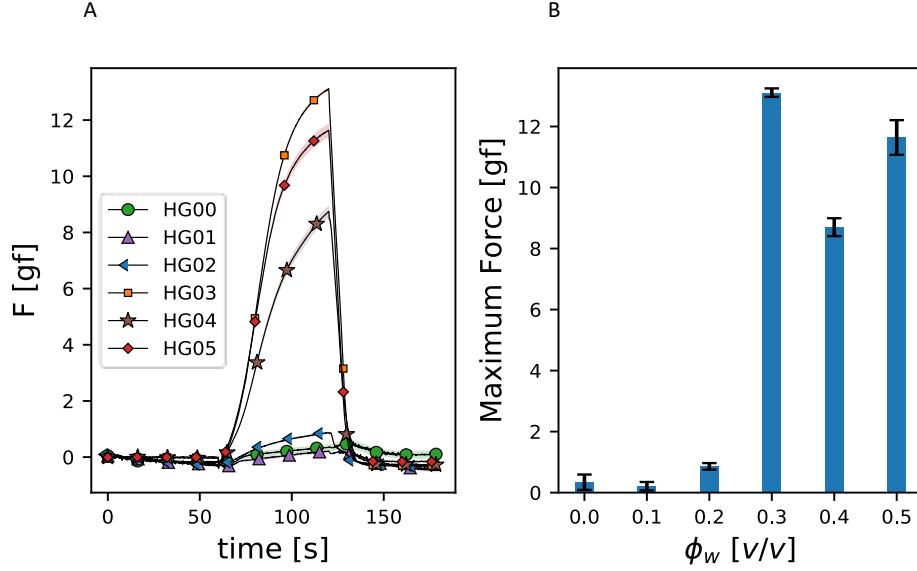
Figure 2.5 Tuning the mechanical properties of SVAs by varying water volume fractions ϕ_w.
A) Force produced by a SVA as a function of time for different ϕ_w. B) Maximum force produced by a SVA as a function of ϕ_w.

minimize errors due to room temperature fluctuations. We have developed a method that uses image processing techniques to measure the linear displacement produced by a SVA, as shown in Figure 2.6. The volume change of a SVA results in the movement of a lever arm contacting the SVA, and the resulting vertical displacement of the tip of the lever arm is then measured.

Since this vertical displacement is small, the curve followed by the tip can be approximated by a straight line; the SVA's displacement is thus proportional to the vertical component of the displacement. A marker on the tip is tracked by a Logitech C930e USB Webcam, which can stream HD 1080P quality video. This webcam is compatible with the MATLAB Image Acquisition and Image Processing Toolboxes. In each test, a checkerboard is placed in the plane of the marker located on the tips of the lever arm. This checkerboard has $2\ mm \times 2\ mm$ black and white squares and is used to estimate the calibration factors (mm/pixel) in x and y directions. Contrast-based filtering is used to identify the outline of
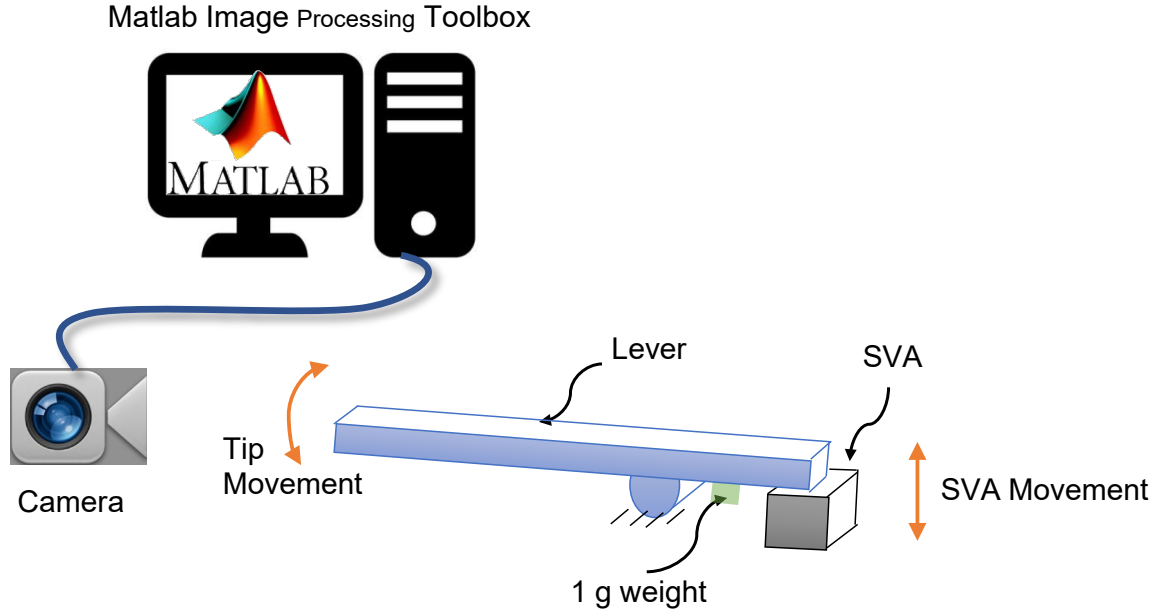
Figure 2.6 SVA displacement measurement setup. A camera is used to track the angular displacement of the tip of a lever arm, which is proportional to the vertical displacement of the SVA (assuming small displacements). The 1 g weight is affixed to the lever arm to ensure that the lever is always in contact with the SVA.

the marker; the marker color is therefore selected to be white against a black background. MATLAB's Camera Calibration Toolbox is used to compensate for lens distortion. The experiment is performed in a water bath at room temperature (25^oC).

2.5   Dynamic Mechanical Analysis (DMA) Tests

Each hydrogel prepolymer recipe is cast into a dogbone shape with $2.5\ mm$ thickness and $1.5\ mm$ neck width. This is done by pouring the prepolymer solutions into PDMS molds with the specified dogbone dimensions and polymerizing them under UV light for 15 seconds. The dogbones are then removed from the PDMS molds and immersed in a large container of DI water to remove excess monomer and DMSO. To measure Young's modulus, the dogbones are loaded into a Dynamic Mechanical Analyzer machine (TA In-

struments DMA850) and subjected to a strain rate of $8\%min^{-1}$. The Young's modulus was obtained from the slope of this stress-strain measurement (Figure 2.7). In addition, we have performed cyclic strains tests using the DMA device to study any material behavior changes over time (Figure 2.8).
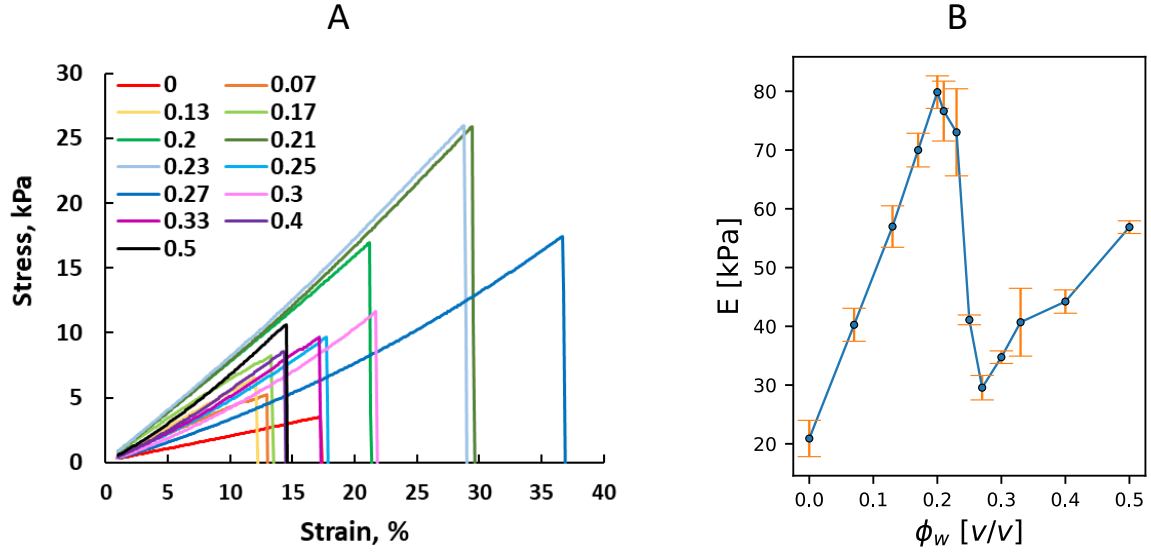
Figure 2.7 Dynamic mechanical analysis (DMA) test. stress-strain curves (left) and derived Young's modulus of the hydrogels as a function of water volume fraction (ϕ_w).

2.6 Crosslink Density Using Flory Theory

The Flory-Rehner rubber elasticity theory provides a simple approach for calculating crosslink density from swelling measurements. The equation is as follows :

$$-[\ln(1-\nu_2) + \nu_2 + \chi_1(\nu_2)^2] = V_1 n[(\nu_2)^{(\frac{1}{3})} - \frac{\nu_2}{2}] \tag{2.1}$$

In the above, ν_2 represents the volume fraction of the polymer in the hydrogel, χ_1 represents the Flory-Huggins interaction parameter for PNIPAAm-water which is equal to 0.5, V_1 represents the solvent (water) molar volume ($18\ cm^3\ mol^-1$), and n represents the density of linear polymer segments bound by crosslinks on both ends. ν_2 can be expressed in terms

20
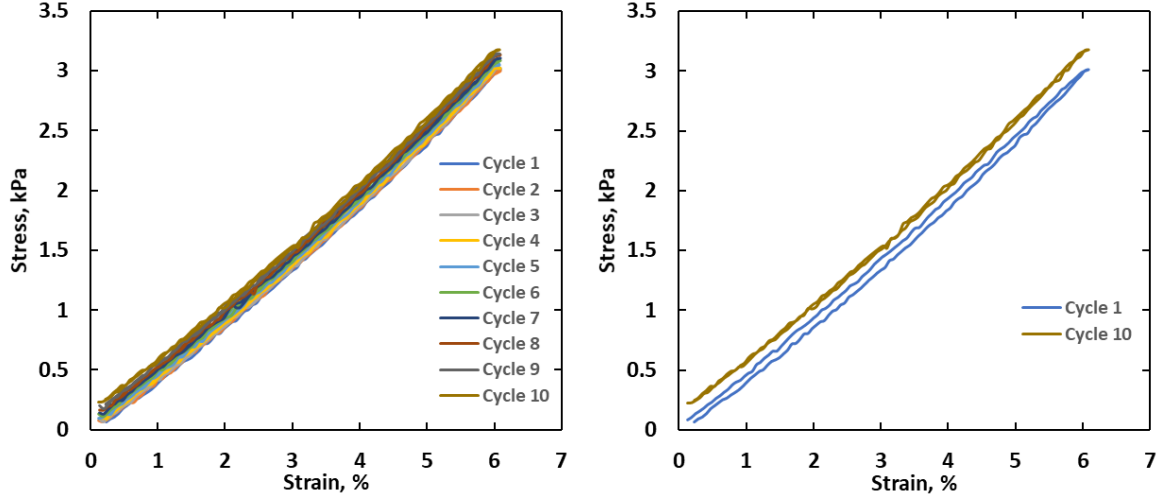
Figure 2.8 Cyclic load test. Stress-strain cycle test of HG03 ($\phi_w = 0.3$) dogbone, demonstrating stability over 10 cycles (left). Stress-strain curves of Cycle 1 and Cycle 10, demonstrating a gradual shift upwards, due to drying-induced stiffening (right). A strain rate of $20\% min^{-1}$ is used to mitigate the effects of drying-induced stiffening.

of the polymer volume ($V_{polymer}$) and gel volume (V_{gel}), as follows:

$$\nu_2 = \frac{V_{polymer}}{V_{gel}} = \frac{\left(\frac{m_{polymer}}{\rho_{polymer}}\right)}{V_{gel}} \tag{2.2}$$

V_{gel} can be measured directly from the dimensions of a regular-shaped hydrogel; $m_{polymer}$ is the dry mass of this hydrogel after freeze-drying. The density of the polymer ($\rho_{polymer}$) can be measured via the following volume relationship:

$$V_{gel} = \frac{m_{water}}{\rho_{water}} + \frac{m_{polymer}}{\rho_{polymer}} \tag{2.3}$$

This can be re-written in the following:

$$\rho_{polymer} = \frac{m_{polymer}}{\left(V_{gel} - \frac{m_{water}}{\rho_{water}}\right)} \tag{2.4}$$

Here, m_{water} represents the mass of the wet hydrogel minus $m_{polymer}$. With these relationships, ν_2 for photo- and thermo-polymerized HG03 PNIPAAm can be calculated, and

21

hence n can be obtained. Furthermore, the average molecular weight of crosslinked polymer segments (M_c) can also be calculated using the following modified equation, assuming the hydrogel is composed of a completely continuous polymer network:

$$-[\ln(1 - \nu_2) + \nu_2 + \chi_1(\nu_2)^2] = (\frac{V_1}{(\bar{\nu}M_c)})[(\nu_2)^{(\frac{1}{3})} - \frac{\nu_2}{2}] \qquad (2.5)$$

Here, $\bar{\nu}$ represents specific volume of the polymer in the hydrogel, represented by the following:

$$\bar{\nu} = \frac{V_{gel}}{m_{polymer}} \qquad (2.6)$$

Table 2.1 lists the key values of relevant properties calculated with this method.

Table 2.1 Values of mass fraction of water, volume fraction of polymer, n, and M_c for photo- and thermo-polymerized HG03 hydrogels.

	Photo	Thermo
m_{water}	0.87	0.85
$V_{Polymer}$	0.26	0.27
$n(\frac{mol}{cm^3})$	7.56×10^{-4}	9.37×10^{-4}
$M_c(\frac{g}{mol})$	149	140

2.7 Scanning Elecron Microscope (SEM) Imaging

To prepare SEM samples, each hydrogel prepolymer recipe was photopolymerized under UV light in a $1\,mm \times 5\,cm \times 7\,cm$ PDMS mold to form sheets. After rinsing in DI water to remove DMSO and excess monomer, the sheets were cut into $1\,mm$ thick slices. These slices were immersed in liquid nitrogen to instantly freeze and then immediately placed in a freeze-drier for 24 hours to remove the ice. The freeze-dried hydrogel slices were then imaged under SEM after sputtering a $5 - 10\,nm$ layer of gold on them. The SEM images for hydrogels with different solvent ratio is shown in Figure 2.9.
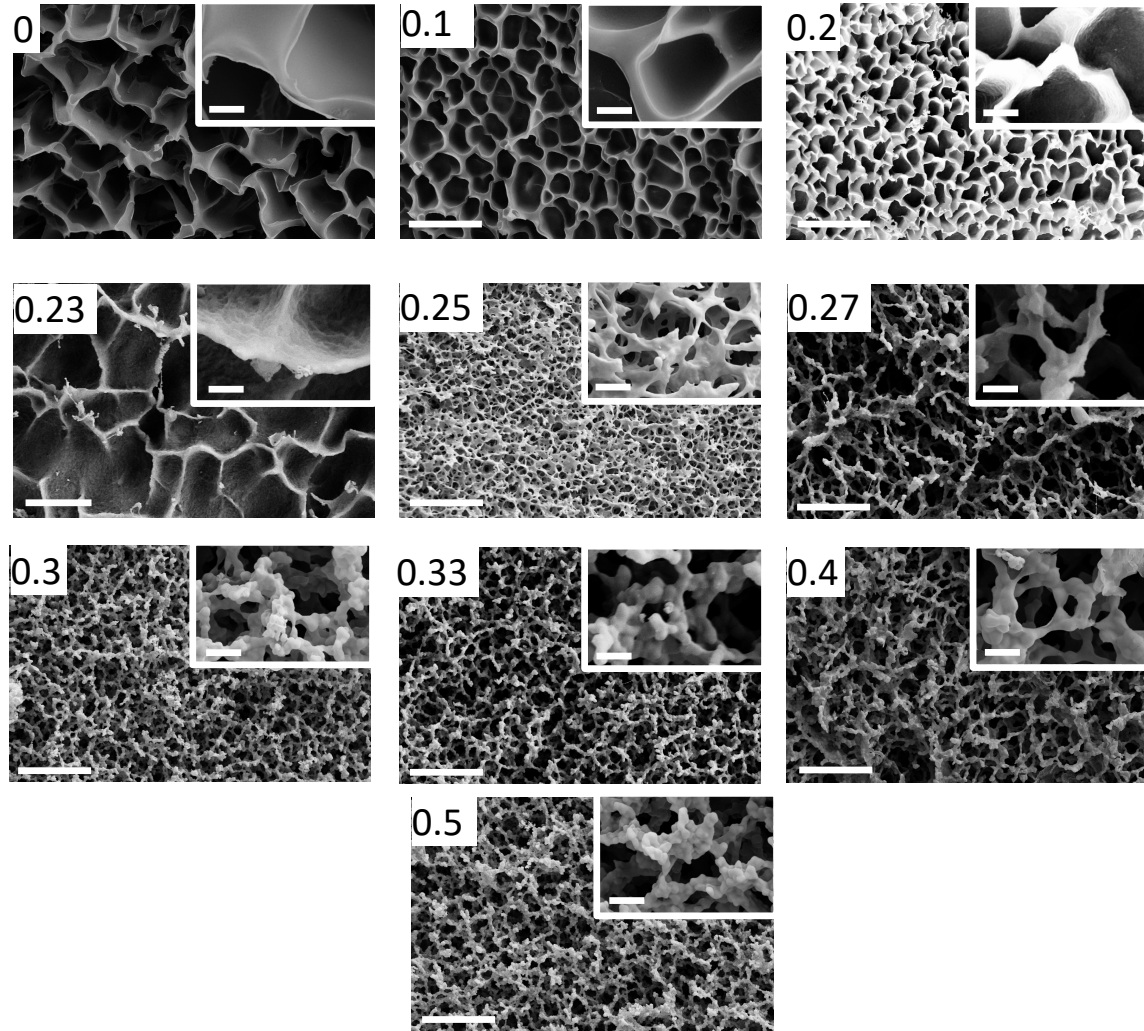
Figure 2.9 SEM images of the hydrogel microstructure. The numbers indicate the water volume fraction (ϕ_w). The scale bars are 10μm and 1μm for the low and high magnifications, respectively [57].

2.8   Studying Pore Wall Deformation Mechanism

We have taken additional SEM images for the HG03 in a shrunken state (Figure 2.10) to see if there is any buckling of the pore walls. Although there might be some buckling observed, they happen at random direction and therefore, they do not result in directional contraction or expansion of the bulk gel which results in a negative Poisson's ratio. In the

23

case of metamaterials by contrast, the buckling happens at microstructures that are ordered and patterned using micromanufacturing techniques such that they buckle all in the same direction resulting in the observed negative Poisson's ratio.
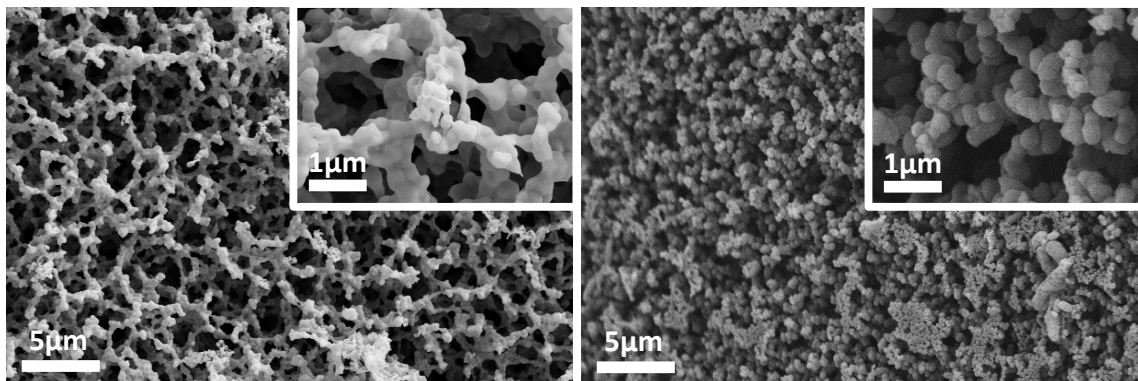
Figure 2.10 SEM images of the HG03 hydrogel (ϕ_w) in swollen state (left) and shrunken state (right).

2.9 Studying the Effect of Freeze-thaw Method on the Pore Structure and Response of the Hydrogel

Based on our prior experience, a freeze-thaw post-treatment with conventional closed-pore PNIPAAm gels (prepared in pure DMSO) results in enhanced swelling performance since the ice crystals can grow and expand or break the close-walled pore boundaries, resulting in a greater degree of pore interconnectivity (Figure 2.11). However, with the open-porous PNIPAAm gel (HG03), as the SEM images in Figure 2.12 shows, the as-prepared HG03 gel and the gel freeze-thawed 5 times in a -20^oC freezer do not show a significant difference in their pore structures.

2.10 Comparing Photopolymerization Swelling Performance to Thermopolymerization

The photopolymerized PNIPAAm sample is fabricated by dissolving $400 \ mg \ mL^{-1}$ NIPAAm and $20 \ mg \ mL^{-1}$ BIS into $2 \ mL$ of DMSO-water mixed solvent (0.27 vol frac-
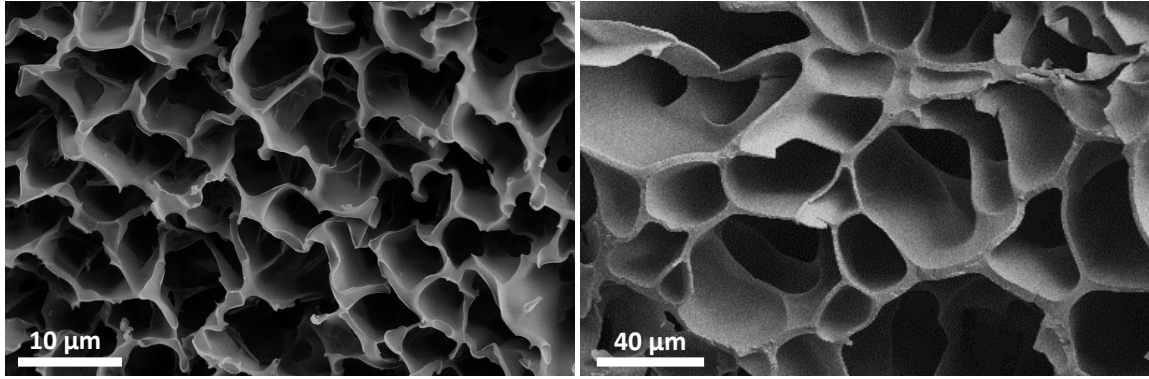
Figure 2.11 SEM images of as-prepared HG00 (left) and HG00 after a single freeze-thaw cycle (right). scale bars inside the figures are different.
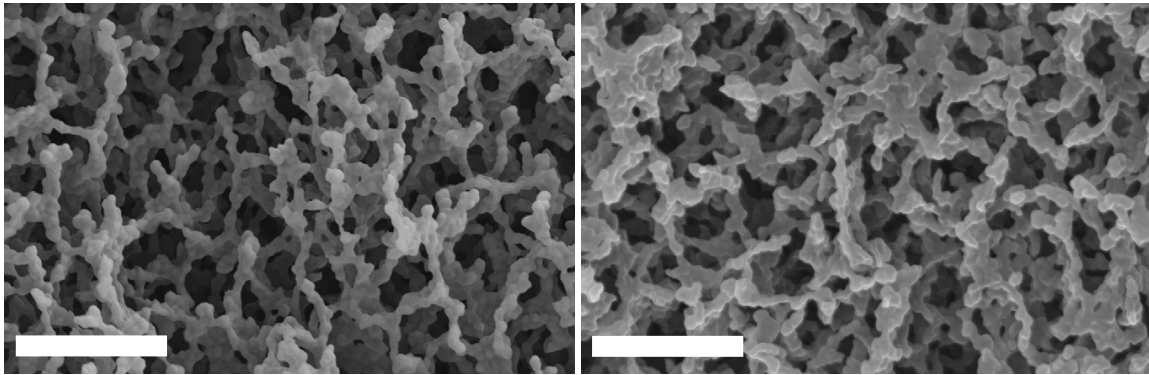
Figure 2.12 SEM images of as-prepared HG03 (left) and HG03 hydrogels after five freeze-thaw cycles (right). scale bars: 5μm.

tion DMSO). 5μL mL^{-1} of Darocur 1173 is added as the photoinitiator and vortexed thoroughly. The prepolymer solution is pipetted into a PDMS mold with dimensions $1\,cm \times 1\,cm \times 1.5\,mm$ and illuminated with UV light for 15s to induce gelation. The photopolymerized PNIPAAm hydrogel is removed from the mold and allowed to soak in DI water for 24 hours to remove unreacted precursors and DMSO. The thermopolymerized PNIPAAm sample is fabricated by dissolving $400\,mg\,mL^{-1}$ NIPAAm and $20\,mg\,mL^{-1}$ BIS into $2mL$ of DMSO-water mixed solvent (0.27 vol fraction DMSO). $20\,mg\,mL^{-1}$ ammonium persulfate thermoinitiator is added, followed by vortexing until fully dissolved. This precursor is then chilled in a $-5^{o}C$ fridge for 15 min, prior to adding $20\,\mu$L mL^{-1}

25

TEMED. After briefly inverting the precursor container several times to facilitate TEMED mixing, the precursor is pipetted into a PDMS mold with dimensions $1\,cm \times 1\,cm \times 1.5\,mm$ and allowed to react for 15 hours. The thermopolymerized PNIPAAm hydrogel is removed from the mold and allowed to soak in DI water for 24 hours to remove unreacted precursors and DMSO. To confirm that thermopolymerized PNIPAAm synthesized under these reaction conditions serves as an adequate control for the photopolymerized PNIPAAm, the reaction conversion is measured. The conversion quantifies how much of the dissolved precursor is consumed in the polymerization reaction, and is defined as follows, where W_{dry} is the weight of the dry hydrogel, C_{solute} is the total concentration of dissolved monomer and crosslinker, and V_{mold} is the volume of the hydrogel mold:

$$Conversion = \frac{W_{dry}}{(C_{solute}V_{mold})} \times 100 \qquad (2.7)$$

Additionally, water content is measured to further validate that the thermopolymerized PNIPAAm synthesized under the above conditions serves as a comparable control.

$$Water\ Content = \frac{(W_{wet} - W_{dry})}{W_{wet}} \times 100 \qquad (2.8)$$

The matching conversion and water content for the photopolymerized and thermopolymerized PNIPAAm hydrogels indicate that the two can be compared directly.

2.11   Effect of Environmental Conditions on SVA Performance

We have studied the effect of environment temperature on SVA performance by measuring the SVA force as the temperature of the water bath is varied. Figure 2.13 shows the SVA force as it is turned on for $60\,s$ and off for $60\,s$ for a total of 10 cycles.

2.12   Cyclic Tests

We have characterized the long-term performance of the SVAs as they go through multiple cycles of expansion/contraction. The SVAs used for this test have not been gone

26
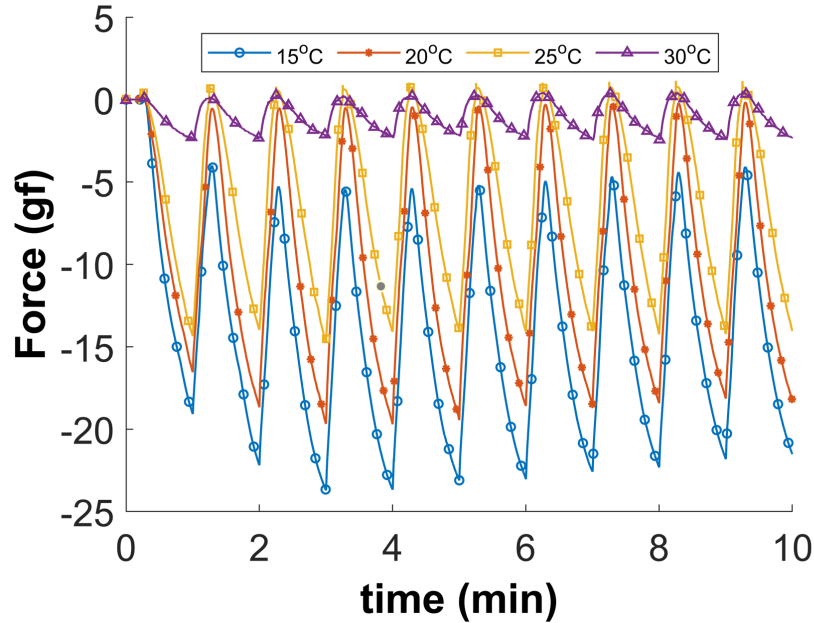
Figure 2.13 Effect of the temperature of the water bath on the force production capacity of the SVAs.

through any heating and cooling cycles prior to this test. Figure 2.14 shows the displacement over 1000 cycles. The temperature change dynamics is also measured by placing a thermocouple inside the SVA. As can be seen, the amplitude of the force is almost the same throughout the time. There is a very small drift which can be related to the settling of the force sensor setup over time. To further evaluate this, the SVA force in the first cycle is plotted against the last cycle. There is a slight improvement in the amplitude of the force and the SVA response seems to be slightly faster. We think this is due to the removal of residual DMSO, monomer and non-crosslinked polymer molecules from the gel when it is initially actuated. Overall, the SVAs does not show significant change in their performance over cyclic loads.
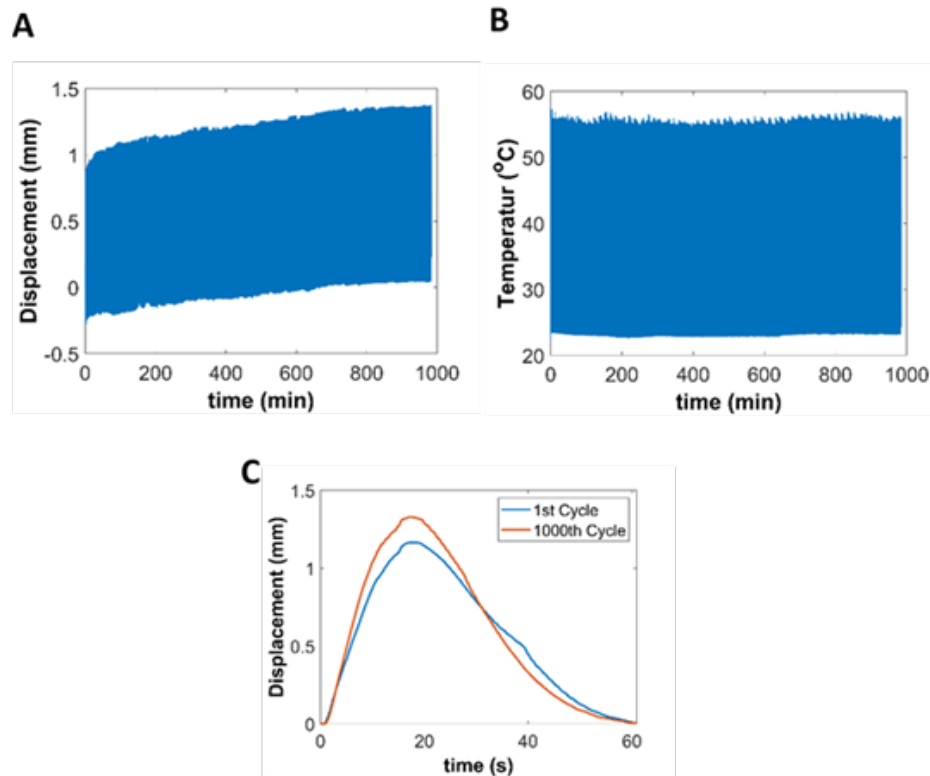
Figure 2.14 Cyclic actuation of SVAs A) Displacement of SVA over 1000 activation cycles. B) The temperature inside the SVA is also plotted. C) the displacement during first cycle and last cycle plotted for comparison.

2.13 Dependency of the Performance of SVAs on Their Size

The volume change of hydrogel depends on temperature and the larger the size of the SVAs are, more time is needed for them to heat up via Joule heating to reach their minimum shrunken volume. To quantify this, we have tested 3 SVAs with different sizes and measured the displacement produced as the heater is turned on for $60\ s$ and off for $60\ s$ for a total of 10 cycles. As can be seen in Figure 2.15, the larger SVAs produced higher deformation, however they need more time to reach that deformation. Ideally, the smaller SVAs perform faster, however, as the number of SVAs increase there is problems in integration and addressing them.

28
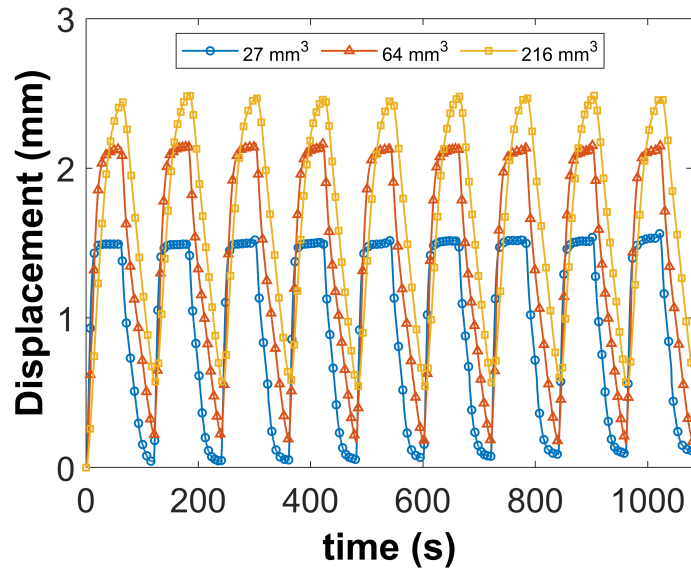
Figure 2.15 The effect of SVA size on the displacement produced as the heater is activated for 10 cycles.

2.14   Kinetics of Temperature Change

In order to quantify the temperature of an SVA, a thermocouple is placed inside a SVA made of H03, close to the Joule heater as shown in Figure 2.16. The temperature and displacement profiles as the heater is turned on for 15 s and then turned and kept off for 45 s are plotted for comparison. During heating, the displacement profile has a high slope because the temperature profile increases rapidly. This is because the energy is input to the system actively. During cooling, the temperature profile and as a result, the displacement profile have lower slope because energy is dissipated through convection and passive cooling.
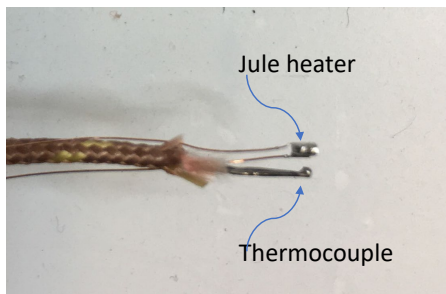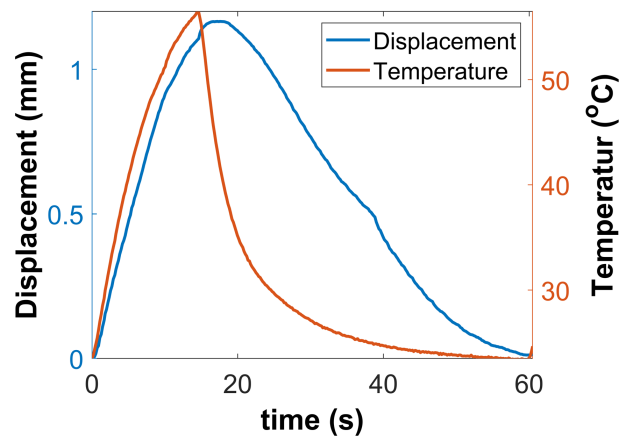
Figure 2.16 Temperature kinetics in SVA actuation A) a thermocouple is placed inside a SVA to measure the kinetics of the temperature change. B) temperature and displacement profiles

Chapter 3

HETEROGENEOUS HYDROGEL STRUCTURES AS MINIATURE

HYPER-REDUNDANT SOFT MANIPULATORS

Stimuli-responsive hydrogels can sense environmental cues and change their volume ac-
cordingly without additional sensors or actuators. This enables a significant reduction in
the size and complexity of devices manufactured with hydrogels. However, their robotic
applications requiring localized and time-varying deformations have been challenging to
realize since the responsive volume change of these materials is typically uniform. Here,
using addressable and tunable hydrogel building blocks – presented in chapter 2 – heteroge-
neous hydrogel structures with programmable, spatiotemporal deformations is presented.
As discussed in chapter 2 SVAs are produced using a mixed-solvent photopolymerization
method, utilizing a fast reaction speed and the cononsolvency property of PNIPAAm to pro-
duce highly interconnected hydrogel pore structures, resulting in tunable swelling ratios,
swelling rates, and Young's moduli in a simple, one-step casting process that is compat-
ible with mass production techniques. By designing the location and swelling properties
of each voxel, and by activating embedded Joule heaters in the voxels, spatiotemporal de-
formations are achieved, enabling heterogeneous hydrogel structures to manipulate objects,
avoid obstacles, generate traveling waves and morph to different shapes. Together, these in-
novations pave the way towards tunable, untethered, and high degree-of-freedom hydrogel
robots that can adapt and respond to changing conditions in unstructured environments.

3.1   Background

Smart hydrogels have attracted great interest in many different fields, such as drug
delivery [53, 58], microfluidics [59, 60], and soft robotics [38], owing to their large and

reversible volume changes in response to a broad range of stimuli without using any additional sensors and actuators. This feature helps reduce the size of devices made of smart hydrogels. Practical soft robotic applications, ranging from basic bending and shortening primitives to complex reconfigurations, all require time-varying and local deformations of bulk hydrogels in order to approach the dexterity of soft organisms in performing tasks such as grasping and manipulation [37, 44]. However, the responsive volume change of smart hydrogels is typically uniform. Two main approaches have been adopted by researchers to achieve nonuniform spatiotemporal deformation in hydrogels [37]. In the first approach, heterogeneous structures in the shape of sheets and rods are fabricated by patterning material domains using manufacturing techniques such as micro- and meso-patterning [61, 62, 63, 64, 65, 66] and 3D printing [67]. Differing swelling properties of neighboring domains upon stimulation results in nonuniform strain fields in these structures, causing them to transform into a variety of complex shapes like coils and conical helices [68, 69]. The range of compatible materials available for each domain, however, is often limited by practical fabrication constraints, such as ink viscosity for 3D printing [67]. Moreover, the geometry and material selected for each domain determine the shape transformations; these features cannot be changed after manufacturing, making on-demand reconfiguration infeasible.

The second approach towards achieving nonuniform spatiotemporal deformations uses an inhomogeneous or time-varying stimulus, such as patterns of structured light [41], local irradiation by near-infrared light [51], or localized electric fields [70]. In these methods, the hydrogel material itself is typically homogeneous, but the stimulus intensity varies across different regions, causing localized and time-varying deformations. These techniques, while suitable for on-demand shape reconfiguration, often require bulky external equipment, ultimately leading to challenges in mobile robot applications.

32

Nature has adopted a hierarchical approach in addressing these challenges by using motor units as building blocks for heterogeneous muscle tissue demonstrating complex spatiotemporally reprogrammable deformations [71, 72]. A motor unit consists of a motor neuron and the muscle fibers innervated by its axonal terminals [73]. It behaves as a stimuli-responsive building block, producing unidirectional deformation in response to electrical stimulus from the central nervous system (CNS). The variations in orientation [74] and response rate [75] of muscle fibers create the structural heterogeneity [76] required for nonuniform hard-coded deformations; the on-demand control over location and intensity of the electrical stimulus provides the spatiotemporal reprogrammability [77, 78, 79].

Virtual voxels have been used for decades as building blocks to represent shapes in 3-D space for computer graphics applications [80]. More recently, voxel-based simulations have been used to predict bulk material properties of structures – including structures made of smart hydrogels – by controlling the material properties of individual virtual voxels [81, 82, 83]. Virtual voxels have also been utilized to simulate heterogeneous structures with robotic functions [84]. However, physical realization of voxels as building blocks have been limited to passive and often rigid materials, and are used in conjunction with additive manufacturing processes to increase their throughput [85]. One recent work has used voxel-based computer simulations to optimize the distribution of active and passive materials in a structure for achieving different goals and the resulting mechanisms are physically realized using cardiomyocytes from a frog as building blocks for creating responsive structures[86].

Inspired by nature's approach for achieving on-demand spatiotemporal deformations in muscle tissue, we introduce addressable and tunable building blocks that can be assembled to create heterogeneous hydrogel structures with *hard-coded* or *reprogrammable*

shape change. These building blocks, herein referred to as soft voxel actuators (SVAs), are shown in **Figure** 3.1, left. The SVA units, consisting of a responsive hydrogel material and corresponding electrical connections, are inspired by the motor units of muscle tissue (Figure 3.1, right). The deformation of SVA units as a result of an electrical stimulus from a microcontroller unit (MCU) is analogous to the contraction of muscle fiber units in response to stimuli from the central nervous system (CNS). The selection of electrical stimuli as opposed to other types of stimuli is advantageous, since it enables addressing SVAs directly by small-footprint microcontrollers without the need for bulky equipment or human intervention. [87].
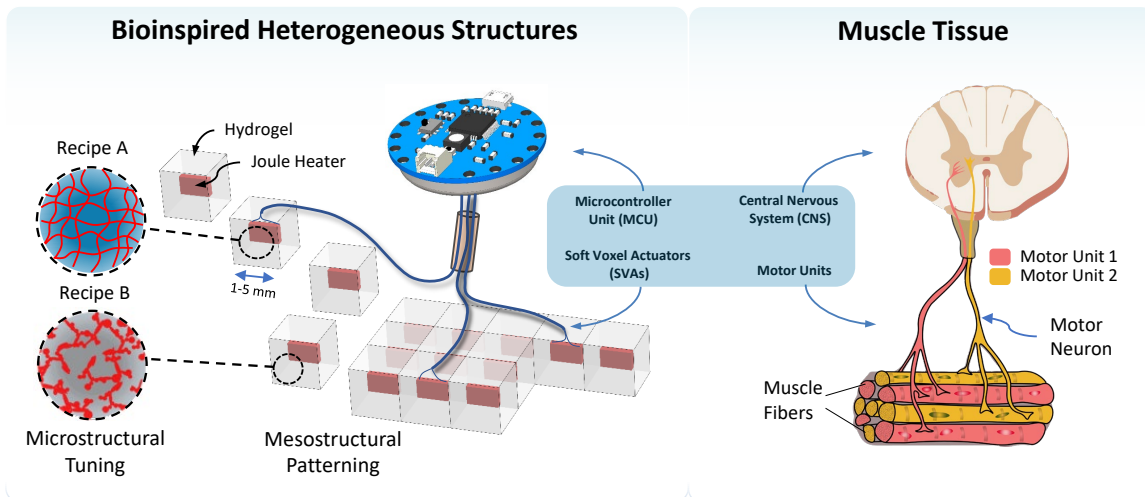
Figure 3.1 Illustration of bioinspired heterogeneous hydrogel structures composed of tunable and addressable voxels. **(Left)** Soft Voxel Actuators (SVAs) are electrically addressable building blocks whose deformations can be controlled by a microcontroller unit (MCU). SVAs are analogous to motor units, consisting of a motor neuron and associated muscle fibers, which deform in response to electrical impulses from the CNS **(Right)**. The microstructure of the hydrogels used to make SVAs can be altered, resulting in tunable material properties.

3.2   Concept

Two types of SVAs have been realized and are described herein: one without an embedded heater (referred to as SVA-I), and one with an embedded heater (referred to as SVA-II), as shown in Figure 3.2. Various combinations of SVA-I and SVA-II can be used for designing and fabricating heterogeneous assemblies. One possible combination, shown in Figure 3.2-(i), uses SVA-I to create pre-programmed voxel assemblies. Based on the specific arrangement of SVA-I consisting of different swelling properties (mainly volume change ratio and rate), complex deformations can be demonstrated. These SVA assemblies deform in response to regular and repeated homogeneous temperature changes (such as the bulk heating and cooling of a water reservoir), generating motions without the need for an on-board energy source. It should be noted that hydrogels expand and contract based on the diffusion of water into and out of their structure when the temperature is passed their critical transition temperature which is around 32° C in case of PNIPAAm hydrogels. Therefore, all our experiments are performed in a water bath. Another combination of SVAs shown in Figure 3.2-(ii), uses thick film surface mount (SMD) resistive elements with a resistance of 10 ohms as Joule heaters in SVA-II units to create time-varying and inhomogeneous temperature fields, resulting in on-demand dynamic deformations and real-time reconfigurability. Details of the Joule heater elements are presented in the 2.

3.3   Hydrogel Synthesis

The ability to select from a broad range of material properties for SVA fabrication can expand the design space of resulting heterogeneous structures. Therefore, a synthesis method that can tune the ratio and rate of hydrogel volume change is required. A variety of physical and chemical methods have been explored to alter the swelling properties
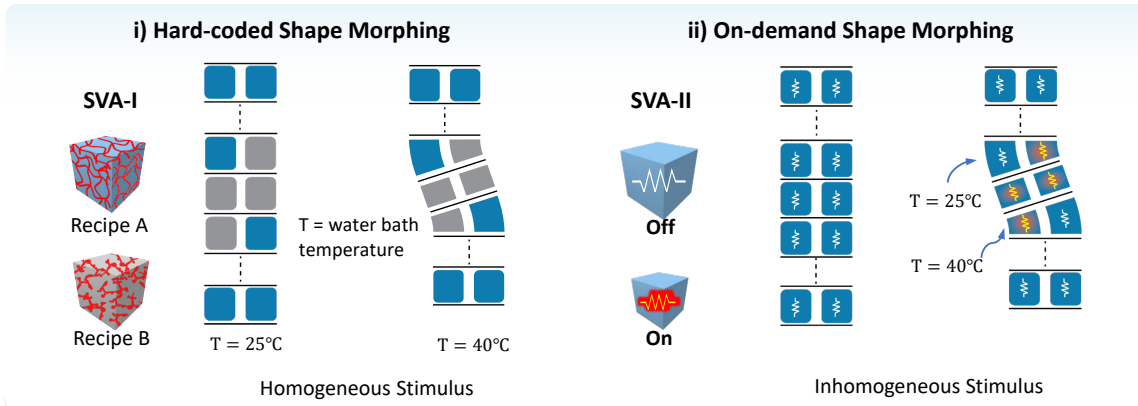
Figure 3.2 Bioinspired heterogeneous hydrogel structures composed of tunable and addressable voxels. **i)** SVAs without embedded Joule heaters (SVA-I) are used to create structures with hard-coded shape morphing that respond to a homogeneous temperature field acting globally on the entire structure through the surrounding water bath. **ii)** SVAs with embedded heaters (SVA-II) are used to create structures with on-demand shape morphing by forming an inhomogeneous temperature field throughout the structure.

of hydrogels [88, 89]. These methods are limited by factors such as the narrow range of achievable swelling properties [90, 91], large trade-offs in mechanical properties [92, 93], long processing times [61, 94], and a need for careful control of synthesis conditions such as temperature [95] and precursor additives [96].

We take advantage of PNIPAAm's cononsolvency, a property of reduced solvation in a mixture of two solvents due to a delicate balance between polymer-solvent and solvent-solvent interactions [97]. Employing a water and dimethyl sulfoxide (DMSO) mixed solvent in the PNIPAAm hydrogel precursor solution, followed by rapid photopolymerization to induce interconnected open pores, significantly enhanced the rate of water transport into and out of the hydrogel matrix and thus the actuation speed. The microstructure of the gel is altered by changing the water volume fraction (φ_w) in the mixed water/DMSO solvent. The SVA swelling rate and displacement, which are directly related to its hydrogel

microstructure, are therefore tuned by merely adjusting φ_w. Polymerization solvent composition is known to affect the swelling properties of the synthesized PNIPAAm hydrogels [98, 99, 100, 101, 102]. The combination of the mixed solvent method with a fast 15 s photopolymerization step is critical for inducing and fixing local aggregations of polymer chains in place, resulting in PNIPAAm hydrogels with open pore structures (**Figure 3.3**-A(i)). Such open pore structures exhibit significantly enhanced rates of thermoresponsive volume change in both heating and cooling phases, compared to conventional hours-long mixed solvent thermopolymerization methods (control experiment), in which the precursors are constantly diffusing towards a homogeneous molecular equilibrium throughout the duration of the reaction, leading to a less interconnected pore structure with thicker pore walls (Figure 3.3-A(ii)). For details see [103]. In order to ensure a valid comparison, the recipe for a representative thermopolymerized control hydrogel was carefully tuned using the initiator concentration while leaving all other components of the precursor solution unchanged, choosing a reaction time such that the conversion and water content match those of the photopolymerized hydrogel (2.10). It is readily observed that with equivalent water content, reaction conversion, and reaction solvent composition, the thermopolymerized hydrogel deswells as fast as the photopolymerized hydrogel (Figure 3.3-B(i)) and the two reach nearly identical shrunken volumes. However the reswelling speed of the thermopolymerized control sample is ∼25 times slower than the photopolymerized sample, which can be attributed to the lower observable tortuosity present in the photopolymerized sample Figure 3.3-B(ii). The Young's Modulus of the thermopolymerized hydrogel is ∼10 times higher than that of the photopolymerized one.

The effect of varying φ_w on the hydrogel microstructure has been investigated by scanning electron microscopy (SEM), as shown in **Figure** 3.4. Six hydrogels consisting of various φ_w were synthesized; they are each represented by a character code ranging from
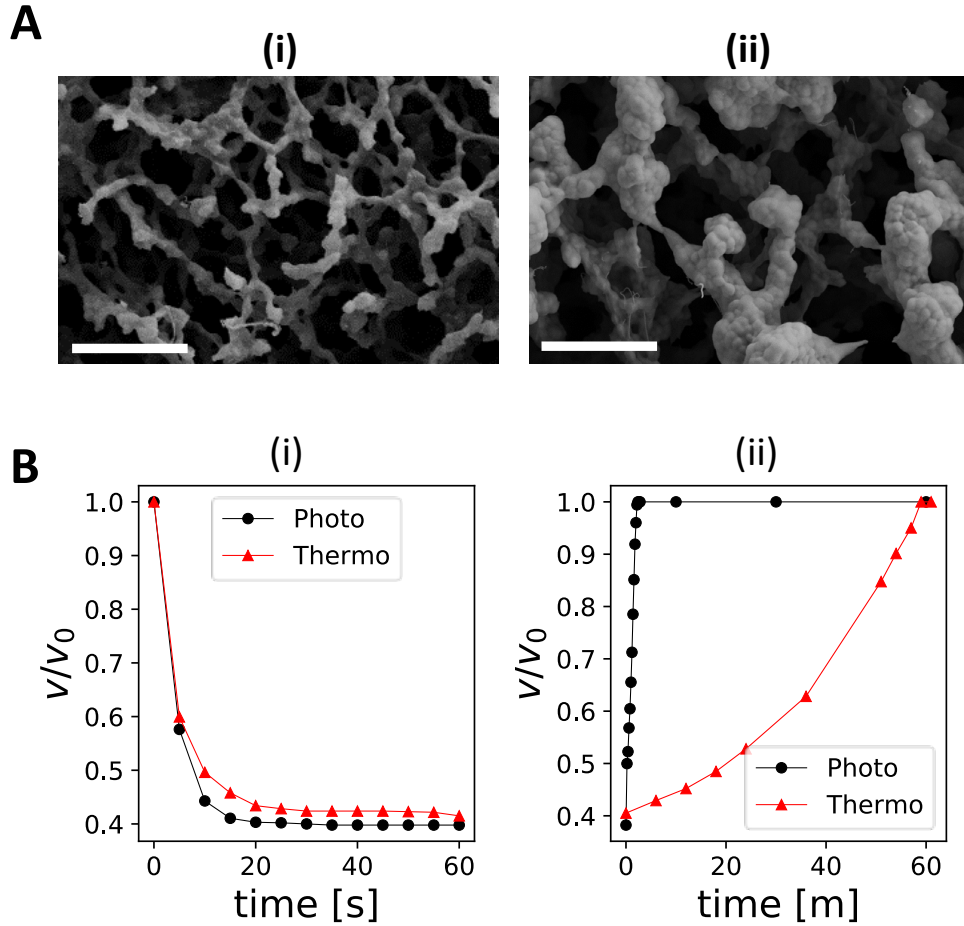
Figure 3.3 Comparison of photopolymerization and thermopolymerization methods on gel microstructure and performance. **A)** SEM micrographs of photopolymerized (i) and thermopolymerized (ii) hydrogels synthesized in water volume fraction $\varphi_w = 0.27$ (scale bar = $5\,\mu m$). **B)** Deswelling (i) and swelling (ii) rates of photopolymerized and thermopolymerized hydrogels synthesized in water volume fraction $\varphi_w = 0.27$.

HG00 (representing a hydrogel with $\varphi_w = 0.0$) to HG05 (representing a hydrogel with $\varphi_w = 0.5$). Details of the SEM imaging procedure are described in 2. Distinct changes in the microstructure can be observed as a function of φ_w, which impacts a variety of other material properties. When φ_w is increased from 0.0 to 0.2, pore size decreases and the pore wall surface begins to change from smooth to rough. We define $\varphi_w = 0.2$ as a critical water volume fraction, at which the microstructure of the gel starts to change from a closed-pore

to an open-pore structure. SEM images for other values of φ_w are presented in Figure 2.9.
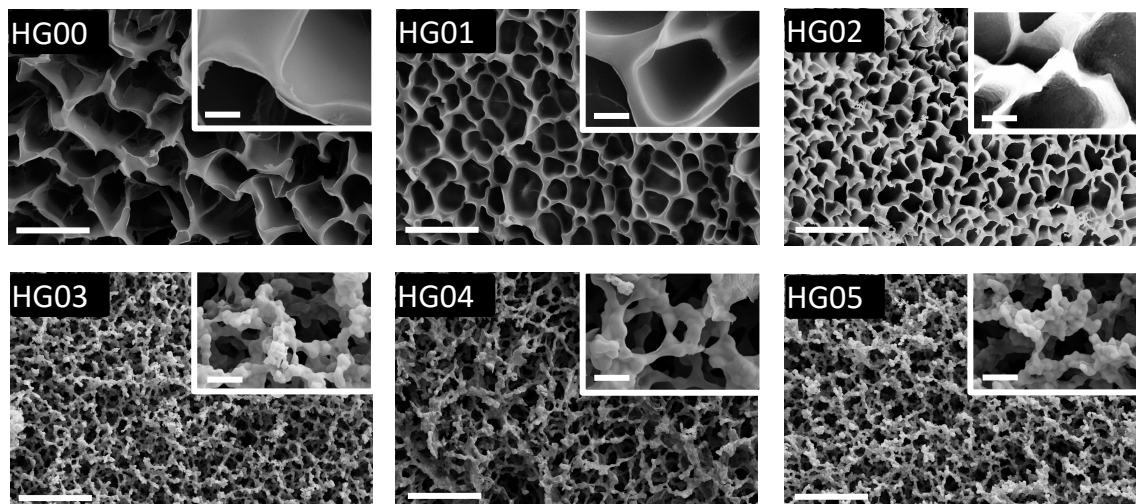
Figure 3.4 Tunable material properties using mixed solvent photopolymerization. SEM images showing the effect of φ_w on pore structure of the photopolymerized PNIPAAm hydrogel (scale bars $10\,\mu m$ and $1\,\mu m$ for low and high magnification, respectively).

The changes in hydrogel microstructure play a role in the dynamic response of SVAs. The linear displacement generated by a SVA unit is measured using a vision-based test setup as described in Figure 2.6. **Figure 3.5**-A plots the time evolution of the displacement (D) of SVA units with different values of φ_w as each SVA's embedded heater is turned on for $60\,s$ and then turned off for $60\,s$. The displacement over time of the hydrogel made with $\varphi_w = 0.0$ is included as the basis for comparison across all tests. The negative displacement observed is because the SVAs initially expand instead of contract as the heater is turned on which might be due to water slightly expanding and vaporizing. Two performance criteria for the SVA units, deformation rate (DR) and maximum displacement (MD), are extracted from the data in Figure 3.5-A and are shown in Figure 3.5-B,C respectively. During both heating and cooling, DR is small for $\varphi_w < 0.2$. At $\varphi_w = 0.2$, the DR during heating is more than 36 times the DR during cooling. As a result, fast and large deformations are observed during the $60\,s$ of heating, and almost no deformation is observed during the $60\,s$

of cooling. Highest DR (in both heating and cooling) occurs in gels with $\varphi_w = 0.3$, while MD peaks at $\varphi_w = 0.2$ and decrease thereafter. In addition to swelling properties, other mechanical properties such as Young's modulus and force produced by the SVAs can also be tuned by adjusting φ_w 2.
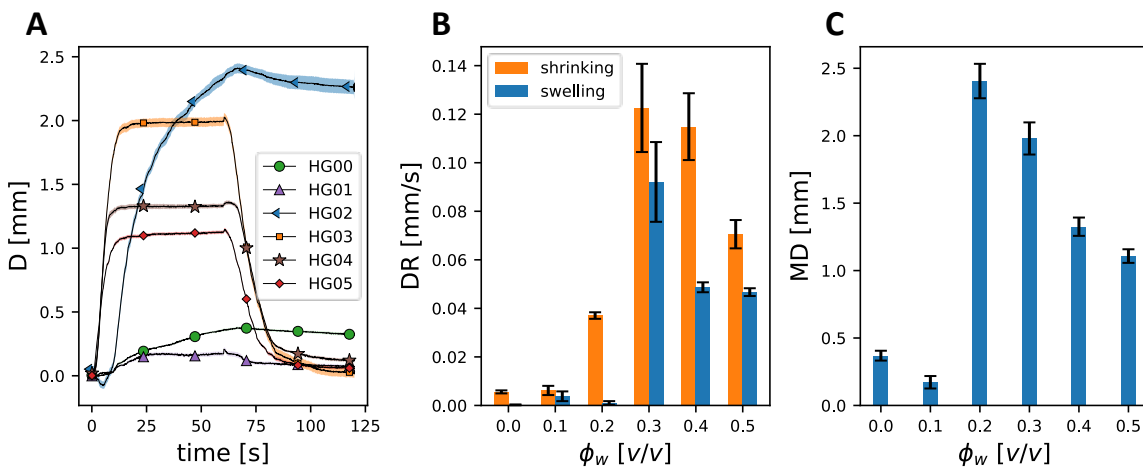
Figure 3.5 Tunable material properties using mixed solvent photopolymerization. **A)** Displacement (D) over time generated by SVA-II units with different values of φ_w under a $1\,gf$ load, as measured by the setup described in 2.3. **C,D)** Displacement rate (DR) and maximum displacement (MD) of SVA-II units as a function of φ_w.

3.4   Hard-coded Shape Morphing

A variety of heterogeneous structures can be produced that transform into different configurations, depending on their hard-coded material domains. As a first example, a beam with only two material domains is fabricated from HG00 and HG02 hydrogels (**Figure 3.6**-(i)). At $20\,^{\circ}$C, the beam is in its equilibrium position. As the temperature increases to $45\,^{\circ}$C, the HG02 hydrogel shrinks more than HG00 (from Figure 3.5-B,C, both MD and DR are higher for HG02), which results in a stress mismatch. To balance these stresses, the beam bends into a circular shape as seen in Figure 3.6-(ii) ,(iii). We will henceforth refer to this

structure as a 'gripper'.

Figure 3.6 Realization of structural inhomogeneity through patterning of hydrogels with different swelling properties. **i)** A two-material, two-region structure made of HG00 and HG03 regions **ii,iii)** The bilayer structure can almost bend into a circle when the surrounding water bath temperature is raised above or below the transition temperature of PNIPAAm hydrogel (32 °C)

A second example uses HG00 and HG02 hydrogels again, but this time with 8 material domains, as shown in **Figure 3.7**-(i-iii). The beams in these figures consist of different arrangements of HG00 and HG02 voxels, and as a result exhibit different deformations when subjected to a homogeneous temperature change in the surrounding water from 20 °C to 45 °C.

Patterning material domains can be used to leverage the shape transformations into unique functions tied to structural heterogeneity. To demonstrate this *structure–function* relationship, two different structures, Str-I and Str-II, are made with different combinations of HG00, HG02, and HG03, as shown in **Figure** 3.8. These structures represent a
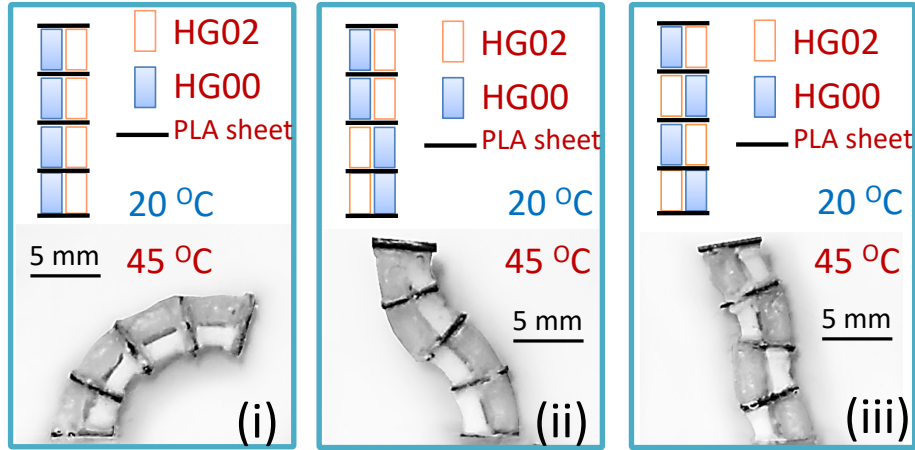
Figure 3.7 Realization of structural inhomogeneity through patterning of hydrogels with different swelling properties. **i-iii)** Increasing the number of material domains in the structure enables it to achieve more diverse shapes. When the surrounding water bath temperature is increased, each structure reconfigures into a different shape, depending on its arrangement of SVA-I units.

combination of the structures in Figure 3.6 and Figure 3.7. In response to a global cyclic temperature change from 20 °C to 45 °C and back to 20 °C, these structures are observed to bend towards an object, grasp it (by wrapping around it), and transport it to another location.

The geometric configuration of material domains in both structures are the same. However, the 'gripper' portion of Str-I is a combination of HG00/HG03 domains, whereas in Str-II it is a combination of HG00/HG02 domains. As a result of this minor material difference, the object grasped by Str-I and Str-II moves along different trajectories, as seen in **Figure** 3.9A, despite an identical set of initial conditions. Due to the high DR of HG03 during the cooling phase (Figure 3.5-B), the gripper in Str-I opens and the object is released in the early stages of the cooling phase. The gripper in Str-II, on the other hand, does not open at the same time as Str-I and continues to hold the object throughout its cooling phase; this can be attributed to the lower DR of the HG02 layer compared to HG03. To illustrate these differences, the x and y coordinates of the object over time are plotted in Figure
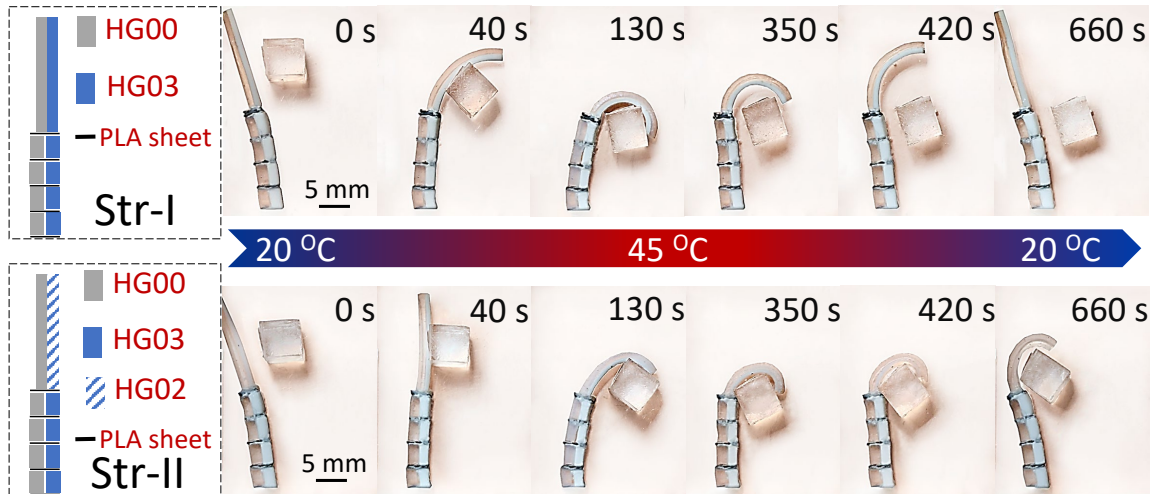
Figure 3.8 Realization of structural inhomogeneity through patterning of hydrogels with different swelling properties. Hybrid structures comprised of substructures with the SVA arrangements in Figure 3.6 and Figure 3.7 are capable of manipulating objects. The material distribution in two example structures, denoted by Str-I and Str-II, is shown in the schematic on the far left. The snapshots display the configurations of the two structures over time as the global water bath temperature is increased and then decreased.

3.9-B, and the time when the object is released by each structure is indicated. Achieving inhomogeneous deformations in response to a homogeneous global stimulus using structures with hard-coded deformations as described simplifies the system and eliminates the need for on-board power sources.

3.5 On-demand Shape Morphing

For applications in dynamic, unstructured environments, such as underwater robotic exploration, it is less useful to pre-program complex trajectories into a structure, since global stimulus control is not always feasible. To enable on-demand thermoresponsive shape morphing in these conditions, SVA-II units may be employed, as depicted in Figure
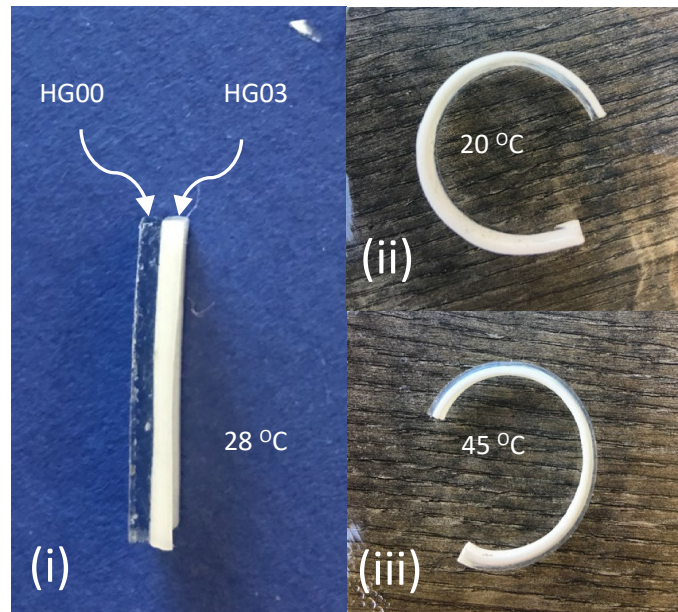
43
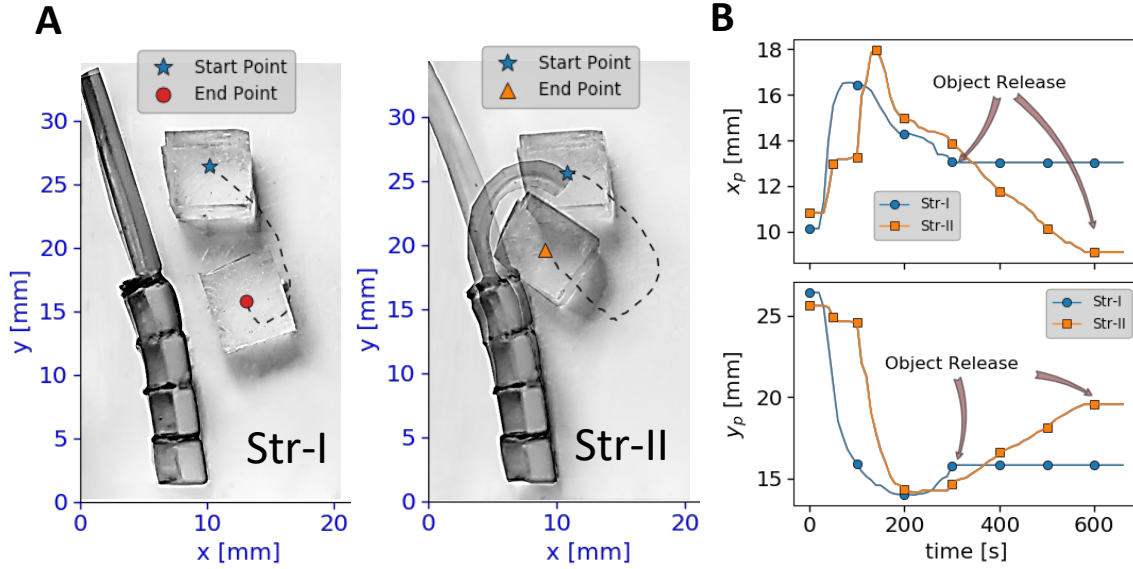
Figure 3.9 Realization of structural inhomogeneity through patterning of hydrogels with different swelling properties. **A)** Image showing the start position, end position, and trajectory of the object manipulated by Str-I (left) and Str-II (right). **B)** Time evolution of the x and y coordinates of the manipulated object's center of mass. Str-I releases the object a $t = 300$ s, while Str-II releases it at $t = 600$ s, demonstrating the versatility of the voxel-based assembly approach to creating heterogeneous structures with diverse functions.

3.2-(ii). The $40 \times 11 \times 5mm$ structure shown in **Figure 3.10**-A was assembled using 16 SVA-II units. These SVAs are made of HG03, which exhibits the highest DR observed across all recipes (Figure 3.5-B). The first example of on-demand shape morphing is illustrated in Figure 3.10-B(i), in which the structure morphs into an 'S' shape and a 'reverse S' shape when particular SVAs are actuated via commands from a microcontroller. A second example of on-demand shape morphing is illustrated in Figure 3.10-B(ii); it highlights how the curvature of a structure may be varied as a function of the voltage supplied to the SVA-II units.

Moving from static to dynamic on-demand shape changes requires time-varying acti-

44
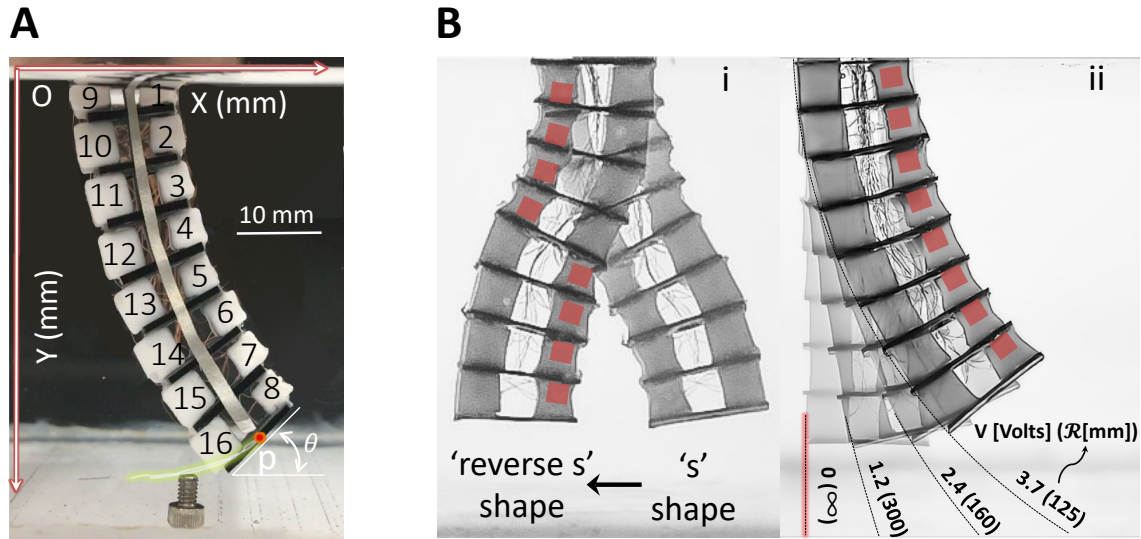
Figure 3.10 A miniature heterogeneous structure consisting of 16 addressable SVA-II units. **A)** SVA numbering scheme and the coordinate system used to measure the position of the point p and the angle θ of the end plate. **B)** On-demand shape morphing of the structure. i) The structure morphs from an 'S' shape to a 'reverse S' shape when particular SVAs are activated. ii) The structure's radius of curvature ($\mathcal{R}$) depends on the activation voltage (V) applied to SVAs 1-8.

vation of SVAs. As demonstrated in **Figure** 3.11, the choice of SVA actuation pattern can influence the end-effector trajectory of a structure. In this experiment, SVAs 1 thorough 8 are activated according to patterns denoted by P1 and P2. Each SVA is activated with maximum voltage (3.7 V) for 15 s before the next SVA is activated.

While complex motion of SVA-II-based structures may be achieved using simple on (3.7 V) and off (0 V) activation signals, as discussed, intermediate voltages may also be applied to further enhance the complexity of shape change in soft heterogeneous structures. To demonstrate this, phase-shifted sinusoidal voltages were used as activation signals to generate longitudinal traveling waves in the structure. A pair of SVAs (comprising a SVA on the left and its adjacent SVA on the right) are activated using the same sinusoidal signal; SVAs 4 and 12 were not activated, to serve as a geometric reference point. The sinusoidal voltages applied to every SVA pair were $\frac{\pi}{8} \ rad$ out of phase with the voltages applied to its

45
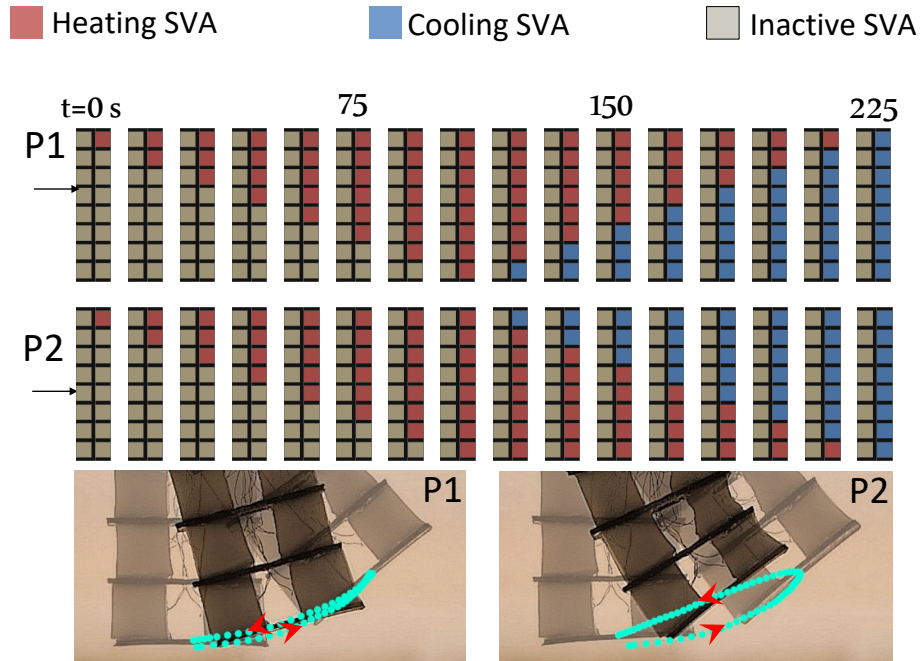
Figure 3.11 Dynamic shape changes are implemented by sequentially activating SVAs. In this case, SVAs 1 through 8 are activated according to the patterns labeled P1 and P2. The trajectory followed by the tip of the structure (shown at the bottom) can thus be adjusted on-demand.

nearest active SVA pair. As an example, sinusoidal signals for four SVA pairs are shown in **Figure** 3.12. A contraction wave was formed as a result of this input signal pattern and traveled along the length of the structure, as illustrated in **Figure** 3.13. Every point on the structure oscillates in a sinusoidal manner as the wave passes through it. The midpoint of the inactive SVA pair, which is highlighted by a yellow square in Figure 3.13, is shown as a reference point on the structure. Additionally, by sending the sinusoidal signals to SVAs located on only one side of the structure, for example SVAs 1 through 8, transverse traveling waves were generated in the structure.

The ability to control the trajectory of the structure's end-effector, as shown in Figure 3.11, is essential to successful functioning of the device in unstructured environments, in which working conditions may change during operation. As depicted in **Figure** 3.14,
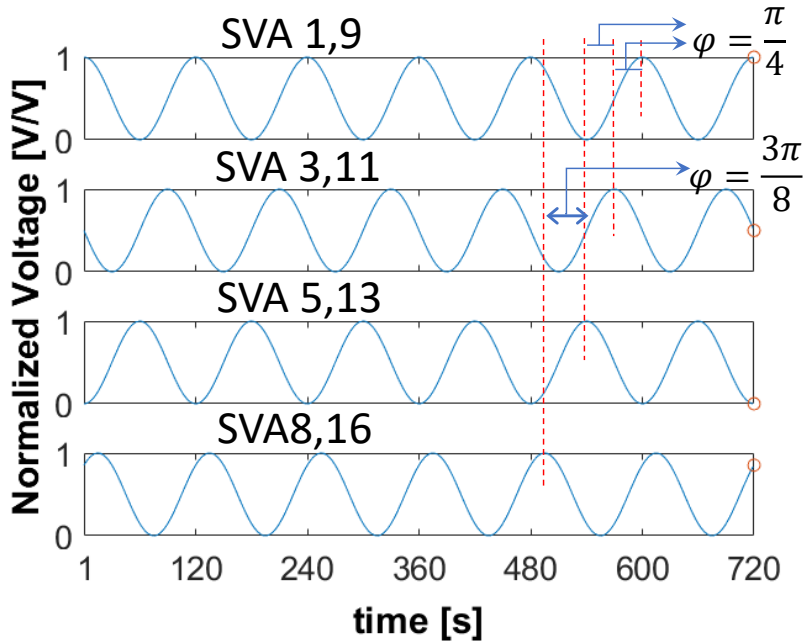
Figure 3.12 Normalized sinusoidal voltages used to create longitudinal traveling waves in the structure. The voltages applied to 8 of the 16 SVAs are shown here. The SVAs are activated in pairs, and the voltage applied to each SVA pair is $\frac{\pi}{8}\ rad$ out of phase with respect to the voltage applied to the next active pair.
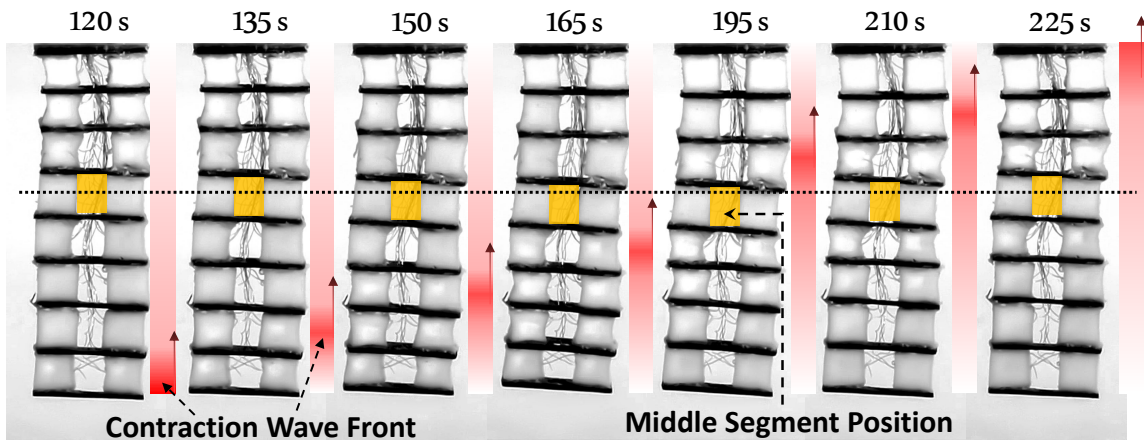
Figure 3.13 The longitudinal traveling waves generated as a result of activation voltages shown in Figure 3.12. One SVA pair, indicated by the yellow square, is kept inactive in order to serve as a reference point.

47
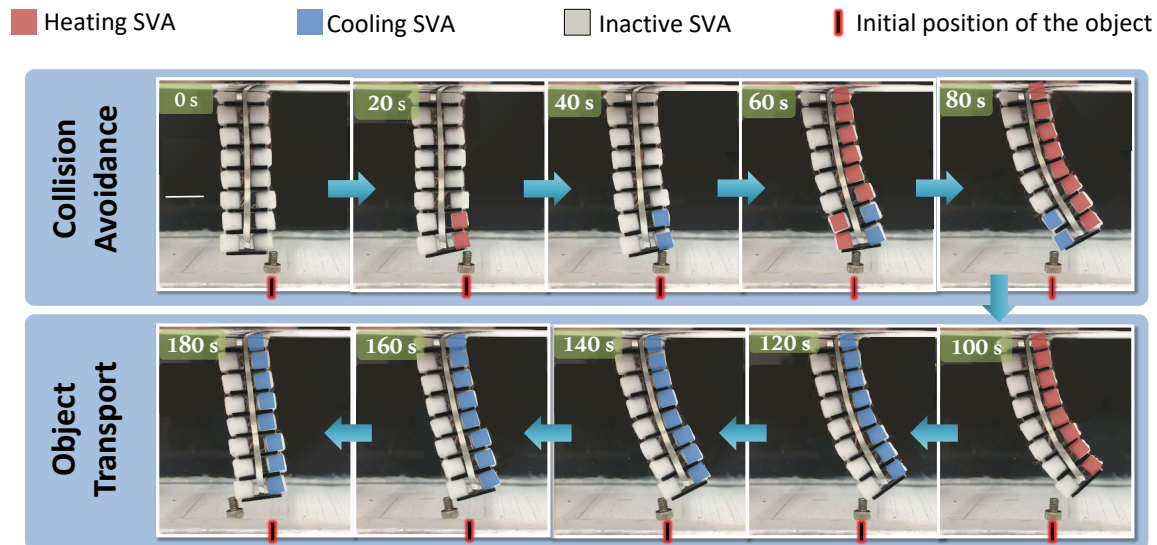
Figure 3.14 Example usage of hyper-redundancy in manipulator with on-demand control of deformation. The structure can avoid collisions with objects or transport them, depending on the sequence of voltage commands from the microcontroller unit.

time-sequenced switching of selected SVA-II units within the structure makes it possible to accomplish various robotic tasks such as collision avoidance (top row) and object transport (bottom row). The trajectory of the end point p and the angle θ of the end plate over time (p and θ are defined in Figure 3.10-A) during each of these two tasks is displayed in Figure 3.15. The on-demand control of reorientation and translation of the end-effector made it possible to complete these two tasks, indicating that highly redundant time-varying deformations in heterogeneous structures are achievable using individually addressable SVA-II units.

3.6 Conclusions

To summarize, we have developed the following tools to increase the variety and complexity of shape transformations in heterogeneous hydrogel structures: a voxel-based assembly design for patterning material domains, and a unique mixed-solvent photopolymer-
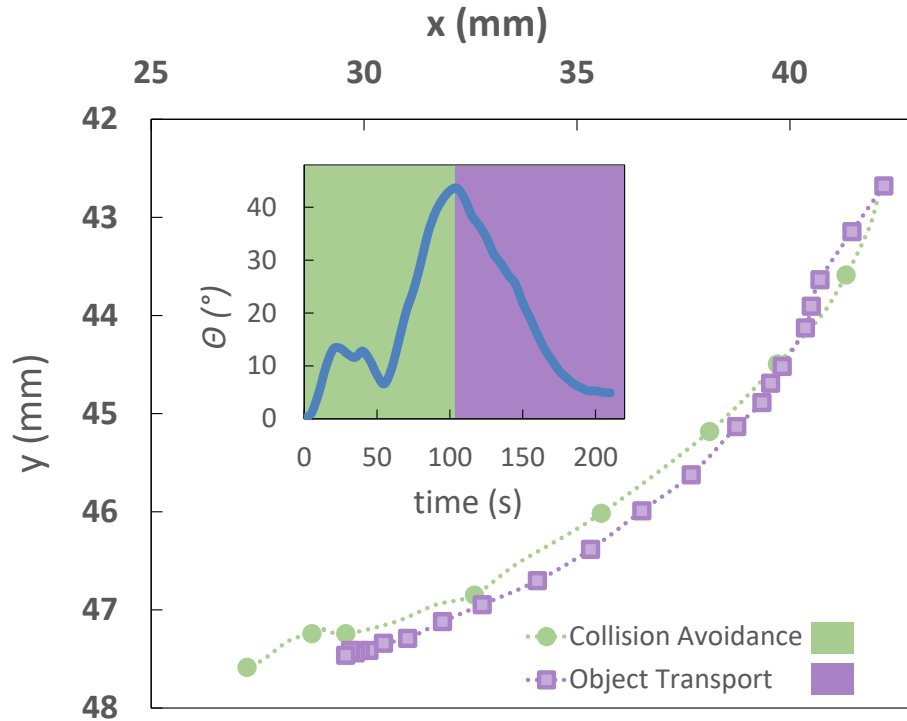
Figure 3.15 Trajectory of the point p on the tip of the structure as it first avoids and then transports the object. The inset shows the angle θ of the end plate as a function of time.

ization hydrogel synthesis method for tuning swelling properties of the voxels. These tools offer a higher number of design parameters, namely, the configuration of the voxels, the material properties of each voxel, and the activation voltage of each voxel (in the case of SVA-II). This rich set of design parameters can be specified to build structures that meet the requirements of a variety of tasks. The resulting heterogeneous structures can generate complex time-varying trajectories and traveling waves, enabling them to interact with unstructured environments in ways that could not be realized in bulk hydrogels or that would require sophisticated integration and manufacturing.

The simplicity of these tools advances the utility of hydrogel structures in robotics applications in a meaningful way because they can be used in robotics research laboratories that lack sophisticated material processing facilities.

While this dissertation focuses specifically on PNIPAAm hydrogel voxels, soft and rigid voxels made of other types of responsive or non-responsive materials can also be incorporated into heterogeneous assemblies. Closed-loop control of the deformation of the structures presented in this dissertation could be achieved by integrating strain- and force-sensitive voxels, made of similar functional hydrogels, that serve as sensors. In addition, multi-objective optimization across material properties and voxel configurations can be used to design structures with higher force production capacity and energy efficiency. Currently, integrating multiple active degrees of freedom (DOFs) in miniaturized soft robots is challenging due to space limitations. Each SVA can be considered as an active DOF and we have demonstrated that the integration of a high number of SVAs in a small footprint, such as the 16-voxel structure presented in this chapter, is possible. To address the challenges of fabricating large-scale assemblies consisting of hundreds of voxels, automated methods must be developed for scalable manufacturing and assembly of voxels.

Chapter 4

MINIATURE UNTETHERED UNDERWATER WALKING ROBOT

Current soft actuators rely on additional hardware such as pumps, high voltage supplies, light generation sources and magnetic field generators for their operation. These components resist miniaturization and embedding them into small-scale soft robots is challenging. This limits the mobile applications of systems that need to be entirely untethered, especially in hyper-redundant robots, where a high number of actuators are needed. Here, we introduce miniature and untethered robots made of the soft voxel actuators (SVAs) presented in Chapter 2. SVAs weighing only 100 mg require small-footprint microcontrollers for their operation, which can be embedded within the robotic system. We have demonstrated the advantages of SVA-based systems through a hyper-redundant gripper with 32 actuators and an untethered miniature robot for underwater mobile applications. Since SVAs are electrically activated, closed-loop control of the SVA-based soft robots is easily achieved with embedded microcontrollers.

4.1 Background

Inspired by biology, soft robot developers try to utilize the advantages inherent in soft, compliant matter to achieve safer interactions around humans or more robust locomotion and manipulation in unstructured environments [6, 7, 8, 104]. Soft pneumatic actuators (SPAs) [28, 29] are the most widely used category of soft robotic actuators. SPAs use passive materials like silicone and rely on rigid components such as motors and pumps that are difficult to downscale. Therefore, manufacturing small-scale soft actuators which have applications as envisioned by [39] has remained a bottleneck in the development of miniaturized soft robots [40].
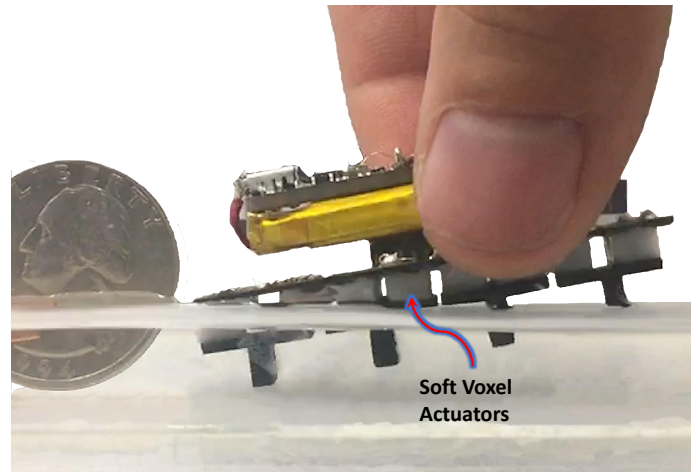
Figure 4.1 An untethered miniature underwater walking robot using 8 SVAs is made which weighs only 20 g including battery and electronics.

Stimuli-responsive soft materials have shown promise in solving some of these challenges [52, 53, 54]. The changes in the stress/strain distribution of these materials in response to variations in pH, temperature, electric field, magnetic field, and light results in motions such as bending, twisting, or elongation. However, the equipment needed to create variable stimuli such as structured light [41] or magnetic fields [42] are still bulky and must be carried externally to the mobile system. Temperature responsive hydrogels, by contrast, can be stimulated electrically using Joule heating [87]. Electrical stimulation can be confined to small regions, making it possible to create more precise motion [105]. We have previously reported solving some of the challenges associated with temperature responsive poly(N-isopropylacrylamide) (PNIPAAm) based hydrogels such as slow response and tunability of mechanical properties. We have also introduced blocks called soft voxel actuators (SVAs), which are electrically activated by Joule heaters [57]. Here, we demonstrate how SVAs support the development of soft robots which are miniature and untethered – two key characteristics that are challenging to realize with pneumatic soft actuators. We introduce a miniature and completely untethered robot for underwater applications; this robot, which weighs only 20 g including its battery and electronics, can be seen in Fig. 4.1.

We also demonstrate the use of SVAs to build a miniature gripper with hyper-redundant DOFs as shown in Fig. 4.2. This gripper uses two manipulators each with 16 actuators and dimensions of $10 \times 40 \times 4.5 \, mm^3$.

4.2 Assembling the Robots Using SVAs

A voxel actuator can be made in different shapes and dimensions based on design requirements. Manufacturing a SVA is performed via a molding process in which a hydrogel precurosor solution is poured into a mold, a Joule heater is inserted into the mold and the solution is then polymerized with a UV LED. Surface mount resistors (10 ohm SMD resistor 0805) were chosen as the heating elements. For the construction of the hyper-redundant gripper, the voxels are made as cubes of $4.5 \times 4.5 \times 4.5 \, mm^3$ as shown in Fig. 4.2. In the case of the untethered walking robot, voxels of $8 \times 4.5 \times 3 \, mm^3$ are used. Details of hydrogel synthesis, material characterization and SVA manufacturing are discussed in Chapter 2.

4.3 Results

Hydrogels expand and contract based on the diffusion of water into and out of their structure when the temperature is passed their critical transition temperature – which is around 32° C in case of PNIPAAm hydrogels. Therefore, all the experiments have been performed in a water bath. Fig. 3.2 shows a schematic of a SVA. When the embedded Joule heater is turned on, the temperature increases and the volume of the hydrogel decreases. When the heater turns off, the SVA cools down and its volume increases. We have shown that a SVA can produce a force of $0.12 \, N$, equivalent to nearly $12 \, g$ or 120 times its own weight [57]. To demonstrate how SVAs support the development of miniature and untethered soft robots, we describe two different robotic platforms in the following sections.

4.3.1 Case Study I: Miniature Hyper-redundant Soft Gripper

The structure shown in Fig. 4.2A was assembled using 32 SVA units. The SVAs are connected together using a 0.1 mm thick 3D printed PLA sheets. Dynamic on-demand shape changes are achieved through time-varying activation of SVAs. In this experiment, SVAs 1 thorough 8 on the right side of the left arm and on the left side of the right arm are activated leading to bending of the arms in opposite direction and closing of the gripper. Each SVA is activated with maximum voltage (3.7 V). The demonstrated miniaturized continuum gripper with 32 degrees of freedom in a $40 \times 11 \times 5 \, \text{mm}^3$ footprint represents the highest reported electrically-addressable number of DOFs in a soft manipulator of these dimensions.
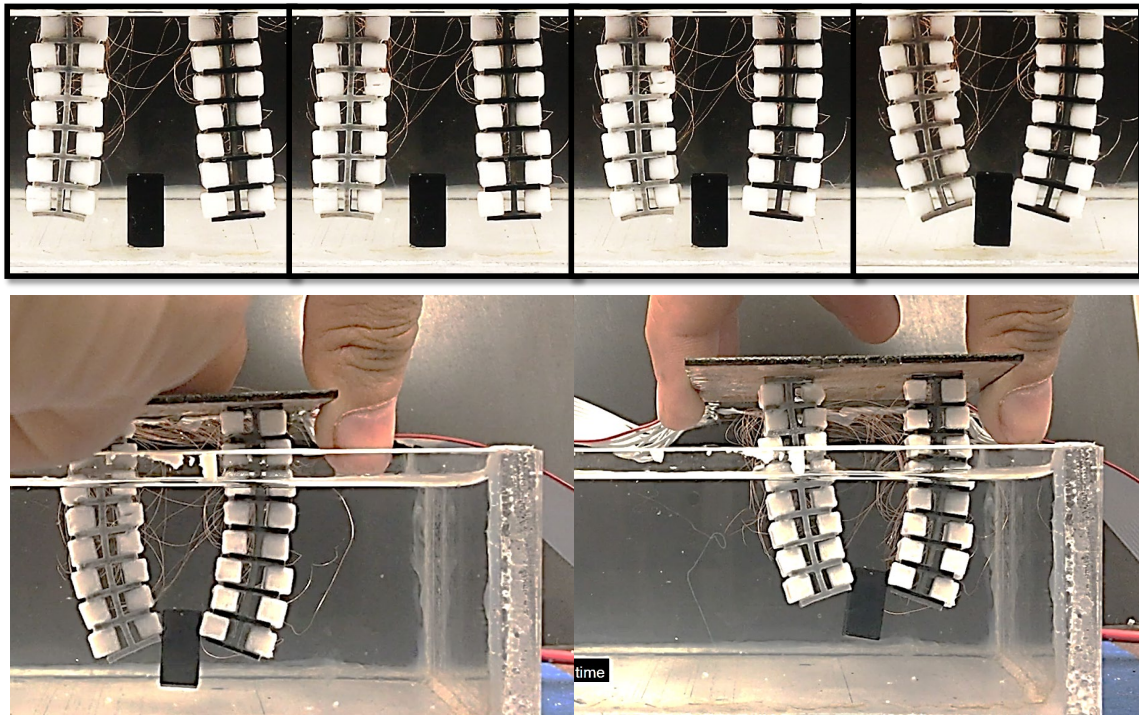
Figure 4.2 Activation of SVAs results in local increase in the temperature which leads to deformations that control the overall motion of the gripper. The gripper can produce enough force to carry a 10 g load.

4.3.2   Case Study II: Untethered Miniature Underwater Walking Robot

The robot shown in Figure 4.1 has four legs. Each leg is a two-DOF manipulator composed of two SVAs and a 3D printed extension as shown in Figure 4.3A. The workspace of the tip of this manipulator is plotted in Fig. 4.3B. To amplify the movement of the tip and measure it more precisely, a needle is attached to the tip of the 3D printed extension. A spherical marker is attached to the end of the needle and functions as a marker for tracking using a camera (Fig. 4.3C). The needle is only attached for recording the trajectories and was not present in the final robot prototype. We have created circular and oval trajectories using sine wave voltages as input to the SVAs. Each SVA is actuated using a sine wave with a phase shift with respect to other SVA. As the phase shift between the two SVAs in a manipulator is varied, the shape of the trajectory changes. Figure 4.3D shows different trajectories of the tip of the needle as a function of phase shift in the sinusoidal excitation voltages. To create an untethered walking robot, four manipulators discussed above are assembled in an array. The array is attached to a microcontroller board (Adafruit Itsy Bitsy M0) and a lithium ion battery is added to the system as shown in as shown in Fig. 4.3E. The movement of the miniature underwater walking robot is shown as a time-lapse in Fig. 4.3F.

4.3.3   Comparing Actuation of SVAs using Electrical and Light Signals

Hydrogels can be made to respond to different stimuli such as PH, Light or heat. On-demand shape changes are achieved using light as a control signal [106]. In case of temperature responsive hydrogels such as the one presented in this work, any stimulus that can change the temperature of the gel could be used for actuation. Therefore, addition of light absorbing agents that can convert light energy to heat can result in a light responsive hydrogel. Gold nanoparticles are among the highly used light absorbing agents. Under
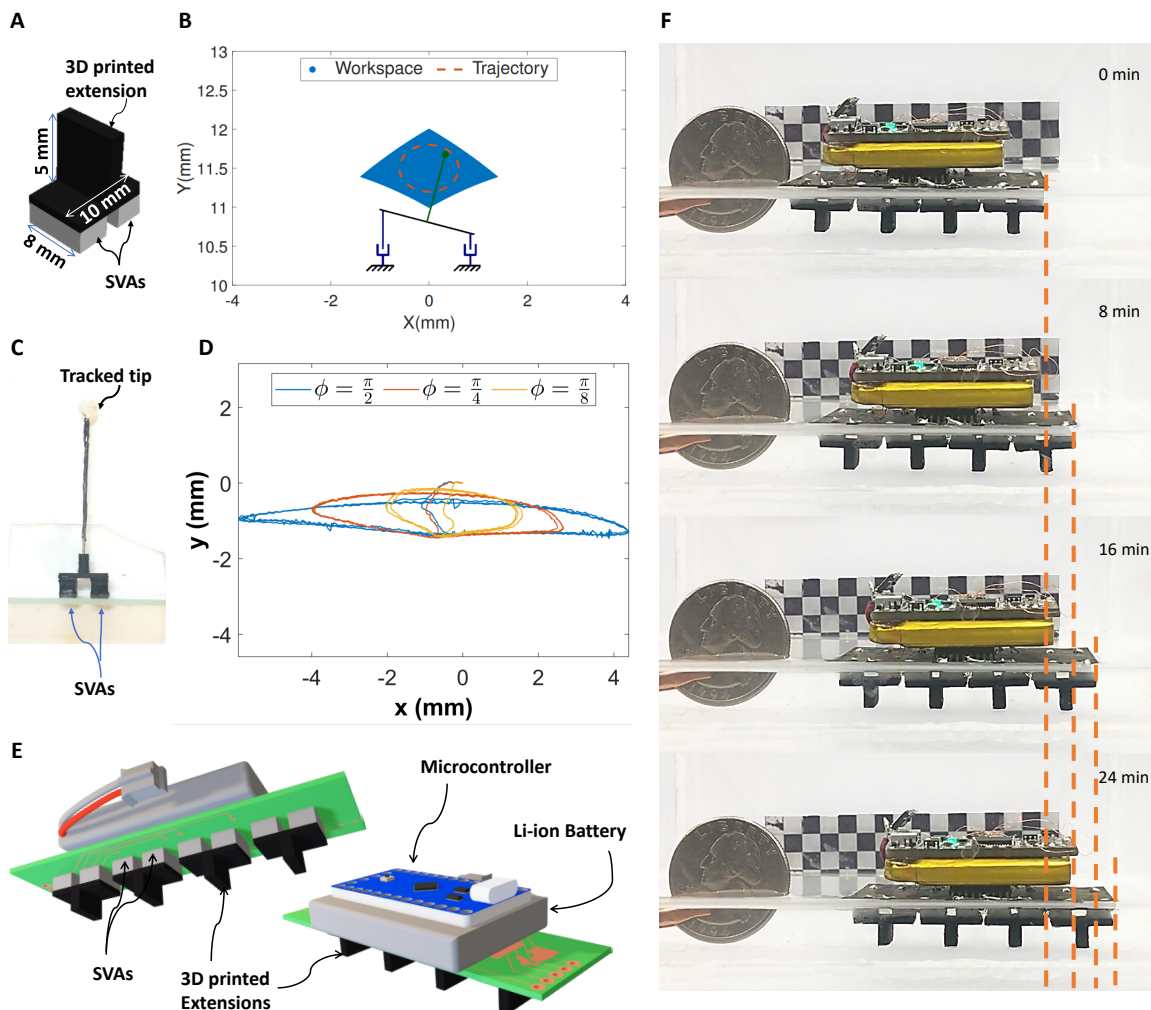
Figure 4.3 A) A two degrees of freedom manipulator using two SVAs and a 3D printed extension. B) The workspace of the tip of this manipulator. C) A needle is attached to the tip of the 3D printed extension to amplify the movement of the tip. D) Different trajectories of the tip of the needle as a function of phase shift in the sinusoidal excitation voltages. E) A microcontroller board and a lithium ion battery is added to the system to make an untethered robot. F) Time-lapse of the movement of the miniature underwater walking robot (see Movie S1 for details).

illumination at their plasmonic resonance wavelength, they can turn incident light into efficient nano sources of heat remotely controllable by light. One such light responsive hydrogel is previously demonstrated in Zhao, Yusen, et al. "Soft phototactic swimmer based

on self-sustained hydrogel oscillator." Science Robotics 4.33 (2019). Here, to show some
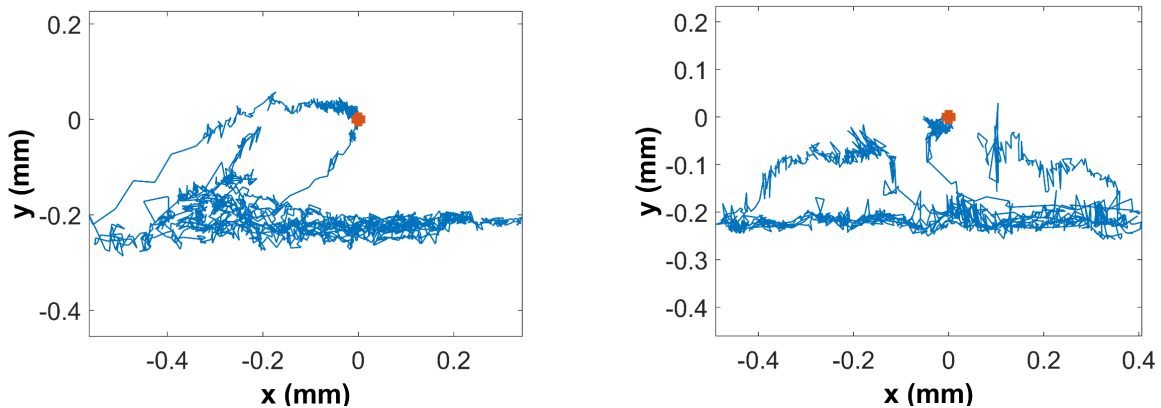
Figure 4.4 Trajectories produced using a light responding hydrogel. Light responding SVAs are activated using a laser source pointed manually by a human operator.

possibilities, polypyrrole as a light absorbing material is used to create SVAs that respond to a light beam. Using this light-responsive gel, a manipulator similar to Fig. 4.3C is built using two SVAs. As before, the goal is to move the tip of the mechanism in an oval loop. The trajectory of the tip is recorded using a camera and is shown in Figure 4.4. It is clearly seen that using light as a control signal results in a random trajectory which is far from the desired one. This is because the laser beam is manually shined on the SVAs. Even if a motorized mechanism is used to shine the light, it only complicates the system making it less usable as a mobile robotic platform. In contrast, the electric stimulation results in a much smoother trajectory that is repeatable over many cycles. It is also possible to program the desired trajectory by varying the activation voltage of SVAs. In this experiment, two sinusoidal voltages are used that have a phase shift that result in circular motion of the tip as discussed before. Animals use electric signals for activation of their muscles and the analogy of SVAs to motor units was the source of inspiration to stay with electric signals as opposed to other activation modes so that the resulting mechanisms are more independent of the environment and are more easily controlled.

4.3.4 Case Study III: Demonstration of a Closed-loop Controller Through a miniature Starfish Inspired Robot

Up to this point, it has been shown that using electrical signals are advantageous in providing a facile method of controlling the deformation of SVAs. To show the full potential of the SVAs, a closed-loop control algorithm is implemented in a robotic platform inspired by starfish. This mechanism has the same structure as the untethered robot shown in Figure 4.1, however instead of the two DOF manipulators touching the ground and moving the robot, the robot is stationary in an upside down configuration and manipulates an object as shown in Figure 4.5D. As shown in Figure 4.5A-C, a circuit board, which serves as the fixed base of the manipulator, is attached to one side of the two SVAs; the 3D printed T-shaped extension is attached to the other side. The circuit board and extension are attached to the SVAs with superglue to ensure that they remain in contact with the SVAs during the experiments. Since hydrogels must be immersed in water to absorb water when cooling, all experiments are conducted in a tank of deionized (DI), room-temperature water.

4.3.4.1 Experimental Setup

In a starfish, the podia moves in a loop and creates the desired motion for manipulation and locomotion. In Section 4.3.3 it is shown that creating a loop is possible through the use of sinusoidal signals. However, using predefined signals limits the movement to a certain pattern. For creating different motions to fit the requirements of different tasks, it is necessary to be able to control the movement of the arm on-demand based on a feedback from the environment. For this purpose, using a camera, the position of the tip of the podia is tracked and used as feedback in the control algorithm. The experiment setup is shown in Figure 4.6A. For calibrating the camera, a checkerboard is used and the entire experiment is performed in a warer tank as illustrated in Figure 4.6B. A Logitech C930e USB Webcam
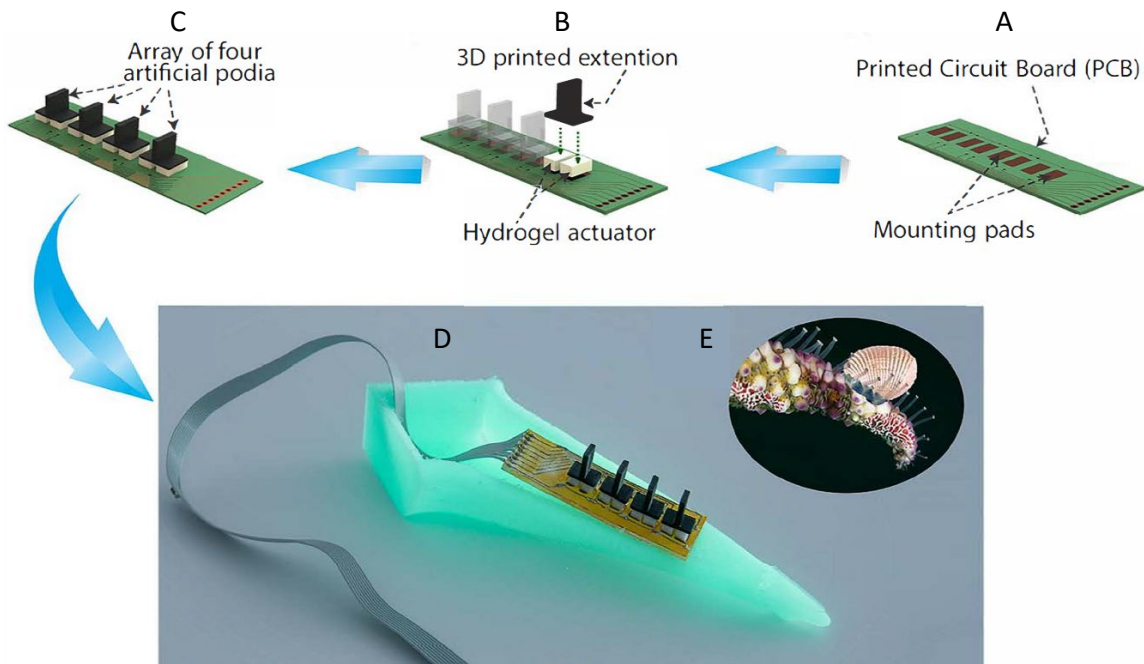
Figure 4.5 A-C) Steps for assembling SVAs into printed circuit board and adding 3D printed podia. D) The completed prototype E) A starfish transporting food (a clam) towards its mouth.
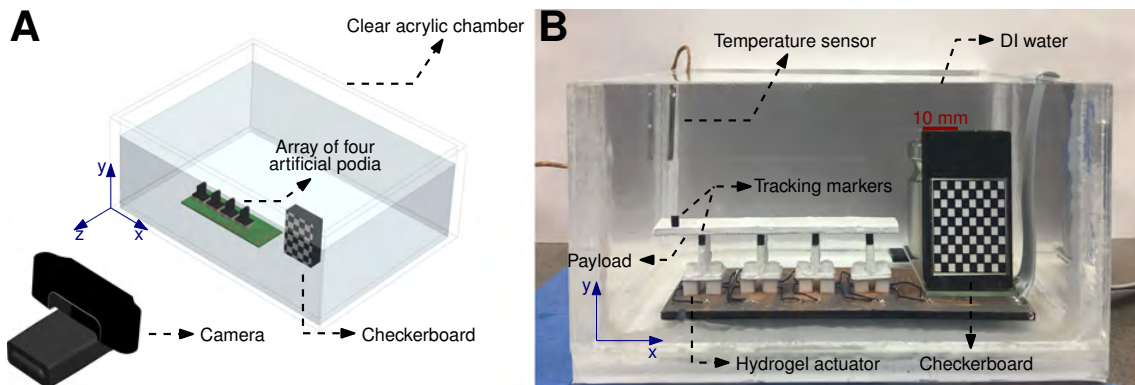
Figure 4.6 Trajectories produced using a light responding hydrogel. Light responding SVAs are activated using a laser source pointed manually by a human operator.

is placed in front of the tank to send real-time data to the image processing program in MATLAB which tracks the position of a marker on the manipulator tip. These measurements of the manipulator tip's position over time are transmitted back to the controller. We used a black-and-white checkerboard with 2 mm × 2 mm squares to estimate the camera

calibration factors (mm/pixel) along the x and y axis (Figure 4.6). White was selected as the color of the tank's background, and black was selected as the color of the manipulator tip's marker to facilitate contrast-based filtering between the foreground and background. The Camera Calibration Toolbox in MATLAB was initially used to compensate for lens distortion, but since this increased the image processing time by 30% without significantly improving the image data, the original camera images were subsequently used without compensation. All control algorithms are implemented in MATLAB; the controller output is sent to an Arduino Mega2560, which acts as the physical communication layer between MATLAB and a PCA9685 MOSFET board. This MOSFET board, with 16 discrete output channels, receives a PWM signal from the controller and applies it (maximum: 3.7 V) at higher current to the corresponding Joule heater.

4.3.4.2 Experimental validation of controller

The details of the system modeling, identification, controller design and performance are discussed in Appendix A. Here, only the results related to experimental validation of the controller is presented. Since the H_∞-optimal controller exhibited higher tracking accuracy in simulation both with and without disturbance and noise (Figure A.4), it was selected for experimental implementation. Using the designed control gain for H_∞, we have implemented the output-feedback tracking framework depicted in Fig. A.3b on the hydrogel-based manipulator (Fig. A.1). Half-ellipse and quarter-ellipse paths were also used as reference trajectories. Sources of noise in the experiment arise in the testing environment and vision-based feedback. Disturbances include modeling and manufacturing errors. The MAE and NMAE values are reported for one cycle per trajectory in Table 4.1, though three repeating cycles per trajectory were collected.

Figure 4.7a compares the trajectory of a manipulator with the 25 mm extension driven by the controller Equation (A.8) along an elliptical reference trajectory. Controller perfor-

60
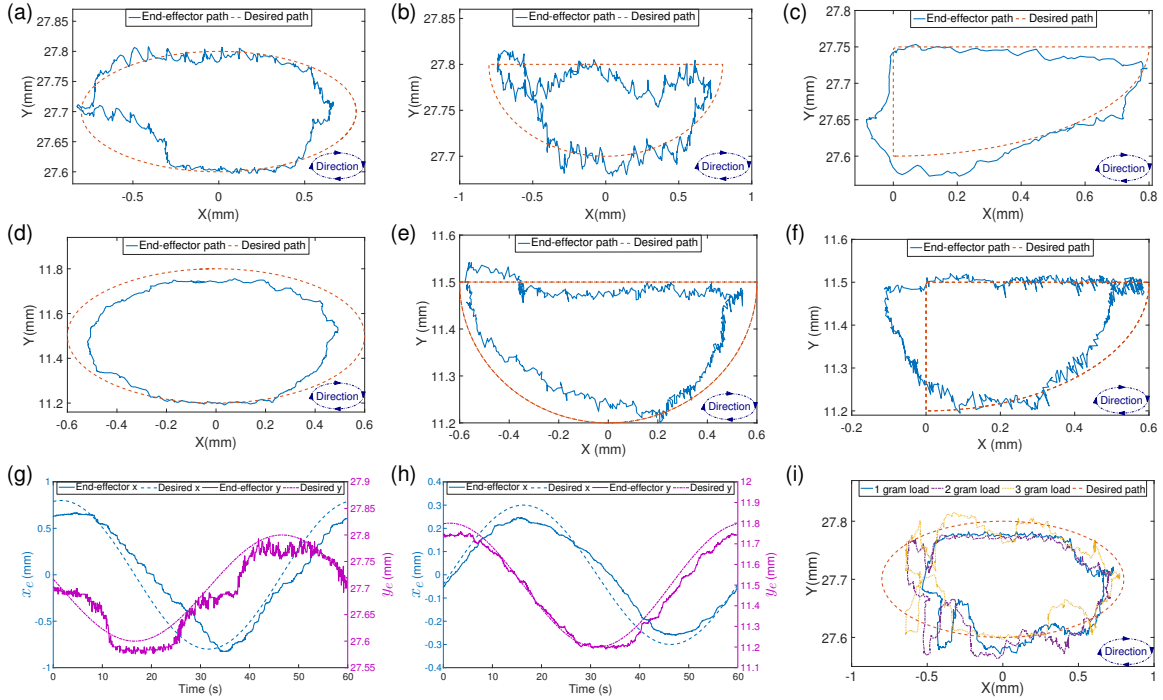
Figure 4.7 Tracking reference and experimental trajectories of manipulator tip in Cartesian coordinates. 25 mm manipulator tracking: (a) an elliptical trajectory; (b) a half-ellipse; (c) a quarter-ellipse. 9 mm manipulator tracking: (d) an elliptical trajectory; (e) a half-ellipse; (f) a quarter-ellipse. (g) 25 mm manipulator tracking an elliptical trajectory: x, y coordinates over time separately. (h) 9 mm manipulator tracking an elliptical trajectory: x, y coordinates over time separately. (i) 25 mm manipulator tracking an elliptical trajectory under 1 g, 2 g, and 3 g.

mance was evaluated using a half-ellipse and quarter-ellipse reference trajectory as well, to verify the ability of the controlled system to track straight lines and sharp turns (Figs. 4.7b and 4.7c). Figures 4.7d, 4.7e ,and 4.7f show the controlled position of the 9 mm extension's tip using the same reference trajectories. Figures 4.7g and 4.7h illustrate the time evolution of the x and y coordinates separately for the two extensions.

In order to further characterize our system's actuation capabilities, the manipulator's trajectory-tracking performance under load was studied, as shown in Fig. 4.7i. Loads (stainless steel nuts) weighing 1 g, 2 g, and 3 g were placed on the 25 mm extension, as

Table 4.1 (N)MAE of H_∞ controller performance in experiment.

d	Reference	Load	x	y	$x - y$	NMAE
(mm)	trajectory	(g)	(mm)	(mm)	(mm)	%
25	Ellipse	-	0.123	0.042	0.131	8.1
25	Half Ellipse	-	0.119	0.023	0.123	7.6
25	Quarter Ellipse	-	0.112	0.026	0.119	7.4
9	Ellipse	-	0.088	0.033	0.099	7.4
9	Half Ellipse	-	0.129	0.058	0.132	9.8
9	Quarter Ellipse	-	0.161	0.061	0.171	12.8
25	Ellipse	1	0.140	0.022	0.144	8.9
25	Ellipse	2	0.162	0.021	0.162	10.1
25	Ellipse	3	0.164	0.022	0.164	10.2

shown in Fig. A.2b. The manipulator was commanded to follow the same elliptical trajectory as in the unloaded case. The results show that the addition of a weight of up to 3 g increases the trajectory tracking NMAE from 8.1% to 10.2% (see Table 4.1). Despite the increase in error, each actuator is still able to function under a load as large as 12.5 times its own weight (0.12 g). As shown in Table 4.1, the experimental NMAE values are higher than the simulation values, but remain below 15%.

4.3.4.3 Payload transport application

Inspired by the way starfish transport food using their tube feet (Figs. 4.8b and 4.8c) [107, 108], we configured an array of four 9 mm manipulators, as shown in Fig. 4.8e, and applied the proposed H_∞-optimal controller in (A.8) and Fig. A.3b to each manipulator in order to transport a payload across their tips. The payload being transported is a clear acrylic plate. The manipulators are commanded to track reference trajectories as depicted in Fig. 4.8a, with phase shifts between adjacent manipulators. The payload moves to the right as the ma-

Table 4.2 Payload displacement ΔX with different reference trajectories for the manipulators.

Reference trajectory	Payload weight + load (g)	Time for one gait cycle (s)	ΔX after five gait cycles (mm)
Ellipse	2.7	60	5.66
Half-ellipse	2.7	50	4.55
Quarter-ellipse	2.7	40	7.10
Ellipse	2.7+1	60	4.75
Ellipse	2.7+2	60	4.84
Ellipse	2.7+3	60	2.30

nipulators complete repeated cycles of the reference trajectories ("gait cycles"), as shown in Figs. 4.8d and 4.8e. The data from Fig. 4.8d on the duration of one gait cycle and the payload displacement in each tested scenario including the ones with extra added loads on the payload are reported in Table 4.2. A video of the payload transport is attached as supplementary material. The payload's position is recorded but not controlled in this exemplar application, since our goal in this chapter was to demonstrate a use-case for trajectory tracking control. However, many other platforms and applications are possible, including bio-inspired ones [109]. Through this example, we have demonstrated how trajectory tracking control of systems with soft actuators, when applied to even simple platforms such as this 2-DOF manipulator, may be used to complete complex tasks such as object transport when used in parallel. This type of design can be used to simplify and decouple the control structures in future applications to reduce computational expense.

4.4 Conclusions

We have shown that the voxel-based design and manufacturing strategy, combined with an electrically addressable smart material, can lead to the creation of miniaturized soft

robots with a high number of DOFs. These robots can be used for tasks in which redundancy is needed for example to handle continuously changing tasks in unstructured environments. This has been demonstrated through a miniaturized hyper-redundant soft robot with 16 SVA units. SVAs can be easily integrated into robotic systems. They help greatly reduce the size of the robots. In addition, sice the SVAs are electrically controlled, they can be connected directly to small footprint microcontrollers and other electronics. The electronics and power supply can be embedded in the robot and cut the tether from the entire system. We have demonstrated this through a miniature underwater walking robot that do not rely on external signals or power which can be beneficial in applications such as under water data collection and ocean monitoring. The SVAs introduced in Chapter 2 are the first demonstration of active, soft voxels that are made of stimuli-responsive materials. Using SVAs as building blocks offers higher number of design parameters, namely, the configuration of the SVAs, the material properties of each SVA, and the activation voltage of each SVA. Multi-objective optimization can be used in future to optimize this rich set of design parameters to build structures that have higher force production capacity and energy efficiency.
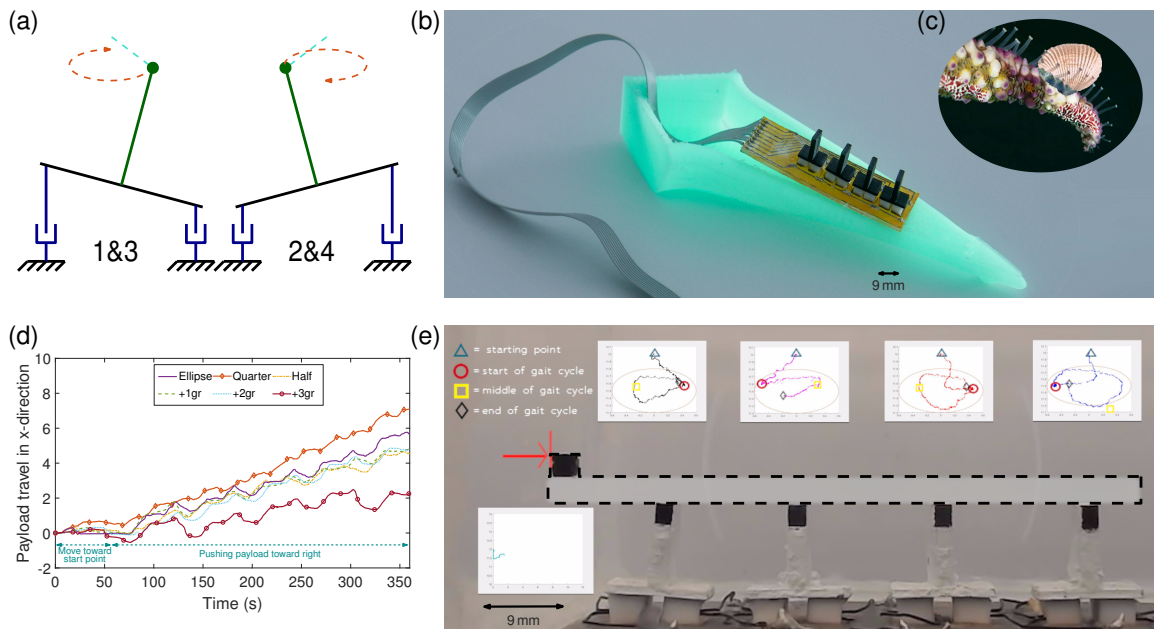
Figure 4.8 Control of four 9 mm manipulators in series for payload transport, in a manner similar to food transport by starfish tube feet. (a) The manipulators, numbered 1 to 4 from left to right, are commanded to first follow the cyan dashed lines from their initial positions to their starting positions on the reference trajectories, and then follow these trajectories, shown as red dashed lines. Manipulators 1 and 3 have a phase shift of $180°$ compared to manipulators 2 and 4. (b) Illustration of a starfish-inspired robotic platform with four hydrogel-actuated manipulators. (c) Real starfish transporting a clam on its tube feet. (d) Displacement of the payload as a function of time for different reference trajectories and load weights. (e) Array of four manipulators functioning as described in (a) to transport the payload. Image was taken when the manipulators completed the first gait cycle. The payload is a clear flat acrylic plate with a black square on its left side. The positions of the manipulator tips are marked by triangles at their initial locations, circles at the start of the gait cycle, squares at the middle of the gait cycle, and diamonds at the end of the gait cycle.

Chapter 5

CONCLUSIONS AND FUTURE WORK

This Ph.D. research is performed as part of office of the naval research (ONR) funded project titled 'Octopus-Inspired Autonomous Arms for Soft Robotics with Adaptive Motions'. The team consisted of roboticists, material scientists, and controls engineers conducted research on multiple disciplines simultaneously, which has helped inform the progress of one field by considering the requirements of the other. This unique combination resulted in solving some of the key technical challenges ahead of soft robotics in general and of miniature, untethered soft robots in particular. This research demonstrates broader impacts on the soft robotics community by demonstrating alternatives to the way the robots can be created, which will be discussed in this chapter.

5.1 Technical and Scientific Impact

The technical contribution of this dissertation in material science can be explained as improving the performance of PNIPAAm-based hydrogels to make them usable in soft robotic systems. These improvements include:

- Increasing speed of the hydrogel response to temperature. Prior to this improvement, the gel response was slow; meaningful robotic movement could not be produced in reasonable amount of time.

- Using a synthesis technique based on photopolymerization to minimize the polymerization time (to under 15 sec) and facilitate the fabrication of hydrogel structures. Prior research focused on improving the response rate without considering the ease of manufacturing and therefore the resulting gels were of less interest in the robotics

66

community.

- Expanding the knowledge on underlying the mechanisms of transport phenomena in temperature-responsive hydrogles as well as the effect of their micro-structure on their response.

- Expanding the knowledge on the mechanism of pore formation in hydrogels based on cononsolvency effect.

- Studying hydrogel response tuning based on simple alterations of ingredients.

In terms of manufacturing, a bottom-up assembly approach inspired by biology has been selected to facilitate the fabrication of soft robots. Using building blocks to assemble soft robots has several advantages:

- Building blocks can be selected from a wide range of materials.

- They can contain essential components such as sensors and processors.

- The manufacturing of a building block is very simple and therefore they can be mass produced easily.

These features facilitates the fabrication of multimaterial structures. This is critical while the range of compatible materials for 3D printing is still limited. Inclusion of electronics in the soft robot structure would also be performed more easily.

5.1.1   Broader Impact on Soft Robotics Community

Soft robotics has quickly turned into a broad area of research since its introduction. A number of challenges still remain in this field, which, if addressed, will make soft robots more useful for solving a wider range of problems. One of these challenges is to cut the

tether from robots and enable them to operate as mobile devices. Another challenge is to reduce the size of the robots. An even tougher problem would arise when trying to solve both the aforementioned challenges simultaneously. Addressing these challenges require innovative approaches and usually requires progress in multiple fields. However, the progress in one field is often made without considering the limitations of the other fields. This problem is more profound in the field of material science regarding the development on novel materials for soft actuators and sensors. For instance, stimuli-responsive hydrogels are usually developed using complex processes and specialized equipment and are consequently less accessible to robotics community.

Within the field of heterogeneous hydrogel structures, the presented methods in material synthesis and manufacturing techniques have helped to achieve unique desirable features that are highly demanded in hydrogels and soft robotics research simultaneously. In the literature surveyed, individual features might have been achieved separately. However, since some of the goals are contrary to each other, reaching one makes the other harder to achieve. For example, improving the response rate of hydrogels is highly regarded from a materials research perspective but is often accompanied by complications in synthesis which require additional processing complexities. Parallel improvements have been made through a collaboration between teams of material scientists and roboticists allowing considerations from one field to inform the other.

In addition, by introducing the first addressable hydrogel voxels, the field is further advanced by creating on-demand actuation and shape change of heterogeneous structures –a feature that improves the motion of a structure from hard-coded to on-demand programmable. As mentioned above, on-demand programmable shape change is one of the main goals of research in this field which is hard to achieve using the current technologies. It should be emphasized that the control signals are electrical signals, a feature inspired by biology in contrast to the previously demonstrated heterogeneous structures which use light

68

signals or global temperature changes. Therefore, the robotic systems can be miniaturized and fully untethered simultaneously.

5.1.2 Broader Impact on Society

This research on soft robotics have many potential applications in biology, medicine and environmental science. The small footprint soft robots developed are low cost and can be manufactured in large numbers. A swarm of these robots can operate under water to collect environmental data, thanks to the intrinsic compatibility of hydrogels and water. The miniature robots can be sent inside the human body to perform drug delivery, biopsies, and tasks that require a high number of degrees of freedom in robotic manipulators. In addition to the capability of soft robots to deal with unstructured environment, they are intrinsically safe around humans. This can enhance the application of robots to daily life uses such as household robots and assistant robots for elderly people which are challenging using rigid robots.

5.2 Future Work

The research presented in this dissertation has opened the doors to a variety of other research opportunities. Some of these new research in the field of control of soft robots and in-depth analysis of the hydrogel materials have already been started by different teams consisting of Ph.D., Masters and undergraduate students. An introduction to these work will be presented here and future opportunities will be discussed.

5.2.1 In-depth analysis of noncosolvencey phenomenon

While the research in this dissertation provides a method of altering the properties of temperature-responsive PNIMPAAm hydrogels by means of mixed solvent method, the mechanisms of pore formation in this method is not fully understood. To study these mech-

anisms, our collaborators in the University of California, Los Angeles (UCLA) have started in-depth study of the hydrogels produced by the mixed solvent method. It is understood that the coil to globule transition of polymer chains in presence of a second solvent (Figure 5.1) results in the formation of pores.
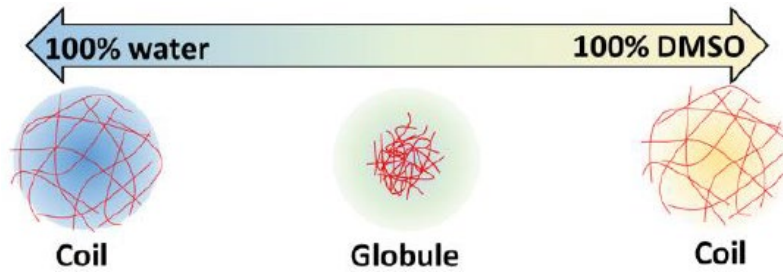
Figure 5.1

In addition, a 3D printing technique has been demonstrated. A sample 3D printed structure is shown in Figure 5.2. The results of this research has been accepted for publication in the journal Advanced Materials [103]. Future work will focus on 3D printing of voxels with embedded soft heaters to remove the rigid components from the voxels and increase their production rate.
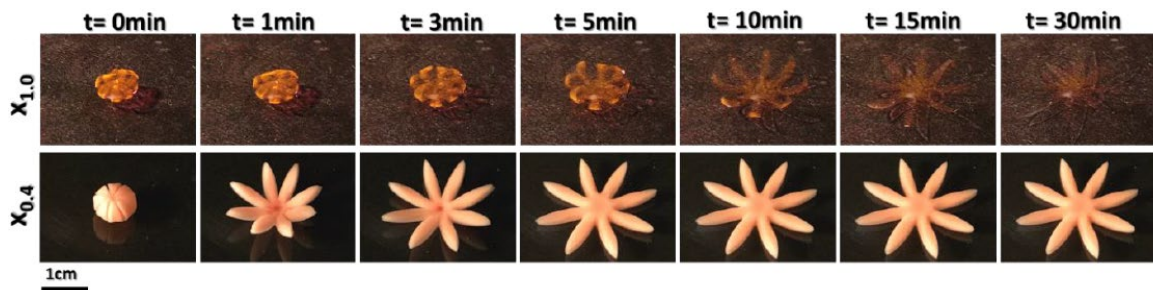
Figure 5.2

5.2.2 Control of the Hyper-redundant Robotic Arm

The electrical stimulation of SVAs helps the control engineers to implement and test their algorithm on the developed robot prototypes. In A we have discussed the an example

70

of such controller in a mechanism consisting of two SVAs. More complex structures such as the 16 DOF miniature manipulator discussed in 3 can also be controlled on the same basis which is discussed in a more recent work [109]. So far, all the sensing required for the closed-loop control was performed using a camera. For embedded systems it is essential that sensors are embedded in the robot. Future work includes finding sensor solutions that can detect the motion of the robot and can be embedded in the robot.

5.2.3 Dynamic Simulation of the Voxel-based Robots

While the finite element modeling provides accurate information about the deformation of the hydrogels considering the details of the transport of water in the porous structures, the time required for such simulations are usually long. For soft robot prototyping, it is essential to have tools that can predict the motion of the robot and provide insight about the performance of a particular design. Different tools have been developed for this purpose such as SOFA [110] which uses a hybrid FEM and lumped model engine and Vox-CAD [111] which is based on a voxel-based, mass-spring lattice modeling. Work is in progress to expand the capabilities of VoxCAD by adding functionality such as controlling individual voxel deformation instead of a global deformation function. An example gripper is shown in Figure 5.3

5.2.4 A 3-dimensional prototype of the hyper-redundant robot

Extending the motion of the miniature hyper-redundant arm discussed in Chapter 3 to 3D is the next step in the development of this arm. This next version would be modular such that different arm segments can be attached together to achieve more complex robots. Each segment has its own computation power, sensors and power supply making it completely independent of other segments. Each segment would be able to communicate with other segments to perform a shared goal. This prototype can help control engineers to explore the

71
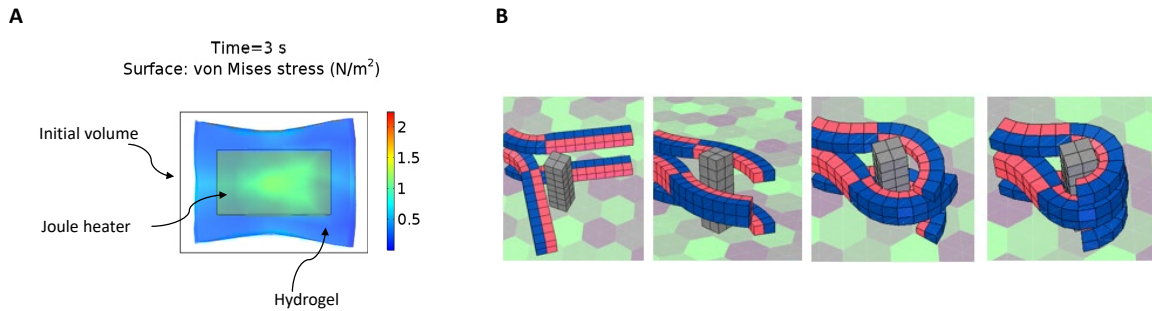
Figure 5.3 Dynamic simulations using FEM and mass-spring methods. A) FEM simulation of a voxel contraction as the Joule heater is turned using COMSOL. B) Mass-spring model simulation of a gripper using a modified version of VoxCAD.
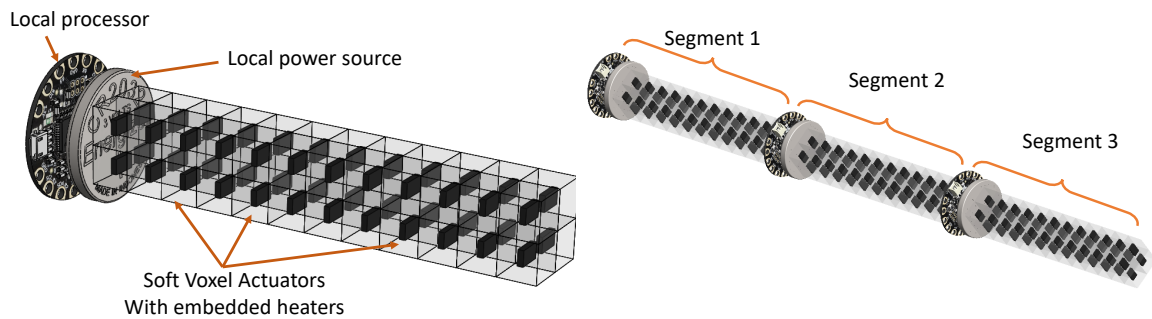
Figure 5.4 The concept of a 3-dimensional miniature arm segment with embedded power and processor (left). An assembly of segments forming a more complex arm (right)

distributed sensing and control algorithms inspired by octopus where some of the control task is not performed by a central nervous system but by a distributed neural network across its arms. A schematic of the idea of a 3D segmented arm is shown in Figure 5.4.

5.2.5 Expanding the Functionality of the Robots

It is widely accepted that soft robots can outperform rigid robots in terms of adaptability. For example, a robot that needs to be at one size for performing routine tasks and shrink in order to fit into tight spaces could in theory be made out of soft materials. In practice however, limitations such as controlling the soft robots and embedding efficient sensors for feedback have so far prevented the demonstration of such tasks by soft robots.
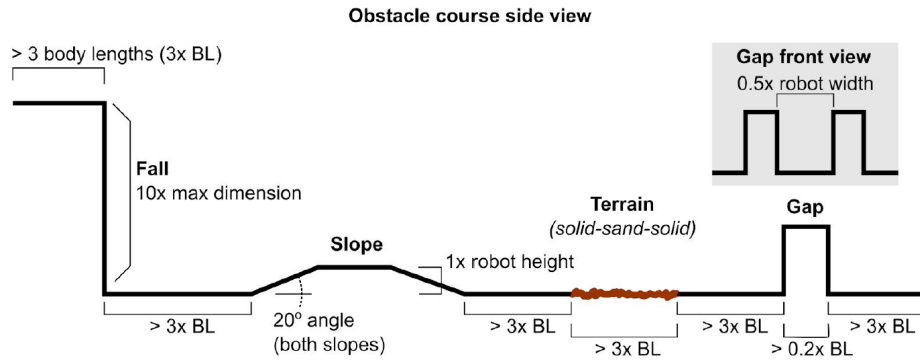
Figure 5.5 Schematic showing the requirements, setup and goals in robotic competition as part of IEEE RoboSoft conference.

These challenges are known to soft robotics community and there has been increasing effort in addressing them. For instance, the relatively new IEEE soft robotics conference (RoboSoft) has started a robotic competition the goal of which is to invite the community to solve some of the mentioned challenges. Figure 5.5 shows the schematic of the competition goals, setup and requirements. Making soft robots using SVAs that can perform some of the tasks mentioned in Figure 5.5 is one of the routes to follow in the future towards more impactful soft robots that can deal with real world situations.

5.2.6   A Swarm of Untethered Octopus Inspired Robots

As a more advanced future application of the methods presented in this thesis, miniature continuum manipulators can be assembled into more complex robots, as shown in Figure 5.6 in order to perform higher level tasks. These robots can operate autonomously and communicate through the built in wireless communication hardware. Regarding the low production cost, a swarm of these robots can be produced and be used for data collection and monitoring of environmental conditions.

Figure 5.6 The concept of an octopus inspired robot with multiple arms and embedded power and processor. A swarm of these low cost robots can be used for ocean monitoring.

REFERENCES

[1] S. Li, J. J. Stampfli, H. J. Xu, E. Malkin, E. V. Diaz, D. Rus, and R. J. Wood, "A Vacuum-driven Origami "Magic-ball" Soft Gripper," in *2019 International Conference on Robotics and Automation (ICRA)*, vol. 2019-May. IEEE, may 2019, pp. 7401–7408. [Online]. Available: https://ieeexplore.ieee.org/document/8794068/

[2] N. T. Jafferis, E. F. Helbling, M. Karpelson, and R. J. Wood, "Untethered flight of an insect-sized flapping-wing microscale aerial vehicle," *Nature*, vol. 570, no. 7762, pp. 491–495, jun 2019. [Online]. Available: http://dx.doi.org/10.1038/s41586-019-1322-0http://www.nature.com/articles/s41586-019-1322-0

[3] R. Khodambashi, S. Berman, X. He, and D. M. Aukes, "Miniaturized Untethered Soft Robots Using Hydrogel-based Soft Voxel Actuators *," in *Proceedings of 4th IEEE International Conference on Soft Robotics (RoboSoft)*. IEEE, 2021.

[4] M. Rogóż, H. Zeng, C. Xuan, D. S. Wiersma, and P. Wasylczyk, "Light-Driven Soft Robot Mimics Caterpillar Locomotion in Natural Scale," *Advanced Optical Materials*, vol. 4, no. 11, pp. 1689–1694, nov 2016. [Online]. Available: http://doi.wiley.com/10.1002/adom.201600503

[5] M. T. Tolley, R. F. Shepherd, B. Mosadegh, K. C. Galloway, M. Wehner, M. Karpelson, R. J. Wood, and G. M. Whitesides, "A Resilient, Untethered Soft Robot," *Soft Robotics*, vol. 1, no. 3, pp. 213–223, sep 2014. [Online]. Available: https://www.liebertpub.com/doi/10.1089/soro.2014.0008http://online.liebertpub.com/doi/abs/10.1089/soro.2014.0008

[6] R. V. Martinez, J. L. Branch, C. R. Fish, L. Jin, R. F. Shepherd, R. M. D. Nunes, Z. Suo, and G. M. Whitesides, "Robotic Tentacles with Three-Dimensional Mobility Based on Flexible Elastomers," *Advanced Materials*, vol. 25, no. 2, pp. 205–212, jan 2013. [Online]. Available: http://doi.wiley.com/10.1002/adma.201203002

[7] C. Laschi, M. Cianchetti, B. Mazzolai, L. Margheri, M. Follador, and P. Dario, "Soft Robot Arm Inspired by the Octopus," *Advanced Robotics*, vol. 26, no. 7, pp. 709–727, jan 2012. [Online]. Available: https://www.tandfonline.com/doi/full/10.1163/156855312X626343

[8] R. Adam Bilodeau, E. L. White, and R. K. Kramer, "Monolithic fabrication of sensors and actuators in a soft robotic gripper," in *2015 IEEE/RSJ International Conference on Intelligent Robots and Systems (IROS)*, vol. 2015-Decem. IEEE, sep 2015, pp. 2324–2329. [Online]. Available: http://ieeexplore.ieee.org/document/7353690/

[9] Y. Liu, M. Pharr, and G. A. Salvatore, "Lab-on-Skin: A Review of Flexible and Stretchable Electronics for Wearable Health Monitoring," *ACS Nano*, vol. 11, no. 10, pp. 9614–9635, oct 2017. [Online]. Available: https://pubs.acs.org/doi/10.1021/acsnano.7b04898

[10] M. Amjadi, K.-U. Kyung, I. Park, and M. Sitti, "Stretchable, Skin-Mountable, and Wearable Strain Sensors and Their Potential Applications: A Review," *Advanced Functional Materials*, vol. 26, no. 11, pp. 1678–1698, mar 2016. [Online]. Available: http://doi.wiley.com/10.1002/adfm.201504755

[11] F. L. Hammond, Y. Menguc, and R. J. Wood, "Toward a modular soft sensor-embedded glove for human hand motion and tactile pressure measurement," in *2014 IEEE/RSJ International Conference on Intelligent Robots and Systems*, no. Iros. IEEE, sep 2014, pp. 4000–4007. [Online]. Available: http://ieeexplore.ieee.org/document/6943125/

[12] J.-B. Chossat, Y.-L. Park, R. J. Wood, and V. Duchaine, "A Soft Strain Sensor Based on Ionic and Metal Liquids," *IEEE Sensors Journal*, vol. 13, no. 9, pp. 3405–3414, sep 2013. [Online]. Available: http://ieeexplore.ieee.org/document/6517240/

[13] X. Wang, R. Guo, and J. Liu, "Liquid Metal Based Soft Robotics: Materials, Designs, and Applications," *Advanced Materials Technologies*, vol. 4, no. 2, p. 1800549, dec 2018. [Online]. Available: https://onlinelibrary.wiley.com/doi/abs/10.1002/admt.201800549

[14] Y. Ren, X. Sun, and J. Liu, "Advances in Liquid Metal-Enabled Flexible and Wearable Sensors," *Micromachines*, vol. 11, no. 2, p. 200, feb 2020. [Online]. Available: https://www.mdpi.com/2072-666X/11/2/200

[15] A. Georgopoulou and F. Clemens, "Piezoresistive Elastomer-Based Composite Strain Sensors and Their Applications," *ACS Applied Electronic Materials*, vol. 2, no. 7, pp. 1826–1842, jul 2020. [Online]. Available: https://pubs.acs.org/doi/10.1021/acsaelm.0c00278

[16] A. Turgut, M. O. Tuhin, O. Toprakci, M. A. Pasquinelli, R. J. Spontak, and H. A. K. Toprakci, "Thermoplastic Elastomer Systems Containing Carbon Nanofibers as Soft Piezoresistive Sensors," *ACS Omega*, vol. 3, no. 10, pp. 12 648–12 657, oct 2018. [Online]. Available: https://pubs.acs.org/doi/10.1021/acsomega.8b01740

[17] M. Melnykowycz, M. Tschudin, and F. Clemens, "Piezoresistive Soft Condensed Matter Sensor for Body-Mounted Vital Function Applications," *Sensors*, vol. 16, no. 3, p. 326, mar 2016. [Online]. Available: http://www.mdpi.com/1424-8220/16/3/326

[18] C. J. Hohimer, G. Petrossian, A. Ameli, C. Mo, and P. Pötschke, "3D printed conductive thermoplastic polyurethane/carbon nanotube composites for capacitive and piezoresistive sensing in soft pneumatic actuators," *Additive Manufacturing*, vol. 34, no. April, p. 101281, aug 2020. [Online]. Available: https://doi.org/10.1016/j.addma.2020.101281https://linkinghub.elsevier.com/retrieve/pii/S2214860420306539

[19] P.-J. Cao, Y. Liu, W. Asghar, C. Hu, F. Li, Y. Wu, Y. Li, Z. Yu, S. Li, J. Shang, X. Liu, and R.-W. Li, "A Stretchable Capacitive Strain Sensor Having Adjustable Elastic Modulus Capability for Wide-Range Force Detection," *Advanced Engineering Materials*, vol. 22, no. 3, p. 1901239, mar 2020. [Online]. Available: https://onlinelibrary.wiley.com/doi/abs/10.1002/adem.201901239

[20] E. L. White, M. C. Yuen, J. C. Case, and R. K. Kramer, "Low-Cost, Facile, and Scalable Manufacturing of Capacitive Sensors for Soft Systems," *Advanced Materials Technologies*, vol. 2, no. 9, p. 1700072, sep 2017. [Online]. Available: http://doi.wiley.com/10.1002/admt.201700072

[21] A. Frutiger, J. T. Muth, D. M. Vogt, Y. Mengüç, A. Campo, A. D. Valentine, C. J. Walsh, and J. A. Lewis, "Capacitive Soft Strain Sensors via Multicore-Shell Fiber Printing," *Advanced Materials*, vol. 27, no. 15, pp. 2440–2446, apr 2015. [Online]. Available: http://doi.wiley.com/10.1002/adma.201500072

[22] J. Chen, Y. Zhu, J. Huang, J. Zhang, D. Pan, J. Zhou, J. E. Ryu, A. Umar, and Z. Guo, "Advances in Responsively Conductive Polymer Composites and Sensing Applications," *Polymer Reviews*, vol. 61, no. 1, pp. 157–193, jan 2021. [Online]. Available: https://doi.org/10.1080/15583724.2020.1734818https://www.tandfonline.com/doi/full/10.1080/15583724.2020.1734818

[23] O. Kanoun, A. Bouhamed, R. Ramalingame, J. R. Bautista-Quijano, D. Rajendran, and A. Al-Hamry, "Review on Conductive Polymer/CNTs Nanocomposites Based Flexible and Stretchable Strain and Pressure Sensors," *Sensors*, vol. 21, no. 2, p. 341, jan 2021. [Online]. Available: https://www.mdpi.com/1424-8220/21/2/341

[24] C. Harito, L. Utari, B. R. Putra, B. Yuliarto, S. Purwanto, S. Z. J. Zaidi, D. V. Bavykin, F. Marken, and F. C. Walsh, "Review—The Development of Wearable Polymer-Based Sensors: Perspectives," *Journal of The Electrochemical Society*, vol. 167, no. 3, p. 037566, feb 2020. [Online]. Available: https://iopscience.iop.org/article/10.1149/1945-7111/ab697c

[25] D. J. Preston, P. Rothemund, H. J. Jiang, M. P. Nemitz, J. Rawson, Z. Suo, and G. M. Whitesides, "Digital logic for soft devices," *Proceedings of the National Academy of Sciences*, vol. 116, no. 16, pp. 7750–7759, apr 2019. [Online]. Available: http://www.pnas.org/lookup/doi/10.1073/pnas.1820672116

[26] M. Garrad, G. Soter, A. T. Conn, H. Hauser, and J. Rossiter, "A soft matter computer for soft robots," *Science Robotics*, vol. 4, no. 33, p. eaaw6060, aug 2019. [Online]. Available: https://robotics.sciencemag.org/lookup/doi/10.1126/scirobotics.aaw6060

[27] R. Daniel, J. R. Rubens, R. Sarpeshkar, and T. K. Lu, "Synthetic analog computation in living cells," *Nature*, vol. 497, no. 7451, pp. 619–623, may 2013. [Online]. Available: http://www.nature.com/articles/nature12148

[28] B. Gorissen, D. Reynaerts, S. Konishi, K. Yoshida, J. W. Kim, and M. De Volder, "Elastic Inflatable Actuators for Soft Robotic Applications," *Advanced Materials*, vol. 29, no. 43, pp. 1–14, 2017.

[29] C. Branyan, C. Fleming, J. Remaley, A. Kothari, K. Tumer, R. L. Hatton, and Y. Menguc, "Soft snake robots: Mechanical design and geometric gait implementation," in *2017 IEEE International Conference on Robotics and Biomimetics (ROBIO)*, vol. 2018-Janua.   IEEE, dec 2017, pp. 282–289. [Online]. Available: http://ieeexplore.ieee.org/document/8324431/

[30] M. Cianchetti, A. Licofonte, M. Follador, F. Rogai, and C. Laschi, "Bioinspired Soft Actuation System Using Shape Memory Alloys," *Actuators*, vol. 3, no. 3, pp. 226–244, jul 2014. [Online]. Available: http://www.mdpi.com/2076-0825/3/3/226

[31] F. Carpi, D. D. Rossi, R. Kornbluh, R. Pelrine, and P. Sommer-Larsen, *Dielectric Elastomers as Electromechanical Transducers*.   Elsevier, 2008. [Online]. Available: http://store.elsevier.com/product.jsp?isbn=9780080474885{&}{_}requestid=1399603https://linkinghub.elsevier.com/retrieve/pii/B9780080474885X00019

[32] G.-Y. Gu, J. Zhu, L.-M. Zhu, and X. Zhu, "A survey on dielectric elastomer actuators for soft robots," *Bioinspiration & Biomimetics*, vol. 12, no. 1, p. 011003, jan 2017. [Online]. Available: http://iopscience.iop.org.libproxy1.nus.edu.sg/article/10.1088/1748-3190/12/1/011003/pdfhttps://iopscience.iop.org/article/10.1088/1748-3190/12/1/011003

[33] R. S. Kularatne, H. Kim, J. M. Boothby, and T. H. Ware, "Liquid crystal elastomer actuators: Synthesis, alignment, and applications," *Journal of Polymer Science Part B: Polymer Physics*, vol. 55, no. 5, pp. 395–411, mar 2017. [Online]. Available: http://doi.wiley.com/10.1002/polb.24287

[34] T. H. Ware, M. E. McConney, J. J. Wie, V. P. Tondiglia, and T. J. White, "Voxelated liquid crystal elastomers," *Science*, vol. 347, no. 6225, pp. 982–984, feb 2015. [Online]. Available: http://www.sciencemag.org/lookup/doi/10.1126/science.1261019https://www.sciencemag.org/lookup/doi/10.1126/science.1261019

[35] P. Calvert, "Hydrogels for Soft Machines," *Advanced Materials*, vol. 21, no. 7, pp. 743–756, feb 2009. [Online]. Available: http://doi.wiley.com/10.1002/adma.200800534

[36] X. Liu, J. Liu, S. Lin, and X. Zhao, "Hydrogel machines," *Materials Today*, vol. 36, no. xx, pp. 102–124, jun 2020. [Online]. Available: https://doi.org/10.1016/j.mattod.2019.12.026https://linkinghub.elsevier.com/retrieve/pii/S1369702119308995

[37] L. Ionov, "Hydrogel-based actuators: possibilities and limitations," *Materials Today*, vol. 17, no. 10, pp. 494–503, dec 2014. [Online]. Available: http://dx.doi.org/10.1016/j.mattod.2014.07.002https://linkinghub.elsevier.com/retrieve/pii/S1369702114002521

[38] H. Banerjee, M. Suhail, and H. Ren, "Hydrogel Actuators and Sensors for Biomedical Soft Robots: Brief Overview with Impending Challenges," *Biomimetics*, vol. 3, no. 3, p. 15, jul 2018. [Online]. Available: http://www.mdpi.com/2313-7673/3/3/15

[39] L. Hines, K. Petersen, G. Z. Lum, and M. Sitti, "Soft Actuators for Small-Scale Robotics," *Advanced Materials*, vol. 29, no. 13, p. 1603483, apr 2017. [Online]. Available: http://doi.wiley.com/10.1002/adma.201603483

[40] C. Majidi, "Soft-Matter Engineering for Soft Robotics," *Advanced Materials Technologies*, vol. 4, no. 2, p. 1800477, dec 2018. [Online]. Available: https://onlinelibrary.wiley.com/doi/abs/10.1002/admt.201800477

[41] S. Palagi, A. G. Mark, S. Y. Reigh, K. Melde, T. Qiu, H. Zeng, C. Parmeggiani, D. Martella, A. Sanchez-Castillo, N. Kapernaum, F. Giesselmann, D. S. Wiersma, E. Lauga, and P. Fischer, "Structured light enables biomimetic swimming and versatile locomotion of photoresponsive soft microrobots," *Nature Materials*, vol. 15, no. 6, pp. 647–653, jun 2016. [Online]. Available: http://www.nature.com/articles/nmat4569

[42] Y. Kim, H. Yuk, R. Zhao, S. A. Chester, and X. Zhao, "Printing ferromagnetic domains for untethered fast-transforming soft materials," *Nature*, vol. 558, no. 7709, pp. 274–279, jun 2018. [Online]. Available: http://www.nature.com/articles/s41586-018-0185-0

[43] Y. Lee, W. J. Song, and J.-Y. Sun, "Hydrogel soft robotics," *Materials Today Physics*, vol. 15, p. 100258, 2020. [Online]. Available: https://doi.org/10.1016/j.mtphys.2020.100258

[44] O. Erol, A. Pantula, W. Liu, and D. H. Gracias, "Transformer Hydrogels: A Review," *Advanced Materials Technologies*, vol. 4, no. 4, p. 1900043, apr 2019. [Online]. Available: https://onlinelibrary.wiley.com/doi/abs/10.1002/admt.201900043

[45] A. Sydney Gladman, E. A. Matsumoto, R. G. Nuzzo, L. Mahadevan, and J. A. Lewis, "Biomimetic 4D printing," *Nature Materials*, vol. 15, no. 4, pp. 413–418, 2016.

[46] P. Ma, B. Niu, J. Lin, T. Kang, J. Qian, Z. L. Wu, and Q. Zheng, "Sequentially Controlled Deformations of Patterned Hydrogels into 3D Configurations with Multilevel Structures," *Macromolecular Rapid Communications*, vol. 40, no. 3, p. 1800681, feb 2019. [Online]. Available: https://onlinelibrary.wiley.com/doi/abs/10.1002/marc.201800681

[47] S.-j. J. Jeon, A. W. Hauser, and R. C. Hayward, "Shape-Morphing Materials from Stimuli-Responsive Hydrogel Hybrids," *Accounts of Chemical Research*, vol. 50, no. 2, pp. 161–169, feb 2017. [Online]. Available: https://pubs.acs.org/doi/10.1021/acs.accounts.6b00570

[48] J. Wang, J. Wang, Z. Chen, S. Fang, Y. Zhu, R. H. Baughman, and L. Jiang, "Tunable, Fast, Robust Hydrogel Actuators Based on Evaporation-Programmed Heterogeneous Structures," *Chemistry of Materials*, vol. 29, no. 22, pp. 9793–9801, nov 2017. [Online]. Available: https://pubs.acs.org/doi/10.1021/acs.chemmater.7b03953

[49] C. Ma, W. Lu, X. Yang, J. He, X. Le, L. Wang, J. Zhang, M. J. Serpe, Y. Huang, and T. Chen, "Bioinspired Anisotropic Hydrogel Actuators with On-Off Switchable and Color-Tunable Fluorescence Behaviors," *Advanced Functional Materials*, vol. 28, no. 7, p. 1704568, feb 2018. [Online]. Available: http://doi.wiley.com/10.1002/adfm.201704568

[50] J. Duan, X. Liang, K. Zhu, J. Guo, and L. Zhang, "Bilayer hydrogel actuators with tight interfacial adhesion fully constructed from natural polysaccharides," *Soft Matter*, vol. 13, no. 2, pp. 345–354, 2017. [Online]. Available: http://xlink.rsc.org/?DOI=C6SM02089E

[51] A. Mourran, H. Zhang, R. Vinokur, and M. Möller, "Soft Microrobots Employing Nonequilibrium Actuation via Plasmonic Heating," *Advanced Materials*, vol. 29, no. 2, 2017.

[52] T. W. J. Steele and H.-A. Klok, "Stimuli-Sensitive and -Responsive Polymer Biomaterials," *Biomacromolecules*, vol. 19, no. 5, pp. 1375–1377, may 2018. [Online]. Available: https://pubs.acs.org/doi/10.1021/acs.biomac.8b00145

[53] M. A. C. Stuart, W. T. S. Huck, J. Genzer, M. Müller, C. Ober, M. Stamm, G. B. Sukhorukov, I. Szleifer, V. V. Tsukruk, M. Urban, F. Winnik, S. Zauscher, I. Luzinov, and S. Minko, "Emerging applications of stimuli-responsive polymer materials," *Nature Materials*, vol. 9, no. 2, pp. 101–113, feb 2010. [Online]. Available: http://dx.doi.org/10.1038/nmat2614http://www.nature.com/articles/nmat2614

[54] E. M. White, J. Yatvin, J. B. Grubbs, J. A. Bilbrey, and J. Locklin, "Advances in smart materials: Stimuli-responsive hydrogel thin films," *Journal of Polymer Science Part B: Polymer Physics*, vol. 51, no. 14, pp. 1084–1099, jul 2013. [Online]. Available: http://doi.wiley.com/10.1002/polb.23312

[55] A. Ghosh, C. Yoon, F. Ongaro, S. Scheggi, F. M. Selaru, S. Misra, and D. H. Gracias, "Stimuli-Responsive Soft Untethered Grippers for Drug Delivery and Robotic Surgery," *Frontiers in Mechanical Engineering*, vol. 3, no. July, pp. 1–9, jul 2017. [Online]. Available: http://journal.frontiersin.org/article/10.3389/fmech.2017.00007/full

[56] J. Shintake, V. Cacucciolo, D. Floreano, and H. Shea, "Soft Robotic Grippers," *Advanced Materials*, vol. 30, no. 29, p. 1707035, jul 2018. [Online]. Available: http://doi.wiley.com/10.1002/adma.201707035

[57] R. Khodambashi, Y. Alsaid, R. Rico, H. Marvi, M. M. Peet, R. E. Fisher, S. Berman, X. He, and D. M. Aukes, "Heterogeneous Hydrogel Structures with Spatiotemporal Reconfigurability using Addressable and Tunable Voxels," *Advanced Materials*, vol. 2005906, pp. 1–9, 2021.

[58] N. Annabi, A. Tamayol, J. A. Uquillas, M. Akbari, L. E. Bertassoni, C. Cha, G. Camci-Unal, M. R. Dokmeci, N. A. Peppas, and A. Khademhosseini, "25th Anniversary Article: Rational Design and Applications of Hydrogels in Regenerative Medicine," *Advanced Materials*, vol. 26, no. 1, pp. 85–124, jan 2014. [Online]. Available: http://doi.wiley.com/10.1002/adma.201303233

[59] L. D'Eramo, B. Chollet, M. Leman, E. Martwong, M. Li, H. Geisler, J. Dupire, M. Kerdraon, C. Vergne, F. Monti, Y. Tran, and P. Tabeling, "Microfluidic actuators based on temperature-responsive hydrogels," *Microsystems & Nanoengineering*, vol. 4, no. 1, pp. 1–7, 2018. [Online]. Available: http://dx.doi.org/10.1038/micronano.2017.69

[60] C. B. Goy, R. E. Chaile, and R. E. Madrid, "Microfluidics and hydrogel: A powerful combination," *Reactive and Functional Polymers*, vol. 145, no. June, 2019.

[61] X. Zhou, T. Li, J. Wang, F. Chen, D. Zhou, Q. Liu, B. Li, J. Cheng, X. Zhou, and B. Zheng, "Mechanochemical Regulated Origami with Tough Hydrogels by Ion Transfer Printing," *ACS Applied Materials & Interfaces*, vol. 10, no. 10, pp. 9077–9084, mar 2018. [Online]. Available: https://pubs.acs.org/doi/10.1021/acsami.8b01610

[62] Y. Klein, E. Efrati, and E. Sharon, "Shaping of Elastic Sheets by Prescription of Non-Euclidean Metrics," *Science*, vol. 315, no. 5815, pp. 1116–1120, feb 2007. [Online]. Available: https://www.sciencemag.org/lookup/doi/10.1126/science.1135994

[63] J. Kim, J. A. Hanna, M. Byun, C. D. Santangelo, and R. C. Hayward, "Designing responsive buckled surfaces by halftone gel lithography," *Science*, vol. 335, no. 6073, pp. 1201–1205, 2012.

[64] C. Ma, X. Le, X. Tang, J. He, P. Xiao, J. Zheng, H. Xiao, W. Lu, J. Zhang, Y. Huang, and T. Chen, "A Multiresponsive Anisotropic Hydrogel with Macroscopic 3D Complex Deformations," *Advanced Functional Materials*, vol. 26, no. 47, pp. 8670–8676, 2016.

[65] R. M. Erb, J. S. Sander, R. Grisch, and A. R. Studart, "Self-shaping composites with programmable bioinspired microstructures," *Nature Communications*, vol. 4, pp. 1–8, 2013.

[66] L. Huang, R. Jiang, J. Wu, J. Song, H. Bai, B. Li, Q. Zhao, and T. Xie, "Ultrafast Digital Printing toward 4D Shape Changing Materials," *Advanced Materials*, vol. 29, no. 7, pp. 1–6, 2017.

[67] S. Y. Zheng, Y. Shen, F. Zhu, J. Yin, J. Qian, J. Fu, Z. L. Wu, and Q. Zheng, """," *Advanced Functional Materials*, vol. 28, no. 37, pp. 1–8, 2018.

[68] Z. L. Wu, M. Moshe, J. Greener, H. Therien-Aubin, Z. Nie, E. Sharon, and E. Kumacheva, "Three-dimensional shape transformations of hydrogel sheets induced by small-scale modulation of internal stresses," *Nature Communications*, vol. 4, pp. 1–7, 2013.

[69] L. Liu, S. Jiang, Y. Sun, and S. Agarwal, "Giving Direction to Motion and Surface with Ultra-Fast Speed Using Oriented Hydrogel Fibers," *Advanced Functional Materials*, vol. 26, no. 7, pp. 1021–1027, 2016.

[70] M. Y. Choi, Y. Shin, H. S. Lee, S. Y. Kim, and J. H. Na, "Multipolar spatial electric field modulation for freeform electroactive hydrogel actuation," *Scientific Reports*, vol. 10, no. 1, pp. 1–8, 2020. [Online]. Available: http://dx.doi.org/10.1038/s41598-020-59318-3

[71] W. R. Frontera and J. Ochala, "Skeletal Muscle: A Brief Review of Structure and Function," *Calcified Tissue International*, vol. 96, no. 3, pp. 183–195, mar 2015. [Online]. Available: http://link.springer.com/10.1007/s00223-014-9915-y

[72] M. Drost, M. Maenhout, P. Willems, C. Oomens, F. Baaijens, and M. Hesselink, "Spatial and temporal heterogeneity of superficial muscle strain during in situ fixed-end contractions," *Journal of Biomechanics*, vol. 36, no. 7, pp. 1055–1063, jul 2003. [Online]. Available: https://linkinghub.elsevier.com/retrieve/pii/S002192900200461X

[73] F. Buchthal and H. Schmalbruch, "Motor unit of mammalian muscle." *Physiological Reviews*, vol. 60, no. 1, pp. 90–142, jan 1980. [Online]. Available: https://www.physiology.org/doi/10.1152/physrev.1980.60.1.90

[74] W. M. KIER and K. K. SMITH, "Tongues, tentacles and trunks: the biomechanics of movement in muscular-hydrostats," *Zoological Journal of the Linnean Society*, vol. 83, no. 4, pp. 307–324, 1985.

[75] W. M. Kier and F. H. Schachat, "Biochemical comparison of fast- and slow-contracting squid muscle." *The Journal of experimental biology*, vol. 168, pp. 41–56, 1992.

[76] Z. Liu, M. A. Meyers, Z. Zhang, and R. O. Ritchie, "Functional gradients and heterogeneities in biological materials: Design principles, functions, and bioinspired applications," *Progress in Materials Science*, vol. 88, pp. 467–498, 2017. [Online]. Available: http://dx.doi.org/10.1016/j.pmatsci.2017.04.013

[77] S. Hanassy, A. Botvinnik, T. Flash, and B. Hochner, "Stereotypical reaching movements of the octopus involve both bend propagation and arm elongation," *Bioinspiration & Biomimetics*, vol. 10, no. 3, p. 035001, may 2015. [Online]. Available: http://dx.doi.org/10.1088/1748-3190/10/3/035001https://iopscience.iop.org/article/10.1088/1748-3190/10/3/035001

[78] A. Kazakidi, D. P. Tsakiris, D. Angelidis, F. Sotiropoulos, and J. A. Ekaterinaris, "CFD study of aquatic thrust generation by an octopus-like arm under intense prescribed deformations," *Computers and Fluids*, vol. 115, pp. 54–65, 2015. [Online]. Available: http://dx.doi.org/10.1016/j.compfluid.2015.03.009

[79] J. N. Richter, B. Hochner, and M. J. Kuba, "Octopus arm movements under constrained conditions: adaptation, modification and plasticity of motor primitives," *Journal of Experimental Biology*, vol. 218, no. 7, pp. 1069–1076, apr 2015. [Online]. Available: http://jeb.biologists.org/cgi/doi/10.1242/jeb.115915

[80] R. Yagel and D. Cohen, "Volume Graphics," *Computer*, vol. 26, no. 7, pp. 51–64, 1993.

[81] J. Hiller and H. Lipson, "Tunable digital material properties for 3D voxel printers," *Rapid Prototyping Journal*, vol. 16, no. 4, pp. 241–247, 2010.

[82] N. Oxman, "Variable property rapid prototyping," *Virtual and Physical Prototyping*, vol. 6, no. 1, pp. 3–31, mar 2011. [Online]. Available: http://www.tandfonline.com/doi/abs/10.1080/17452759.2011.558588

[83] G. Sossou, F. Demoly, H. Belkebir, H. J. Qi, S. Gomes, and G. Montavon, "Design for 4D printing: A voxel-based modeling and simulation of smart materials," *Materials and Design*, vol. 175, p. 107798, 2019. [Online]. Available: https://doi.org/10.1016/j.matdes.2019.107798

[84] N. Cheney, R. MacCurdy, J. Clune, and H. Lipson, "Unshackling evolution," *ACM SIGEVOlution*, vol. 7, no. 1, pp. 11–23, 2014.

[85] J. Hiller and H. Lipson, "Design and analysis of digital materials for physical 3D voxel printing," *Rapid Prototyping Journal*, vol. 15, no. 2, pp. 137–149, 2009.

[86] S. Kriegman, D. Blackiston, M. Levin, and J. Bongard, "A scalable pipeline for designing reconfigurable organisms," *Proceedings of the National Academy of Sciences of the United States of America*, vol. 117, no. 4, pp. 1853–1859, 2020.

[87] C. Yu, Z. Duan, P. Yuan, Y. Li, Y. Su, X. Zhang, Y. Pan, L. L. Dai, R. G. Nuzzo, Y. Huang, H. Jiang, and J. A. Rogers, "Electronically Programmable, Reversible Shape Change in Two- and Three-Dimensional Hydrogel Structures," *Advanced Materials*, vol. 25, no. 11, pp. 1541–1546, mar 2013. [Online]. Available: http://doi.wiley.com/10.1002/adma.201204180

[88] X. Z. Zhang, X. D. Xu, S. X. Cheng, and R. X. Zhuo, "Strategies to improve the response rate of thermosensitive PNIPAAm hydrogels," *Soft Matter*, vol. 4, no. 3, pp. 385–391, 2008.

[89] A. B. Imran, T. Seki, and Y. Takeoka, "Recent advances in hydrogels in terms of fast stimuli responsiveness and superior mechanical performance," *Polymer Journal*, vol. 42, no. 11, pp. 839–851, 2010. [Online]. Available: http://dx.doi.org/10.1038/pj.2010.87

[90] S. Kim, K. Lee, and C. Cha, "Refined control of thermoresponsive swelling/deswelling and drug release properties of poly(N-isopropylacrylamide) hydrogels using hydrophilic polymer crosslinkers," *Journal of Biomaterials Science, Polymer Edition*, vol. 27, no. 17, pp. 1698–1711, 2016. [Online]. Available: http://dx.doi.org/10.1080/09205063.2016.1230933

[91] D. Gan and L. A. Lyon, "Tunable swelling kinetics in core - shell hydrogel nanoparticles," *Journal of the American Chemical Society*, vol. 123, no. 31, pp. 7511–7517, 2001.

[92] P. Li, X. Hou, L. Qu, X. Dai, and C. Zhang, "PNIPAM-MAPOSS hybrid hydrogels with excellent swelling behavior and enhanced mechanical performance: Preparation and drug release of 5-fluorouracil," *Polymers*, vol. 10, no. 2, 2018.

[93] K. Depa, A. Strachota, M. Šlouf, and J. Hromádková, "Fast temperature-responsive nanocomposite PNIPAM hydrogels with controlled pore wall thickness: Force and rate of T-response," *European Polymer Journal*, vol. 48, no. 12, pp. 1997–2007, dec 2012. [Online]. Available: https://linkinghub.elsevier.com/retrieve/pii/S0014305712003023

[94] C. Ma, T. Li, Q. Zhao, X. Yang, J. Wu, Y. Luo, and T. Xie, "Supramolecular lego assembly towards three-dimensional multi-responsive hydrogels," *Advanced Materials*, vol. 26, no. 32, pp. 5665–5669, 2014.

[95] E. Otsuka, S. Komiya, S. Sasaki, J. Xing, Y. Bando, Y. Hirashima, M. Sugiyama, and A. Suzuki, "Effects of preparation temperature on swelling and mechanical properties of PVA cast gels," *Soft Matter*, vol. 8, no. 31, pp. 8129–8136, 2012.

[96] N. Bodenberger, D. Kubiczek, I. Abrosimova, A. Scharm, F. Kipper, P. Walther, and F. Rosenau, "Evaluation of methods for pore generation and their influence on physio-chemical properties of a protein based hydrogel," *Biotechnology Reports*, vol. 12, pp. 6–12, dec 2016. [Online]. Available: http://dx.doi.org/10.1016/j.btre.2016.09.001https://linkinghub.elsevier.com/retrieve/pii/S2215017X1630039X

[97] A. Pica and G. Graziano, "An alternative explanation of the cononsolvency of poly(N-isopropylacrylamide) in water-methanol solutions," *Physical Chemistry Chemical Physics*, vol. 18, no. 36, pp. 25 601–25 608, 2016.

[98] Q. Wang, C. S. Biswas, M. Galluzzi, Y. Wu, B. Du, and F. J. Stadler, "Random copolymer gels of N-isopropylacrylamide and N-ethylacrylamide: effect of synthesis solvent compositions on their properties," *RSC Advances*, vol. 7, no. 15, pp. 9381–9392, 2017. [Online]. Available: http://dx.doi.org/10.1039/C6RA27348Chttp://xlink.rsc.org/?DOI=C6RA27348C

[99] W.-F. Lee and S.-H. Yen, "Thermoreversible hydrogels. XII. Effect of the polymerization conditions on the swelling behavior of the N-isopropylacrylamide gel," *Journal of Applied Polymer Science*, vol. 78, no. 9, pp. 1604–1611, nov 2000. [Online]. Available: http://doi.wiley.com/10.1002/1097-4628{%}2820001128{%}2978{%}3A9{%}3C1604{%}3A{%}3AAID-APP50{%}3E3.0.CO{%}3B2-V

[100] X. Zhang, R. Zhuo, and Y. Yang, "Using mixed solvent to synthesize temperature sensitive poly(N-isopropylacrylamide) gel with rapid dynamics properties," *Biomaterials*, vol. 23, no. 5, pp. 1313–1318, mar 2002. [Online]. Available: https://linkinghub.elsevier.com/retrieve/pii/S0142961201002496

[101] Q. Feng, L. Z. Du, Q. Z. Yan, and C. C. Ge, "Effects of Synthesis-Solvent on Characteristics of Poly(<i>N-Isopropylacrylamide</i>) Hydrogels Synthesized by Frontal Polymerization," *Advanced Materials Research*, vol. 295-297, pp. 1193–1197, jul 2011. [Online]. Available: https://www.scientific.net/AMR.295-297.1193

[102] H. Tokuyama, N. Ishihara, and S. Sakohara, "Porous poly(N-isopropylacrylamide) gels polymerized in mixed solvents of water and N,N-dimethylformamide,"

Polymer Bulletin, vol. 61, no. 3, pp. 399–405, sep 2008. [Online]. Available: http://link.springer.com/10.1007/s00289-008-0961-3

[103] Y. Alsaid, S. Wu, D. Wu, Y. Du, L. Shi, R. Khodambashi, R. Rico, M. Hua, Y. Yan, Y. Zhao, D. Aukes, and X. He, "Tunable Sponge-Like Hierarchically Porous Hydrogels with Simultaneously Enhanced Diffusivity and Mechanical Properties," *Advanced Materials*, vol. 2008235, no. 2, p. 2008235, 2021.

[104] M. T. Tolley, R. F. Shepherd, B. Mosadegh, K. C. Galloway, M. Wehner, M. Karpelson, R. J. Wood, and G. M. Whitesides, "A Resilient, Untethered Soft Robot," *Soft Robotics*, vol. 1, no. 3, pp. 213–223, sep 2014. [Online]. Available: http://online.liebertpub.com/doi/abs/10.1089/soro.2014.0008https://www.liebertpub.com/doi/10.1089/soro.2014.0008

[105] A. Richter and G. Paschew, "Optoelectrothermic Control of Highly Integrated Polymer-Based MEMS Applied in an Artificial Skin," *Advanced Materials*, vol. 21, no. 9, pp. 979–983, mar 2009. [Online]. Available: http://doi.wiley.com/10.1002/adma.200802737

[106] T. Wang, J. Huang, Y. Yang, E. Zhang, W. Sun, and Z. Tong, "Bioinspired Smart Actuator Based on Graphene Oxide-Polymer Hybrid Hydrogels," *ACS Applied Materials & Interfaces*, vol. 7, no. 42, pp. 23 423–23 430, oct 2015. [Online]. Available: https://pubs.acs.org/doi/10.1021/acsami.5b08248

[107] G. A. KERKUT, "The Forces Exerted by the Tube Feet of the Starfish During Locomotion," *Journal of Experimental Biology*, vol. 30, no. 4, pp. 575–583, 1953.

[108] R. J. Pentreath, "Feeding mechanisms and the functional morphology of podia and spines in some New Zealand ophiuroids (Echinodermata)," *Journal of Zoology*, vol. 161, no. 3, pp. 395–429, may 2010. [Online]. Available: http://doi.wiley.com/10.1111/j.1469-7998.1970.tb04520.x

[109] A. Doroudchi, R. Khodambashi, A. S. Lafmejani, D. M. Aukes, and S. Berman, "Dynamic Modeling of a Hydrogel-based Continuum Robotic Arm with Experimental Validation," in *2020 3rd IEEE International Conference on Soft Robotics (RoboSoft)*. IEEE, may 2020, pp. 695–701. [Online]. Available: https://ieeexplore.ieee.org/document/9116012/

[110] F. Faure, C. Duriez, H. Delingette, J. Allard, B. Gilles, S. Marchesseau, H. Talbot, H. Courtecuisse, G. Bousquet, I. Peterlik, and S. Cotin, "SOFA: A Multi-Model Framework for Interactive Physical Simulation," in *Soft Tissue Biomechanical Modeling for Computer Assisted Surgery*, 2012, vol. 11, pp. 283–321. [Online]. Available: http://link.springer.com/10.1007/8415{_}2012{_}125

[111] J. Hiller and H. Lipson, "Dynamic Simulation of Soft Multimaterial 3D-Printed Objects," *Soft Robotics*, vol. 1, no. 1, pp. 88–101, 2014.

[112] C. Majidi, "Soft Robotics: A Perspective—Current Trends and Prospects for the Future," *Soft Robotics*, vol. 1, no. 1, pp. 5–11, mar 2014. [Online]. Available: https://www.liebertpub.com/doi/10.1089/soro.2013.0001

[113] S. Mantha, S. Pillai, P. Khayambashi, A. Upadhyay, Y. Zhang, O. Tao, H. M. Pham, and S. D. Tran, "Smart Hydrogels in Tissue Engineering and Regenerative Medicine," *Materials*, vol. 12, no. 20, p. 3323, oct 2019. [Online]. Available: https://www.ncbi.nlm.nih.gov/pmc/articles/PMC68/https://www.mdpi.com/1996-1944/12/20/3323

[114] M. Qin, M. Sun, M. Hua, and X. He, "Bioinspired structural color sensors based on responsive soft materials," *Current Opinion in Solid State and Materials Science*, vol. 23, no. 1, pp. 13–27, feb 2019. [Online]. Available: https://doi.org/10.1016/j.cossms.2018.10.001https://linkinghub.elsevier.com/retrieve/pii/S1359028618301347

[115] A. Guiseppi-Elie, "Electroconductive hydrogels: Synthesis, characterization and biomedical applications," *Biomaterials*, vol. 31, no. 10, pp. 2701–2716, apr 2010. [Online]. Available: http://dx.doi.org/10.1016/j.biomaterials.2009.12.052https://linkinghub.elsevier.com/retrieve/pii/S0142961209014392

[116] A. K. Mishra, T. J. Wallin, W. Pan, P. Xu, K. Wang, E. P. Giannelis, B. Mazzolai, and R. F. Shepherd, "Autonomic perspiration in 3D-printed hydrogel actuators," *Science Robotics*, vol. 5, no. 38, p. eaaz3918, jan 2020. [Online]. Available: https://robotics.sciencemag.org/lookup/doi/10.1126/scirobotics.aaz3918

[117] X. Peng, C. Jiao, Y. Zhao, N. Chen, Y. Wu, T. Liu, and H. Wang, "Thermoresponsive Deformable Actuators Prepared by Local Electrochemical Reduction of Poly(N -isopropylacrylamide)/Graphene Oxide Hydrogels," *ACS Applied Nano Materials*, vol. 1, no. 4, pp. 1522–1530, apr 2018. [Online]. Available: http://pubs.acs.org/doi/10.1021/acsanm.8b00022https://pubs.acs.org/doi/10.1021/acsanm.8b00022

[118] X. He, M. Aizenberg, O. Kuksenok, L. D. Zarzar, A. Shastri, A. C. Balazs, and J. Aizenberg, "Synthetic homeostatic materials with chemo-mechano-chemical self-regulation," *Nature*, vol. 487, no. 7406, pp. 214–218, jul 2012. [Online]. Available: http://www.nature.com/articles/nature11223

[119] R. Luo, J. Wu, N.-D. D. Dinh, and C.-H. H. Chen, "Gradient porous elastic hydrogels with shape-memory property and anisotropic responses for programmable locomotion," *Advanced Functional Materials*, vol. 25, no. 47, pp. 7272–7279, dec 2015. [Online]. Available: http://doi.wiley.com/10.1002/adfm.201503434

[120] Y. S. Kim, M. Liu, Y. Ishida, Y. Ebina, M. Osada, T. Sasaki, T. Hikima, M. Takata, and T. Aida, "Thermoresponsive actuation enabled by permittivity switching in an electrostatically anisotropic hydrogel," *Nature Materials*, vol. 14, no. 10, pp. 1002–1007, 2015.

[121] D. Morales, E. Palleau, M. D. Dickey, and O. D. Velev, "Electro-actuated hydrogel walkers with dual responsive legs," *Soft Matter*, vol. 10, no. 9, pp. 1337–1348, 2014.

[122] X. Du, H. Cui, Q. Zhao, J. Wang, H. Chen, and Y. Wang, "Inside-Out 3D Reversible Ion-Triggered Shape-Morphing Hydrogels," *Research*, vol. 2019, pp. 1–12, 2019.

[123] T. D. Nguyen, R. Schulman, Q. Huang, D. H. Gracias, J. Liu, C. Yoon, J. Guo, and A. Cangialosi, "DNA sequence–directed shape change of photopatterned hydrogels via high-degree swelling," *Science*, vol. 357, no. 6356, pp. 1126–1130, 2017.

[124] A. Zolfagharian, A. Z. Kouzani, S. Y. Khoo, A. Noshadi, and A. Kaynak, "3D printed soft parallel actuator," *Smart Materials and Structures*, vol. 27, no. 4, p. 45019, 2018. [Online]. Available: http://dx.doi.org/10.1088/1361-665X/aaab29

[125] R. J. Webster and B. A. Jones, "Design and Kinematic Modeling of Constant Curvature Continuum Robots: A Review," *The International Journal of Robotics Research*, vol. 29, no. 13, pp. 1661–1683, nov 2010. [Online]. Available: http://journals.sagepub.com/doi/10.1177/0278364910368147

[126] S. M. Rezayat Sorkhabadi, P. T. Chinimilli, D. Gaytan-Jenkins, and W. Zhang, "Human Locomotion Activity and Speed Recognition Using Electromyography Based Features," in *2019 Wearable Robotics Association Conference (WearRAcon)*. IEEE, mar 2019, pp. 80–85. [Online]. Available: https://ieeexplore.ieee.org/document/8719626/

[127] L. Ljung, "Perspectives on system identification," *Annual Reviews in Control*, vol. 34, no. 1, pp. 1–12, apr 2010. [Online]. Available: http://dx.doi.org/10.1016/j.arcontrol.2009.12.001https://linkinghub.elsevier.com/retrieve/pii/S1367578810000027

[128] M. Schaller, S. M. R. Sorkhabadi, and W. Zhang, "Robotic Shoe: An Ankle Assistive Device for Gait Plantar Flexion Assistance," in *2020 Design of Medical Devices Conference*. American Society of Mechanical Engineers, apr 2020, pp. 7–9. [Online]. Available: https://asmedigitalcollection.asme.org/BIOMED/proceedings/DMD2020/83549/Minneapolis,Minnesota,USA/1085705

[129] R. K. Lim, M. Q. Phan, and R. W. Longman, "State-Space System Identification with Identified Hankel Matrix," Department of Mechanical and Aerospace Engineering Technical Report 3045," *Department of Mechanical and Aerospace Engineering Technical Report*, no. 3045, pp. 1–36, 1998. [Online]. Available: http://www.dartmouth.edu/{~}mqphan/Resources/TP3045.pdf

[130] P. T. Chinimilli, S. M. Rezayat Sorkhabadi, and W. Zhang, "Assessment of Human Dynamic Gait Stability With a Lower Extremity Assistive Device," *IEEE Transactions on Neural Systems and Rehabilitation Engineering*, vol. 28, no. 3, pp. 669–678, mar 2020. [Online]. Available: https://ieeexplore.ieee.org/document/8974246/

[131] K. J. Aström and R. M. Murray, *Feedback Systems*. Princeton University Press, dec 2008. [Online]. Available: https://www.degruyter.com/document/doi/10.1515/9781400828739/html

[132] A. Farhamfard, M. B. Menhaj, and A. Fakharian, "H^∞ output feedback controller design for flexible needles guidance," in *2016 Artificial Intelligence and Robotics (IRANOPEN)*. IEEE, apr 2016, pp. 164–169. [Online]. Available: http://ieeexplore.ieee.org/document/7529508/

[133] L. Ljung, "Black-box models from input-output measurements," in *IMTC 2001. Proceedings of the 18th IEEE Instrumentation and Measurement Technology Conference. Rediscovering Measurement in the Age of Informatics (Cat. No.01CH 37188)*, vol. 1. IEEE, 2001, pp. 138–146. [Online]. Available: http://ieeexplore.ieee.org/document/928802/

[134] I. P. Sigurd Skogestad, *Multivariable feedback control: analysis and design*. Wiley, 2007, vol. 2.

[135] G.-R. Duan and H.-H. Yu, *LMIs in Control Systems*. CRC Press, 2013.

[136] S. Boyd, L. El Ghaoui, E. Feron, and V. Balakrishnan, *Linear Matrix Inequalities in System and Control Theory*. Society for Industrial and Applied Mathematics, jan 1994. [Online]. Available: http://epubs.siam.org/doi/book/10.1137/1.9781611970777

[137] J. Löfberg, "YALMIP: A toolbox for modeling and optimization in MATLAB," *Proceedings of the IEEE International Symposium on Computer-Aided Control System Design*, pp. 284–289, 2004.

[138] A. Doroudchi, S. Shivakumar, R. E. Fisher, H. Marvi, D. Aukes, X. He, S. Berman, and M. M. Peet, "Decentralized Control of Distributed Actuation in a Segmented Soft Robot Arm," *Proceedings of the IEEE Conference on Decision and Control*, vol. 2018-Decem, no. Cdc, pp. 7002–7009, 2019.

APPENDIX A

TRACKING CONTROL OF A MINIATURE 2-DOF MANIPULATOR WITH

HYDROGEL ACTUATORS

Due to the nature of the complex spatiotemporal dynamics of stimuli-responsive soft materials, closed-loop control of hydrogel-actuated mechanisms has remained a challenge. This paper demonstrates, for the first time, closed-loop trajectory tracking control in real-time of a millimeter-scale, two degree-of-freedom manipulator via *independently-controllable*, temperature-responsive hydrogel actuators. A linear state-space model of the manipulator is developed from input-output measurement data, enabling the straightforward application of control techniques to the system. The Normalized Mean Absolute Error (NMAE) between the modeled and measured displacement of the manipulator's tip is below 10%. We propose an Observer-based controller and a robust H_∞-optimal controller and evaluate their performance in a trajectory tracking output-feedback framework, compared with and without sinusoidal disturbances and noise. We demonstrate in simulation that the H_∞-optimal controller, which is computed using Linear Matrix Inequality (LMI) methods, tracks an elliptical trajectory more accurately than the Observer controller and is more robust to disturbances and noise. We also show experimentally that the H_∞-optimal controller can be used to track different trajectories with an NMAE below 15%, even when the manipulator is subject to a 3 g load, 12.5 times an actuator's weight. Finally, a payload transport scenario is presented as an exemplar application; we demonstrate that an array of four manipulators is capable of moving a payload horizontally by applying the proposed H_∞-optimal trajectory-tracking controller to each manipulator in a decoupled manner.

A.0.1   This subsection is numbered but not shown in the toc

A.1   Background

Soft actuators, composed of deformable matter such as fluids, gels, elastomers, and shape memory alloys (SMAs) [112], are lightweight and noiseless, in contrast to pneumatic systems with pumps and motors. Stimuli-responsive materials have potential applications

in micro-manipulation, sensing, optics [113, 114], and biomedical applications [115]. Hydrogels in particular have the ability to absorb and release water, undergoing reversible volumetric changes that facilitates their use as soft actuators [116]. A variety of hydrogel formulations exist, enabling these materials to change state under different external physical or chemical stimuli [117, 118]. For example, poly(N-isopropylacrylamide), or PNI-PAAM, is a commonly used temperature-responsive hydrogel that contracts when heated.
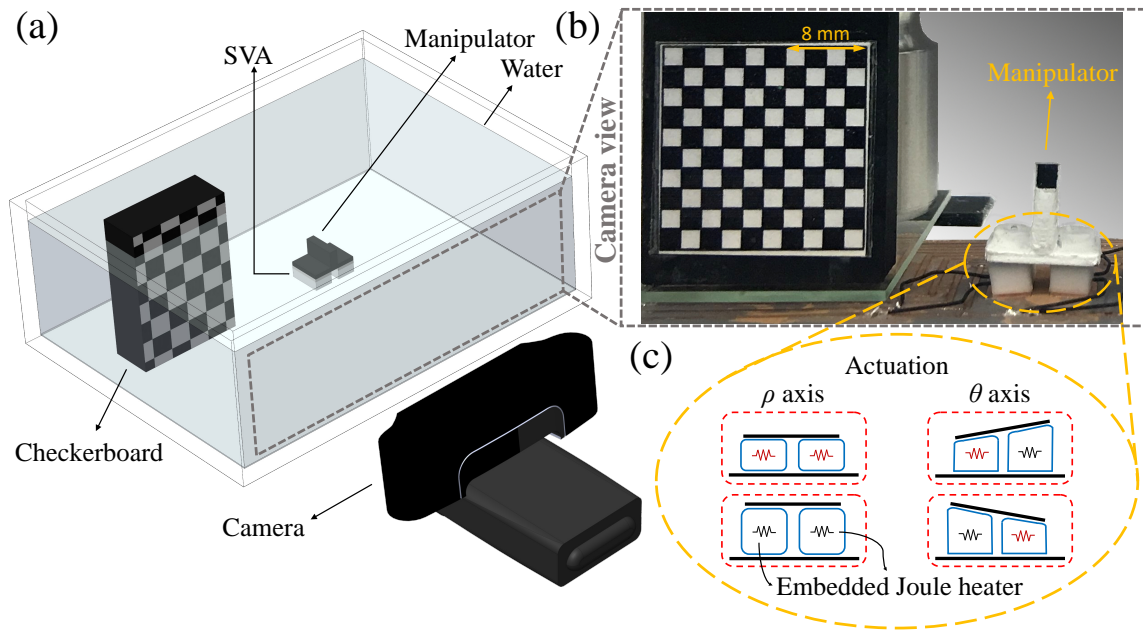
Figure A.1 Experimental setup for tracking control of a 2-DOF manipulator with embedded hydrogel Soft Voxel Actuators (SVAs) [109]. (a) Illustration of a manipulator in a water-filled tank with a camera for vision-based feedback of the manipulator tip. (b) Camera view of the setup, including a fabricated manipulator prototype and checkerboard for camera calibration. (c) Illustration of SVA deformation in various activation states (red = on; black = off).

Hydrogel-based active mechanisms using morphing or bending beams and sheets have been utilized for sensing, smart micro-fluidic valves, optical lensing, and micro-scale swimming and walking [37]. More complicated tasks, such as picking and placing objects with open-loop control methods, have also been demonstrated [106]. Due to the nature of the stimuli, closed-loop control of hydrogel actuators has remained a challenge. Light sources

such as lasers [119], for instance, require sophisticated and bulky equipment to produce motion. The methods used in [120] require bulk heating of the surrounding fluids, which limits their application to confined environments, such as tanks. Electric fields [121] and chemical gradients [122, 123] affect an entire region simultaneously, which means that all actuators placed in these fields are subject to the same stimulus. This results in primitive systems that are capable of performing simple tasks. For instance, novel devices with soft, 3D-printed, parallel, contactless actuators for biomedical applications like cell manipulation and drug release [124] use electro-responsive hydrogels and are stimulated via electric field; the actuators are simultaneously affected by changes in the electric field, resulting in a single controllable degree of actuation for the device. To enable independent actuation of multiple hydrogel actuators, we recently developed a novel approach or fabricating and integrating Soft Voxel Actuators (SVAs) composed of temperature-responsive hydrogel [57]. We also presented a dynamic model for a continuum robotic arm with distributed SVAs and validated the model with open-loop control of independently actuated SVAs [109].

In this chapter, we introduce the design, implementation, and experimental validation of *closed-loop controllers* for hydrogel-actuated robots. We demonstrate our control approach on a millimeter-scale, two degree-of-freedom (DOF) manipulator actuated by two SVAs, shown in Fig. A.1. Many prior control-oriented models developed for similar systems have been governed by the kinematic equations describing rigid links [125, 126], which are less useful in the design of feedback controllers for continuously deformable robots with soft actuators embedded within their structure. To address this, we propose a black-box identified model as in [127, 128] that simplifies system dynamics in the form of a linear state-space representation. Modern control is built upon state-space models and state-space system identification, which makes modern control techniques more practical in application [129, 130]. We apply system identification methods to obtain a linear state-space model of the manipulator, which can be used to implement a wide range of

92

controllers for different applications. We design an H_∞-optimal output-feedback tracking controller [131], similar to the H_∞ output-feedback controller in [132] for flexible needles guidance with a difference that their control system is dynamic rather than static. We then compare it in simulation to an observer-based output-feedback controller. The H_∞-optimal controller is then experimentally validated for planar reference trajectories. Finally, we show that our approach can be used to control more complex mechanisms actuated by SVAs through a demonstration of payload transport by four manipulators.

In summary, the contributions of this paper are as follows:

1. Implementation of active temperature-responsive hydrogel-based actuators (the SVA) as **independently-controllable** units.

2. Development and experimental identification of a linear state-space model of the manipulator that can be used to implement a variety of control techniques. This linear model is sufficiently accurate for control purposes, despite the complex nonlinear dynamics of the actuators.

3. Demonstration of, for the first time, the ability to control a 2-DOF mechanism with **independently-controllable** hydrogel actuators in real time using output-feedback controllers.

4. Demonstration of an exemplar payload transport application using an array of four manipulators with this versatile and computationally-inexpensive technique.

A.2 Manipulator Fabrication

SVAs are fabricated by embedding small Joule heaters within a mold, temperature-responsive PNIPAAM hydrogel in the shape of a rectangular prism, as illustrated in Fig. A.1b and A.1c. When an electric potential is applied across the embedded Joule heater, the actu-

ator shrinks uniformly. The manipulator, also shown in Fig. A.1b, consists of two SVAs affixed to a 3D-printed T-shaped extension, which serves as the end-effector. A standard PNI-PAAM hydrogel precursor solution is used to fabricate the SVAs from thermo-responsive hydrogel, using a recipe described in [57]. Each SVA is $8 \times 4.5 \times 3\,\text{mm}^3$ in its fully swollen state, with a total weight of 0.12 g, including the embedded-Joule heater ($10\,\Omega$ SMD resistor 0805), which is connected to microcontrollers by wires. The T-shaped extension is 3D-printed in nylon using a Markforged M2 3D printer. A circuit board, which serves as the fixed base of the manipulator, is attached to one side of the two SVAs; the T-shaped extension is attached to the other side. The circuit board and extension are attached to the SVAs with superglue to ensure that they remain in contact with the SVAs during the experiments. Since hydrogels must be immersed in water to absorb water when cooling, all experiments are conducted in a tank of deionized (DI), room-temperature water.

A.3   Experimental Setup

Figure A.1 shows the experimental setup used for closed-loop control and tracking of the manipulator's trajectory. A Logitech C930e USB Webcam is placed in front of the tank to send real-time data to the image processing program in MATLAB which tracks the position of a marker on the manipulator tip. These measurements of the manipulator tip's position over time are transmitted back to the controller. We used a black-and-white checkerboard with 2 mm $\times$ 2 mm squares to estimate the camera calibration factors (mm/pixel) along the x and y axis (Fig. A.1). White was selected as the color of the tank's background, and black was selected as the color of the manipulator tip's marker to facilitate contrast-based filtering between the foreground and background. The Camera Calibration Toolbox in MATLAB was initially used to compensate for lens distortion, but since this increased the image processing time by 30% without significantly improving the image data, the original camera images were subsequently used without compensation. All

94

control algorithms are implemented in MATLAB; the controller output is sent to an Arduino Mega2560, which acts as the physical communication layer between MATLAB and a PCA9685 MOSFET board. This MOSFET board, with 16 discrete output channels, receives a PWM signal from the controller and applies it (maximum: 3.7 V) at higher current to the corresponding Joule heater.

A.4   Manipulator Modeling

In this section, the kinematics of the manipulator are derived in order to compute its workspace. A two-dimensional linear state-space model of the manipulator is then defined using black-box system identification methods.

A.4.1   Kinematics and Workspace
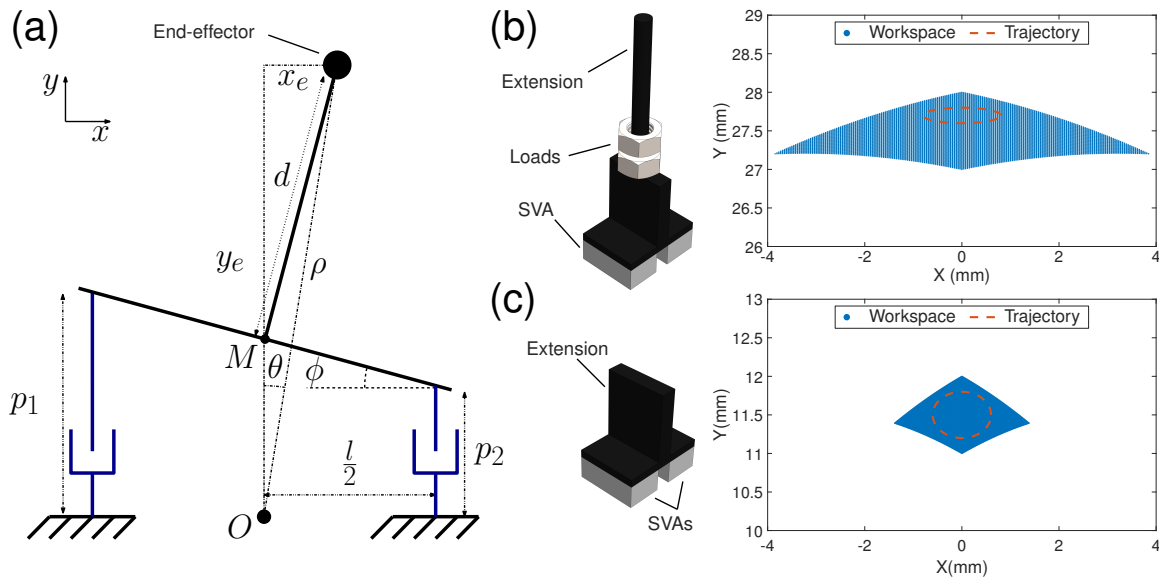

Figure A.2 Schematic and workspace of the manipulator. (a) The 2-DOF parallel mechanism model with two prismatic joints. (b), (c) Workspaces for extensions with lengths $d = 25\,\text{mm}$ and $d = 9\,\text{mm}$, respectively, with exemplar elliptical trajectories overlaid in red. Extra loads are added to the longer extension in (b) to test the robustness of the controller in experiment.

To derive manipulator tip kinematics and workspace, the SVAs are modeled as two prismatic joints, as illustrated in Fig. A.2a. The T-shaped extension is assumed to be rigid compared to the SVAs that are rigidly attached to the extension and circuit board. The SVAs are modeled as linear contractile elements since only one dimension of their volumetric shape change influences the displacement of the manipulator. Thus, with two prismatic actuators connected in parallel, the manipulator may be considered a 2-DOF mechanism. As shown in Fig. A.2a, we define p_1 and p_2 as the linear displacement of each SVA. These values vary between 3 mm in inactivated SVA to 2 mm when activated by the embedded Joule heaters; $l =$ 6.5 mm is the spacing between SVAs, d is the length of the extension, and ϕ shows the extension's angle from the horizontal axis. We assume point M's displacement in the x direction is negligible (Fig. A.2a). The forward kinematics of the manipulator may be computed geometrically for the manipulator tip's, $\boldsymbol{p}_e$, in Cartesian coordinates, x_e and y_e, in the reference frame with origin O, according to

$$\boldsymbol{p_e} = \begin{bmatrix} x_e & y_e \end{bmatrix}^T, \quad \phi = \arctan(\frac{p_1 - p_2}{l}), \tag{A.1}$$

$$x_e = d\sin(\phi), \quad y_e = d\cos(\phi) + \frac{p_1 + p_2}{2}. \tag{A.2}$$

The polar coordinates ρ and θ of the manipulator's tip in this reference frame (see Fig. A.2a) are given by

$$\rho = \sqrt{x_e^2 + y_e^2}, \quad \theta = \arctan\left(\frac{x_e}{y_e}\right). \tag{A.3}$$

As illustrated in Fig. A.1c, if both SVAs are activated simultaneously with the same input voltage, then the manipulator's tip moves along the ρ-axis at a constant θ; if only the left or right SVA is activated, then the tip undergoes an angular displacement at a constant ρ. Other SVA activation patterns produce a combination of displacements in both ρ and θ. Two different extensions with lengths of $d = 25$ mm and $d = 9$ mm were fabricated

and tested, and their workspaces are shown in Figs. A.2b and c, respectively. The longer extension is used to amplify the motion of each actuator, resulting in a larger workspace and making the controller performance easier to measure and evaluate. Extra loads may be added to the shaft of the longer extension, as shown in the left image in Fig. A.2b, in order to experimentally test the robustness of the controller. The shorter extension, by contrast, supports higher loads on the tip during trajectory tracking, as demonstrated in the payload transport application in Section 4.3.4.3.

A.4.2 Linear State-Space Model

As explained in the last section, the displacements of the SVAs and manipulator tip are not decoupled, since the T-shaped extension connecting the actuators to the tip establishes a rigid kinematic transformation from the prismatic motion of the actuators to the 2-DOF planar motion of the end-effector. We model this control system using a two-dimensional linear state-space representation, which enables the implementation of a variety of control methods. Defining $\boldsymbol{x}(t) \in \mathbb{R}^{4 \times 1}$ as the vector of unknown system state variables at time t, $\dot{\boldsymbol{x}}(t)$ as the vector of time derivatives of the state variables, $\boldsymbol{u}(t) = [V_1(t) \quad V_2(t)]^T$ as the vector of inputs, and $\boldsymbol{y}(t) = [\theta(t) \quad \rho(t)]^T$ as the vector of outputs, the state-space model is given by

$$\dot{\boldsymbol{x}}(t) = \boldsymbol{A}\boldsymbol{x}(t) + \boldsymbol{B}\boldsymbol{u}(t),$$

$$\boldsymbol{y}(t) = \boldsymbol{C}\boldsymbol{x}(t) + \boldsymbol{D}\boldsymbol{u}(t) \tag{A.4}$$

where the matrices $\boldsymbol{A}$, $\boldsymbol{B}$, $\boldsymbol{C}$, and $\boldsymbol{D}$ must be determined for each extension (25 mm and 9 mm), separately. Since the state variables of the model are not necessarily measurable, it is crucial to understand the relationship between various input-output models and state-space models in order to accurately identify the state-space model from input-output data [129]. To find and select a model that best represents the system's behavior,

97

a number of models were considered including state-space models of different dimensionalities. the 2-input 2-output showed a good fit to the data and also directly provides the unknown matrices that are required for designing the controller, we identified the system using a state-space model. A, B, C, and D were identified by applying black-box system identification to a set of time series input-output data according to [133], using the MATLAB System Identification Toolbox. The identified matrices for the 25 mm extension were found to be:

$$A = \begin{bmatrix} -0.0007 & -0.0301 & 0.0444 & 6.0548 \\ -0.0016 & -0.0623 & 0.0254 & -1.4325 \\ -0.2613 & 0.6580 & 7.2633 & -374.9846 \\ -0.0243 & 0.1643 & 3.0590 & -44.3024 \end{bmatrix},$$

$$B = \begin{bmatrix} 0.0001 & 0.0003 \\ -0.0000 & -0.0001 \\ -0.0051 & -0.0232 \\ -0.0001 & -0.0042 \end{bmatrix},$$

$$C = \begin{bmatrix} 1.1446 & -0.0046 & -0.0020 & 0.0034 \\ -1.1431 & -3.5368 & 0.0020 & -0.0534 \end{bmatrix},$$

$$D = \begin{bmatrix} 0 & 0 \\ 0 & 0 \end{bmatrix}.$$

Multiple input-output datasets were gathered across various ranges of amplitudes and frequencies to find a state-space model. Among all the input signals, the fastest signal that permitted the hydrogel actuators to respond across their full temperature range was selected as the primary modeling input. Figure A.4a plots two selected input voltages among the data set that were experimentally applied to the SVAs which covers the tip workspace and

depicts a 50% shift in the SVAs' input signal. Since the hydrogel-based SVAs have a relatively slow response, especially during their cooling phase, they were actuated from a starting point of half-actuation (50%) in order to improve both the speed and tracking performance of the manipulator and the signal reaches the minimum and maximum values during the cycle. Fig. A.4b displays the resulting displacement of the manipulator tip and the outputs of the identified model (A.4) for the same inputs. These figures, which are a comprehensive example of comparison between the actual data and the identified model output, show that the model outputs ρ and θ follow the corresponding measured output values throughout the duration of the experiment, with the NMAE for ρ and θ given by 0.026 mm (5.7%) and 0.008 rad (6.6%), respectively. The NMAE value remains below 10% for other tested data sets. Thus, our linear state-space model of the entire mechanism is sufficiently accurate to use in the design of controllers for the manipulator, despite the difficult-to-characterize nonlinear dynamics of the hydrogel actuators themselves.

A.5   Controller Design

It can be shown that the open-loop state-space model (A.4), which has the corresponding transfer function $\boldsymbol{G}_o(s)$, is stable, controllable, and observable. In this section, we design two trajectory tracking controllers based on this state-space model, an observer-based output-feedback controller and an H_∞-optimal output-feedback controller. Block diagrams of the controllers are illustrated in Fig. A.3. Both controllers are designed to track a reference trajectory $\boldsymbol{r}(t) \in \mathbb{R}^{2\times1}$ while attenuating the effects of noise, denoted by $\boldsymbol{n}(t) \in \mathbb{R}^{2\times1}$, and external disturbances, denoted by $\boldsymbol{d}(t) \in \mathbb{R}^{2\times1}$.

A.5.1   Observer-based output-feedback controller

In this type of controller, an observer is designed to compute an estimate $\hat{\boldsymbol{x}}(t)$ of the unknown system state vector $\boldsymbol{x}(t)$ from the control input $\boldsymbol{u}(t)$ and the output $\boldsymbol{y}(t)$. The
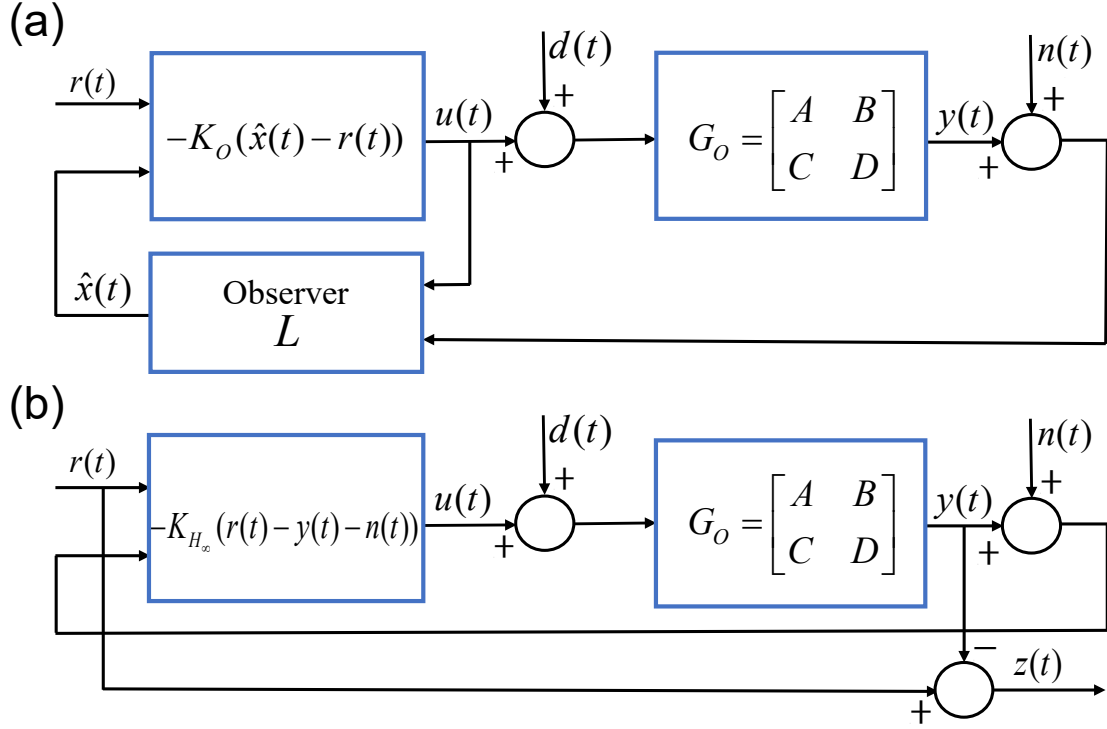
Figure A.3 Block diagrams of the proposed output-feedback controllers with state-space representation in the tracking framework [134]. (a) Observer-based controller. (b) H_∞-optimal controller.

control input is defined as

$$\boldsymbol{u}(t) = -\boldsymbol{K}_O\left(\hat{\boldsymbol{x}}(t) - \boldsymbol{r}(t)\right), \tag{A.5}$$

where $\boldsymbol{K}_O \in \mathbb{R}^{2 \times 4}$ is the feedback gain matrix, which can be computed as though all state variables are measurable, depending only on the $\boldsymbol{A}$ and $\boldsymbol{B}$ matrices. With this control input, the observer is given by

$$\dot{\hat{\boldsymbol{x}}}(t) = (\boldsymbol{A} - \boldsymbol{B}\boldsymbol{K}_O - \boldsymbol{L}\boldsymbol{C})\hat{\boldsymbol{x}}(t) + \boldsymbol{L}\boldsymbol{y}(t), \tag{A.6}$$

where $\boldsymbol{L} \in \mathbb{R}^{4 \times 2}$, the observer gain matrix, must be defined such that $\boldsymbol{A} - \boldsymbol{L}\boldsymbol{C}$ is a Hurwitz matrix [131]. The following $\boldsymbol{K}_O$ and $\boldsymbol{L}$ matrices were computed for the 25 mm extension:

$$
\boldsymbol{K}_O = \begin{bmatrix} -3.8929 & 2.3760 & -0.1061 & 0.2888 \\ 3.6672 & -0.9670 & 0.0949 & -0.2706 \end{bmatrix},
$$

$$
\boldsymbol{L} = \begin{bmatrix} 18.5160 & -21.9676 \\ 0.1852 & -7.7968 \\ -0.0051 & 0.0232 \\ -0.0649 & 0.0042 \end{bmatrix}.
$$

A.5.2 H_∞-optimal output-feedback controller

The H_∞-optimal controller is designed using Linear Matrix Inequality (LMI) methods [135, 136]; MATLAB's YALMIP toolbox [137] is then used to solve the optimization problem numerically. revThe interconnected system $S(\boldsymbol{K}_{H_\infty}, \boldsymbol{G}_o)$ of the optimal gain matrix $\boldsymbol{K}_{H_\infty} \in \mathbb{R}^{2\times2}$ and the open-loop system $\boldsymbol{G}_o(s)$, with external input defined as $\boldsymbol{w} = [\boldsymbol{r}^T \ \boldsymbol{d}^T \ \boldsymbol{n}^T]^T \in \mathbb{R}^{6\times1}$ and external output $\boldsymbol{z} = \boldsymbol{r} - \boldsymbol{y}$, represents the closed-loop system with the H_∞ gain:

$$
\|\boldsymbol{z}\|_{L_2} \ \leq \ \big\|S(\boldsymbol{K}_{H_\infty}, \boldsymbol{G}_o)\big\|_{H_\infty} \|\boldsymbol{w}\|_{L_2}. \tag{A.7}
$$

The optimal gain matrix $\boldsymbol{K}_{H_\infty}$ is obtained as the solution to an optimization problem that minimizes the effect of the external input ($\boldsymbol{w}$) on the external output ($\boldsymbol{z}$). We can prove that the H_∞ gain is bounded using the bounded-real lemma [136] (see Appendix). The control law is designed in the the output-feedback tracking structure:

$$
\boldsymbol{u}(t) = -\boldsymbol{K}_{H_\infty}(\boldsymbol{r}(t) - \boldsymbol{y}(t) - \boldsymbol{n}(t)). \tag{A.8}
$$

The gain matrix for the 25 mm extension was computed as

$$
\boldsymbol{K}_{H_\infty} = \begin{bmatrix} -1.7371 & 2.9015 \\ -0.3775 & -2.4158 \end{bmatrix}.
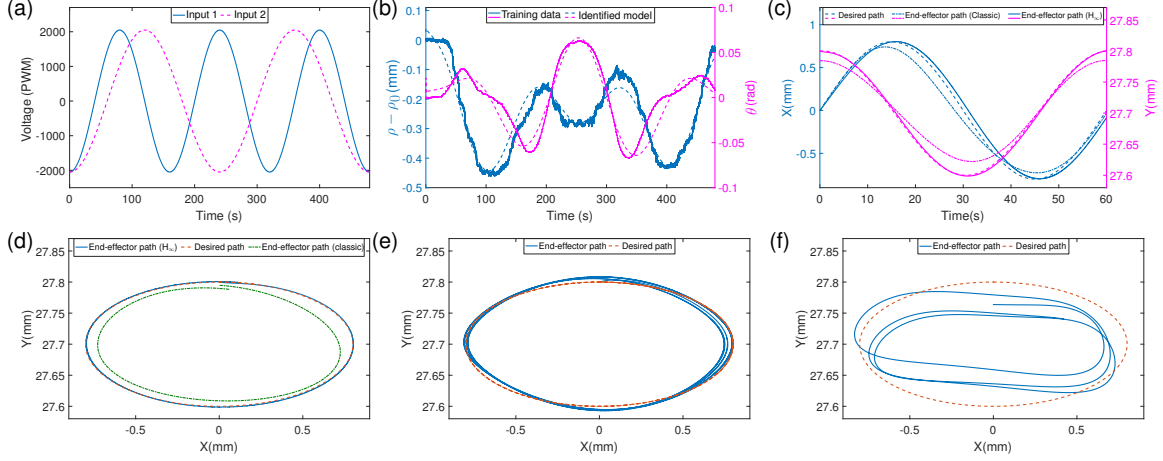$$

101

Figure A.4 Simulation results. (a) 12-bit PWM waveform applied to the SVAs during training. (b) System output and model fitted from training. (c) The x and y coordinates of the manipulator tip over time for the H_∞-optimal and Observer-based controllers, tracking an ellipse. (d) The x-y trajectory of the tip during the simulation in (c). (e) H_∞-optimal controller with noise and disturbance. (f) Observer-based controller with noise and disturbance.

A.6 Results and Discussion

In this section, we study the performance of H_∞ and observer controllers for trajectory tracking. An elliptical reference trajectory is used, defined by

$$\boldsymbol{r}(t) = \begin{bmatrix} \alpha \sin\left(\frac{2\pi}{60}t\right) & \beta + \gamma \cos\left(\frac{2\pi}{60}t\right) \end{bmatrix}^T. \tag{A.9}$$

where $\alpha = 0.8$, $\beta = 27.7$, and $\gamma = 0.1$ for the 25 mm extension, and $\alpha = 0.6$, $\beta = 11.5$, and $\gamma = 0.3$ for the 9 mm extension, to ensure that each path lies in the workspace of its corresponding manipulator (see Fig. A.2). The manipulator's tracking performance degraded at frequencies of higher than one cycle per minute.

Table A.1 N(MAE) of controller performance in simulation (in mm).

Controller	Noise & disturbance	x MAE	y MAE	$x-y$ MAE	$x-y$ NMAE (%)
H_∞	No	0.045	0.006	0.052	3.2
Observer	No	0.065	0.008	0.079	4.9
H_∞	Yes	0.047	0.005	0.055	3.4
Observer	Yes	0.078	0.009	0.096	5.9

A.6.1   Comparison of controllers in simulation

The performance of the two controllers is first compared in simulation in the presence of the following disturbance and noise signals:

$$\boldsymbol{d}(t) = \left[0.00015 \sin\left(\frac{3\pi}{60}t\right) \quad 0.00045 \sin\left(\frac{2\pi}{60}t\right)\right]^T, \tag{A.10}$$

$$\boldsymbol{n}(t) = \left[0.3 \sin\left(\frac{\pi}{60}t\right) \quad 0.3 \sin\left(\frac{0.5\pi}{60}t\right)\right]^T. \tag{A.11}$$

The manipulator with the 25 mm extension was simulated in MATLAB Simulink, using the output-feedback tracking framework depicted in Fig. A.3 and the identified model and controller values designed in the previous section. Figures A.4c and A.4d plot the x and y coordinates and the trajectory of the manipulator tip over time for one cycle (60 s), given an elliptical reference trajectory, from each controller. To observe the effect of adding noise and disturbance in simulation, the sinusoidal functions of $\boldsymbol{n}$ and $\boldsymbol{d}$ were input to the 25 mm manipulator. The tracking trajectories of the manipulator tip produced by each controller are compared in Figs. A.4e and A.4f, separately. Although the simulations are performed across three cycles, only one cycle is shown in the figures and used in the error comparison for clarity. The tracking error for each case is reported in Table A.1.The NMAE values were computed by dividing the mean absolute error (MAE) over their corresponding range. All the values are relatively low, under 10%, indicating accurate tracking.

We can prove that the H_∞ gain is bounded using the bounded-real lemma [136] below.

Lemma: *Suppose that*

$$\boldsymbol{G}(s) = \left[\begin{array}{c|c} \boldsymbol{A} & \boldsymbol{B} \\ \hline \boldsymbol{C} & \boldsymbol{D} \end{array}\right].$$

Then, the following statements are equivalent:

1. $\left\|\boldsymbol{G}(s)\right\|_{H_\infty} \leq \gamma$

2. There exists a $\boldsymbol{P} > 0$ such that

$$\begin{bmatrix} \boldsymbol{A}^T\boldsymbol{P} + \boldsymbol{P}\boldsymbol{A} & \boldsymbol{P}\boldsymbol{B} \\ \boldsymbol{B}^T\boldsymbol{P} & -\gamma\boldsymbol{I} \end{bmatrix} + \frac{1}{\gamma}\begin{bmatrix} \boldsymbol{C}^T \\ \boldsymbol{D}^T \end{bmatrix}\begin{bmatrix} \boldsymbol{C} & \boldsymbol{D} \end{bmatrix} < 0$$

The proof that statement 1 implies 2 requires the Hamiltonian, and the proof that statement 2 implies 1 uses the global stability conditions of the Lyapunov function [136].

A.7   Conclusion

In this chapter, we addressed a trajectory-tracking problem for a millimeter-scale 2-DOF manipulator with soft hydrogel-based actuators. We defined a linear state-space model of the manipulator and fit the matrices of this model using input-output measurement black-box identification. This state-space representation enables the implementation of a range of controllers on the manipulator; in this chapter, the performance of an observer-based controller was compared in simulation to that of an H_∞-optimal controller in an output-feedback framework with and without noise and disturbance. We showed experimentally that different versions of the manipulator are able to track various reference trajectories, even under load, using the H_∞-optimal controller.

Our ability to coordinate independently controllable soft actuators with complex internal dynamics in a robotic system demonstrates progress in the real-time, closed-loop

control of mechanisms with this type of actuator. We expect that researchers will be able to adapt this approach across similar stimuli-responsive materials as they are developed and optimized. This will also permit SVAs, manufactured from a variety of materials, to be used for controlled grasping, manipulation, and locomotion tasks across a variety of new soft robotic platforms, such as octopus-inspired continuum robots [109]. Our approach can be used to design and implement decentralized controllers on segmented mechanisms with distributed hydrogel actuators, as discussed in our related work [109, 138].

In future work, we plan to improve the speed of the image processing algorithms for tracking the manipulator, and ultimately eliminate the use of the camera for position tracking and instead implement this control scheme using embedded sensor feedback. This will enable the application of machine learning techniques to optimize control performance.

APPENDIX B

CURRICULUM VITAE

Roozbeh Khodambashi Emami

rkhodamb@asu.edu   1824 E Don Carlos Ave, Tempe, AZ, 85281   (404) 409-2176

For project details and sample codes please visit my website: https://rkhodambashi.github.io/

EDUCATION

- Ph.D. in Systems Engineering, Arizona State University, *April 2021*
- M.S. in Music Technology**,** Georgia Institute of Technology, *May 2016*
- M.S. in Biomedical Engineering**,** Amirkabir University of Technology, *April 2008*
- B.S. in Mechanical Engineering, Shahrekord University, *April 2005*

Ph.D. Dissertation

R. Khodambashi, "Soft Actuators for Miniature and Untethered Soft Robots Using Stimuli-responsive Hydrogels", Arizona State University, 2021. Committee: Daniel Aukes (chair), T. Sugar, C. Nam.

PUBLICATIONS, INTELLECTUAL PROPERTY, AND PRESENTATIONS

Journal Publications

1. Khodambashi, R., Alsaid, Y., Rico, R., Peet, M. M., Marvi, H., Fisher, R. E., Berman, S., He, X., Aukes, D. M., "Heterogeneous Hydrogel Structures with Spatiotemporal Reconfigurability using Addressable and Tunable Voxels". Adv. Mater. 2021, 2005906. https://doi.org/10.1002/adma.202005906. **Featured on the cover of the journal.**
2. Y. Alsaid, S. Wu, D. Wu, Y. Du, L. Shi, R. Khodambashi, R. Rico, M. Hua, Y. Yan, Y. Zhao, D. Aukes, X. He. "Tunable Sponge-like Hierarchically Porous Hydrogels with Simultaneously Enhanced Diffusivity and Mechanical Properties". Adv. Mater. 2021, 2010344. Accepted for publication.
3. A. Doroudchi, R. Khodambashi, M. Sharifzadeh, D. Li, S. Berman, D. Aukes Tracking Control of a Miniature 2-DOF Manipulator with Hydrogel Actuators", 2021, accepted for publication as a Submission for RA-L and RoboSoft in the IEEE Robotics and Automation Letters (RA-L).
4. Khodambashi R.**,** Najarian S., Golpaygani A.T., Keshtgar A., (2008), **"**A Tactile Sensor for Detection of Skin Surface Morphology and its Application in Telemedicine Systems**"**, *American Journal of Applied Sciences*, 5 (6): 633-638.
5. Mehrizi, A. A., Najarian, S., Khodambashi, R., & Dehkhoda, S. (2011). "A Novel Method of Tactile Assessment of Arteries Using Computational Approach". *International Journal of Academic Research*, 3(2).
6. Darvish, B., Najarian, S., Shirzad, E., & Khodambashi, R. (2009). "A novel tactile force probe for tissue stiffness classification". *American Journal of Applied Sciences*, *6*(3), 512.

Refereed Conference Papers

1. R. Khodambashi, S. Berman, X. He and D. M. Aukes, "Miniaturized Untethered Soft Robots Using Hydrogel-based Soft Voxel Actuators" Proceedings of 4th IEEE International Conference on Soft Robotics (RoboSoft), April 12-16, 2021, Yale University, USA.
2. A. Doroudchi, R. Khodambashi, A. S. Lafmejani, D. M. Aukes and S. Berman, "Dynamic Modeling of a Hydrogel-based Continuum Robotic Arm with Experimental Validation," 2020 3rd IEEE International Conference on Soft Robotics (RoboSoft), New Haven, CT, USA, 2020, pp. 695-701.

3. Khodambashi, R., Weinberg, G., Singhose, W., Rishmawi, S., Murali, V., & Kim, E. (2016, November). "User oriented assessment of vibration suppression by command shaping in a supernumerary wearable robotic arm". In Humanoid Robots (Humanoids), 2016 IEEE-RAS 16th International Conference on (pp. 1067-1072). IEEE.

4. Khodambashi R., Najarian S., Golpaygani A.T., Dehkordi A., (2007), "A Model for Simulating the Mechanical Response of Fingertip to Tactile Stimuli", Proceedings of the 15th. Annual (International) Conference on Mechanical Engineering ISME2007, Amirkabir University of Technology (Tehran Polytechnic), Tehran, Iran.

5. Wang, N., Liu, R., Khodambashi, R., Asmare, N., & Sarioglu, A. F. (2017, January). "Code-division multiplexed resistive pulse sensor networks for spatio-temporal detection of particles in microfluidic devices". In MicroElectro Mechanical Systems (MEMS), 2017 IEEE 30th International Conference on (pp. 362-365). IEEE.

6. Sharifzadeh, Mohammad, Roozbeh Khodambashi, and Daniel M. Aukes. "An Integrated Design and Simulation Environment for Rapid Prototyping of Laminate Robotic Mechanisms." ASME 2018 International Design Engineering Technical Conferences and Computers and Information in Engineering Conference. American Society of Mechanical Engineers, 2018.

Patents, Patent Applications, & Provisional Patents

1. R. Khodambashi, Yousif Alsaid, Ximin He, Daniel Aukes, SHAPE MORPHING SOFT MATERIALS AND ASSEMBLIES INCLUDING THE SAME. US Patent Pending, Non-provisional Application filed June 2020.
   R. Khodambashi, A Darabi, Piezoelectric generator, method of its operation and its application in production, storage and transmission of electric energy, US Patent 10,505,471.

2. Gil Weinberg, R. Khodambashi, "A Wearable Robotic Limb", US Patent Pending, Application No. 62/258,571, GaTech invention disclosure reference number GTRC 7108.

3. R. Khodambashi, S. Najarian, "Tactile Device for Skin Lesion Detection", The Judiciary of Iran, Registration Number: 42618, 24th. September 2007.

4. R. Khodambashi, "Computer System for Studying Vibration Phenomenon for use in Mechanical Vibration Laboratories", The Judiciary of Iran, Registration Number: 43205, 9th. October 2007.

PROFESSIONAL ACTIVITIES AND SERVICE

Peer Reviewer for Journals

IEEE Robotics and Automation Letters (IEEE-RAL); Soft Robotics (SoRo); IOP Smart Materials and Structures (SMS); IOP Material Research Express (MRE); IOP Multifunctional Materials (MFM)

Peer Reviewer for Conferences

International Conference on Robotics and Automation (ICRA); International Conference on Intelligent Robots (IROS); IEEE International Conference on Soft Robotics (RoboSoft)

MEMBERSHIPS AND AWARDS
- University Graduate Fellowship, 2019, Arizona State University.
- Ferdinand A. Stanchi fellowship, 2019, Arizona State University.
- Senator, Georgia Tech Graduate Student Government
- Top 10 entries among 1000+ in '2015 Create the Future Design Contest', NASA.
- Second Prize (500$) for ME6404 course project
- Iranian Elite Association
- Iranian Society of Mechanical Engineers

MENTORING AND LEADERSHIP EXPERIENCE

Fulton Undergraduate Research Initiative (FURI) Mentor, Arizona State University
- Helped students define their research projects and write a proposal.
- Helped students identify the material and equipment needed for their project.
- Worked with the student to budget the project and purchase required items.
- Guided students to conduct the experiments and write reports.

The Vertically Integrated Projects (VIP) Program *Student Mentor,* Georgia Tech
• Leaded the undergraduate VIP class in 'augmented robotic musicianship' project
• Helped the mechatronics design group, comprised of mechanical and electrical engineers in designing a robotic arm.
• Coordinated group meetings and set deadlines for accomplishing designated tasks.
• Cooperated with other groups to share design data and make sure the design meets the criteria for sensing and artificial intelligence groups.

President of volleyball club student organization, 2017-2019 Arizona State University
• Organized campaigns for acquiring new members.
• Organized weekly practice sessions and games.
• Organized friendly matches

CERTIFICATES
- Certificate of attendance in Quality management Systems Internal Audit Training Course (based on ISO9110:2008), TUV Nord academy, Iran-Germany (http://www.tuvnordiran.com).
- Foundations of Programming: Object-Oriented Design, Lynda.com, Issued Oct 2016. Credential ID 953C6B.
- C++ Essential Training, Lynda.com, Issued Sep 2016, Credential ID E77CC3.
- Certificate of attendance in "Process Piping Design" and "Welding Inspection" workshops, Nazeran Yekta Co., Isfahan, Iran (www.nazeranyekta.com).

SOFTWARE AND PROGRAMMING SKILLS

• SolidWorks	• Python	• MATLAB
• Ansys	• C++	• SIMULINK
• MAX/MSP	•Arduino	• LabVIEW

REFERENCES
Available upon request.